COOPERATIVE CONTROL OF PAYLOAD TRANSPORT BY MOBILE MANIPULATOR COLLECTIVES

by

HAO SU

JUNE 2008

A thesis submitted to the Faculty of the Graduate School of the State University of New York at Buffalo in partial fulfillment of the requirements for the degree of

MASTER OF SCIENCE

Department of Mechanical and Aerospace Engineering

State University of New York at Buffalo

Buffalo, New York 14260

To my family and friends

Acknowledgement

I would like to express my gratitude to my advisor, Dr. Venkat Krovi, for all the guidance and help in my graduate study at the University at Buffalo. He introduced the fabulous robotics world to me, and articulated many important concepts and ideas in an insightful and intuitive way. I believe all of these would be invaluable knowledge for my future career.

I am honored to have Dr. Roger Mayne and Dr. Puneet Singla serving on my thesis committee. I am also grateful to Dr. Tarunraj Singh and Dr. John Crassidis for teaching me control theory and Dr. Kemper Lewis for helping me when I first came here.

I would also like to thank all of the ARMLAB members, especially Rajan, Chin Pei, Leng-feng, Anand, Kun, Qiushi, Pat, Madu, Srikanth and Yao. A special thanks to Qiushi: as group partner in so many course projects with me, and the time of coding multi-robot simulator and studying biped locomotion is priceless treasure for me; as lab member, it is you that talked with me and helped me to solve many problems I met; as friend, we play Pingpong (in gym or in lab), tennis and billiard at the depressed moments. For Pat, I have to say you are such a nice guy! You help me and many lab members the practical problems and share your (yes, I know sometimes it is cooked by Mother Miller) fantastic food with us. I am greatly grateful for all your friendship, intelligence, and patience. I thank Chin Pei as a good mentor for teaching and explaining many robotics theories, and provide many guidance and illumination in many critical times.

Thanks Madu and Srikanth for talking homework and research with me, and telling me quite a lot of stuff about India. Li Yuan is the Artificial Wikipedia and GPS in our life, and it is great please to travel with you and talk with you; Xiang Jianping helped me make many important decisions and save me quite a lot money on laundry; my nice roommate Ren Bin makes my life happy and rejoicing. Thanks all my friends at Buffalo, Yang Yan, Liu Li, Chen Tingting, Xu Jingyang, Hao Fang, Xie Wei, Luo Changsong, Chris, Sai. Thank you Yaan for your never-ending encouragement and talk with me. You are an unexpected vista of my life in US.

Finally, I must say that my family has been the biggest help of all throughout my life. Dad, you are a good officer and also good mentor, always help me to find the “optimal solution”. Mom, you made so many contributions for our family. I would not be where I am today without you. My little brother, hope you have good luck in the university!

Thank you all!

Table of Contents

List of Figures

List of Tables

Abstract

Multi-manipulators based mobile manipulation is an important capability to extend the domain of robotic applications. The novel feature endowed by the combination of mobility with manipulation is crucial for a number of applications, ranging from material handling task to planetary exploration. The benefits include increased workspace, reconfigurability, improved disturbance rejection capabilities and robustness to failure. The challenges, however, arise from the compatibility of various holonomic and nonholonomic constraints and kinematic and dynamic redundancy. Moreover, cooperative manipulation would lead to significant dynamic coupling and requires delicate motion coordination. Failure to consider these effects can cause excessive internal forces and high energy consumption, and even destabilize the system.

To deal with these entailed issues, we present a decentralized dynamic control algorithm for a robot collective consisting of multiple nonholonomic wheeled mobile manipulators capable of cooperatively transporting a common payload. The nonholonomic wheeled mobile manipulator consists of a fully-actuated manipulator arm mounted on a disk-wheeled mobile base. In this algorithm, the high level controller deals with motion/force control of the payload, at the same time distributes the motion/force task into individual agents by grasp description matrix. In each individual agent, the low level controller decomposes the system dynamics into decoupled task space (end-effector motions/forces) and a dynamically-consistent null-space (internal motions/forces) component. The agent level control algorithm facilitates the prioritized operational task accomplishment with the end-effector impedance-mode controller and secondary null-space control. The scalability and modularity is guaranteed upon the decentralized

control architecture.

Within the dynamic redundancy resolution framework, a decentralized coordination and formation control with collision avoidance capability is further studied for mobile manipulator collectives.

A variety of numerical simulations are performed for multiple mobile manipulator system carrying a payload (with/without uncertainty) to validate this approach. The simulations test the capability of internal force regulation by cooperative manipulators. The end-effector and mobile base to tracking capability is also verified in the simulations. Multiple mobile manipulator collision avoidance is also studied in simulation.

1 Introduction

Object transport and manipulation is perhaps the most important robotic task in the history of robotics. The electrical and mechanical engineers, by taking advantage of the reverse engineering, have been trying to learn from the nature. Two decades ago, biologists observed that coordinated motion of animal groups is an interesting and suggestive phenomenon in nature. A swarm of bees usually collaboratively waggle dance to communicate for a new flower bush source. Fish schools maneuver and glide ingeniously to maximize the overall impetus by delicate formation. Revealing the benefits and mechanism of these behaviors has been one of the constant research interests of biologists and sociologists are deliberately emulating the collective behavior of nature in the design of multiple mobile agents. On the other hand, the hardware devolvement with the advent of inexpensive, embedded microprocessors has technically enabled the implementation of these behaviors in real world. Self-contained and computationally low cost intelligent robot agents are coming out of laboratories to real world applications.

1.1 Motivation and Application

In the daily life, human beings usually take advantage of two hands to manipulate objects, since single hand manipulation is sometimes incapable or not dexterous enough for some tasks. While for much heavier objects or complex tasks, accumulation of individual capability is desirable and crucial for task implementation. By this analogy, we can see the benefits introduced by cooperation. A couple of different reasons account for deploying multi-robot systems, however, one of the main motivations is that multi-robot systems can be used to enhance the system effectiveness. By the constraints of robot actuation capability, cooperative robots are able to accomplish many tasks that are far beyond of individual robot capability. Ideally, to manipulate any large, heavy payload, we can incorporate as many as smaller, lighter robot modules so as to fulfill the task. This modular and flexible structure allows for “divide and conquer” approach to take care of heavy and complex tasks.

The cooperative robot is also advantageous from the perspective of redundancy and robustness. Using a team of multiple robots would enhance system robustness with respect to the single point failure in the sense that we can reconfigure the team and reassign a new task to each agent. Redundancy is frequently used in the systems that require high fault tolerance and high successful rate, like mars exploration.

Cooperative robotics first comes into the modern engineering researchers’ mind in the late 1980s with a special focus on multiple manipulators and multiple mobile robots. The spectrum of engineering perspective of multi-robot system study is considerably broad and deep. Interested readers can refer to [1, 2] and reference therein for a detailed description of research areas in multi-robot systems. Here, we briefly review some pertained principal research topics.

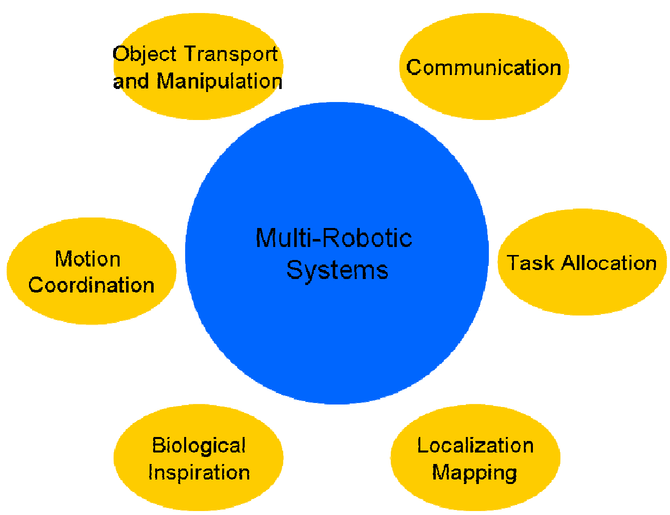

Figure 1: Principal research topics in multi-robot systems [2]

• *Communication:* Communication is of paramount importance for the successful fulfillment of multi-robot systems and it has been extensively studied ever since the debut of multi-robot research. Information exchange across the system affects the interactions among subsystems, and it is possible to categorize the communication schemes as: centralized and decentralized as shown in Figure 2. In the centralized implementation, a central controller makes use of all agent states to command the control signal, while in the decentralized case, each robot module is equipped with individual controller which can only access its own states and the control signal is generated locally.

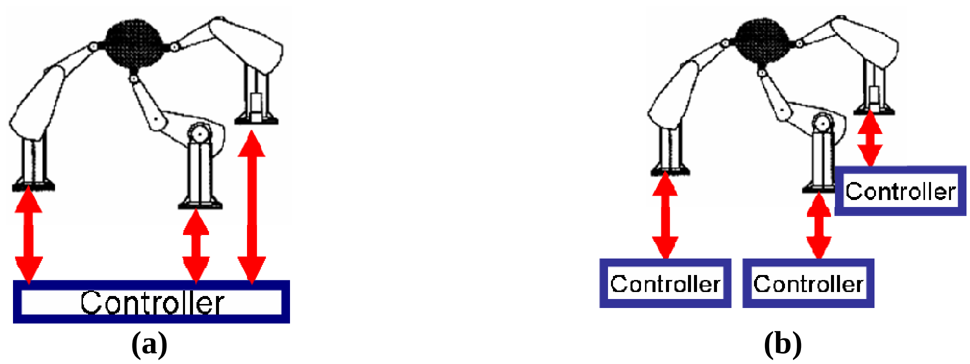

Figure 2 : Controller archtecture: (a) Centralized control, (b) Decentralized control

• *Object transport and manipulation:* Manipulation is perhaps the most important task of robotic system, so the extension of this in multi-robot systems naturally has been one of the important goals in cooperative robots. There are many pertained issues to be considered in this process like synchronization of the subsystems, control of the applied forces and motion planning. Detailed issues would be reviewed in the subsequent section.

• *Motion coordination:* At this level, the system could be composed of a homogenous or heterogeneous se of robots of certain characteristics. Research themes in this domain that have been particularly well studied include multi-robot path planning, traffic control, formation generation, and formation keeping [2]. Most of these issues are now fairly well understood, although demonstration of these techniques in physical multi-robot teams (rather than in simulation) has been limited.

The promise of collaborative robotic system has been fulfilled in support of missions pertaining to national defense, homeland security, and environmental monitoring. Examples of such cooperation includes mobile robot collectives in Figure 3 (a), manned fleet of marine vessels in Figure 3 (b), manned flight aircrafts in Figure 3 (c) and multiple grounded and aerial vehicles in future battlefield as seen in Figure 3 (d). It is necessary to note that some of the ideas and control approaches introduced in this thesis within a robotic paradigm can be applied to these more general multiple robotic systems, like multiple vehicles.

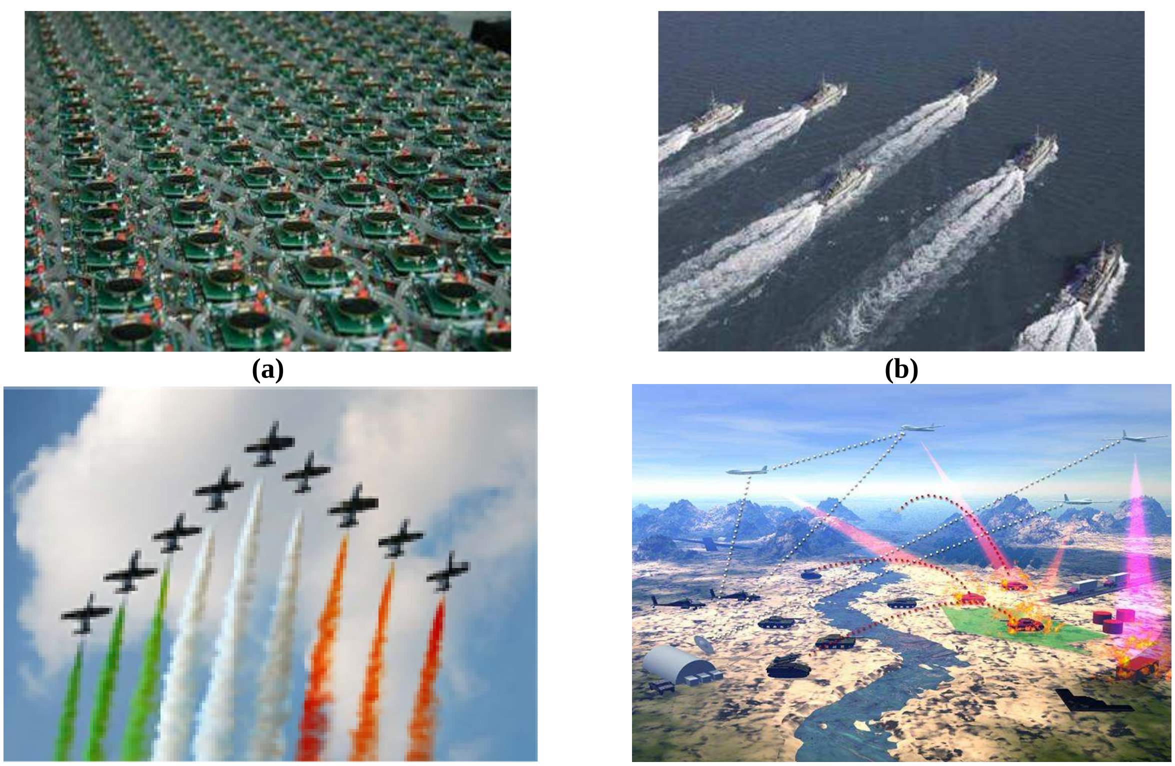

(a) (b) (c) (d)

Figure 3: Engineeing examples of cooperation: (a) EPuck robots, (b) Fleet of marine surface vessels.(c) Italian acrobatic air force unit. (d) Multi vehicles in future battlefield

1.2 Related Works

The analogy between manned/unmanned aerial vehicles and a swarm of bees or a school of fish is perhaps the original biological inspiration for robotics engineers. Natural behavior also provides some envisioning guidance for robotics paradigm of behavior based control that can be described by the relationship between the three primitives of robotics: sense, plan, and act. The first engineering work is motivated by application in the simulation of computer graphics. In 1986, Reynolds [3] made a computer model for coordinating animal motion as bird flocks or fish schools. This pioneering work inspired significant efforts in the study of group behaviors.

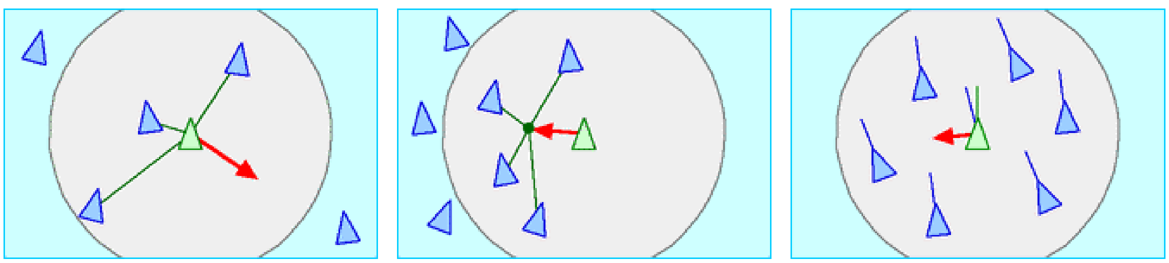

(a) (b) (c)

Figure 4: Three primitive behavior of Boids [3]

Reynolds observed that with the basic flocking model consists of three simple steering behaviors separation, alignment and cohesion, these behaviors could describe how an individual boid maneuvers based on the positions and velocities its nearby flockmates. Figure 4 illustrates the three basic behaviors separation, alignment and cohesion. The individual boid has access to its flockmates within a certain small neighborhood around itself. With these simple behavior and limited perception, a fleet of these simulated "aircrafts" can maneuver and avoid obstacles as shown in Figure 5.

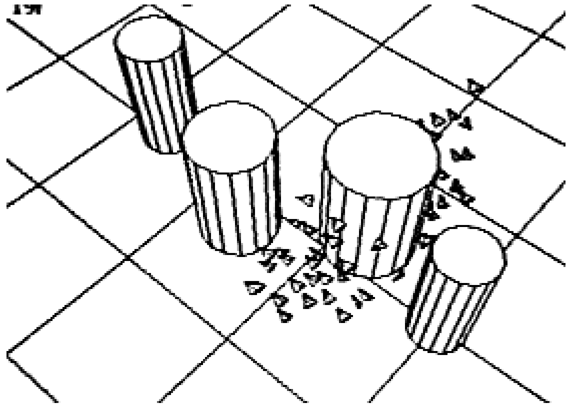

Figure 5: Group behavior of Boids [3]

With this inspiration of computer graphics, researchers take advantage of “reverse engineering” to observe and study the group behavior in nature like the one shown in Figure 6 (a) where a school of fish glides in the sea to decrease power consumption. Fish schools maneuver intelligently to minimize group energy consumption by delicate formation. A group of ants collaboratively make payload transport to achieve the task that is impossible for individual ant. Similar to the origin of computer graphics simulation for multiple agents, the graphics rendering for bee swarms are still an interesting and important work in film industry. More intuitively, the coordination of human group evacuation in emergent condition is posed to be an imperative problem in optimization arena. Emergency evacuation of people group is also getting more and more research attention from the perspective of optimization, like door arrangement, optimal route, and group allocation. Some of the scenarios mentioned above can be visually seen in Figure 6.

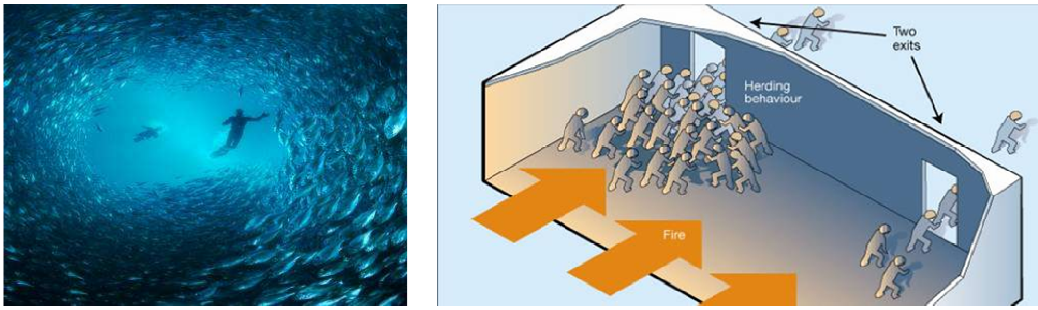

(a) **(b)**

Figure 6: Group behavior in nature and human society

Even though the origin of multi robot comes from the computer graphics simulation and the inspiration of group behavior in nature, we can also trace the similarity and share a lot of common interests in the traditional robotic systems.

(a) **(b)**

Figure 7: Multi-fingered robot and multiple legged robot

Multi-finger robotics has been one of the most popular research arenas in robotic community. Multiple articulated robotic fingers can hold a common payload with shared payload distribution. In this sense, the dynamics of payload system or to say the grasp system in multi-finger robots is exactly the same as in the multiple payload transport system, and most of the research issues in grasp problem, like grasp feasibility, force closure and grasp force optimization would appear in the multiple mobile manipulation scenarios. Imagine that each finger is a fixed based (they all have the common basis) robotic manipulator, the way to control this system in a centralized or decentralized manner is a question to be addressed from the computational perspective.

Another related research area that has been well studied is the multi legged systems. If each leg can be dissembled from the chassis, it can be considered as a mobile manipulator with nonholonomic and holonomic constraints on the wheel. The difference with the multiple mobile manipulator system is that the individual leg is fixed on the common payload, i.e. the chassis, so it can be considered as a special version of the mobile manipulator system. From this token, we can conclude that multiple mobile manipulator system is a more complex, higher mobility system that includes various issues like kinematic constraints (nonholonomic and holonomic), grasp distribution and motion planning.

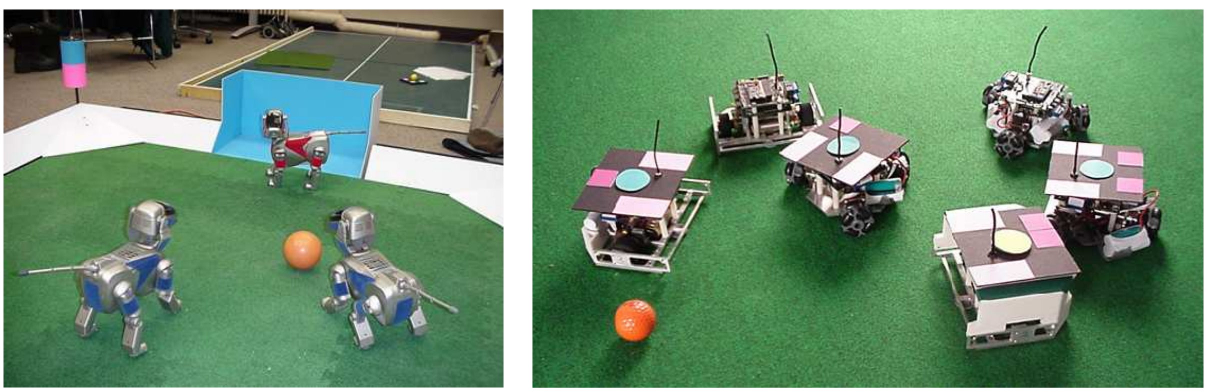

(a) (b)

Figure 8: Mobile robot soccer team and Sony AIBO robot soccer team

Because of these difficulties mentioned above, and most of computer scientists cast research effort on this, it is necessary to note that the inchoate research mainly covers the multiple agent motion coordination and multiple agent communication, particularly in the robot soccer team. For example, as show in Figure 8, the researchers from Carnegie Mellon University and Georgia Institute of Technology first developed 3 vs. 3 agents' robot soccer team in a field of $2\mathrm{m} \times 3\mathrm{m}$ without communication and then a new generation of 4 vs. 4 agents' robot soccer team in a field of $5\mathrm{m} \times 9\mathrm{m}$ with full autonomy.

This research shed light on the communication and coordination issue of multiple mobile manipulator systems.

With all the developed theory and technology, the mobile manipulator system has debut in the laboratory and then later come to the battle field and daily life. The PackBot EOD, developed by iRobot Corporation, can be rapidly deployed as mobile bomb disposal. The weight of this kind of robot is less than 24 kilograms fully loaded, and can be hand carried and deployed by a single operator. This mobile manipulator, shown in Figure 9 (a) has been widely used in Iraq battle field. Researchers from University of Massachusetts Amherst constructed a mobile manipulator hardware platform with redundant kinematic degrees of freedom, a comprehensive sensor suite, and significant end-effector capabilities for manipulation. UMan, the UMass Mobile Manipulator can be seen in Figure 9 (b).

(a)

(b)

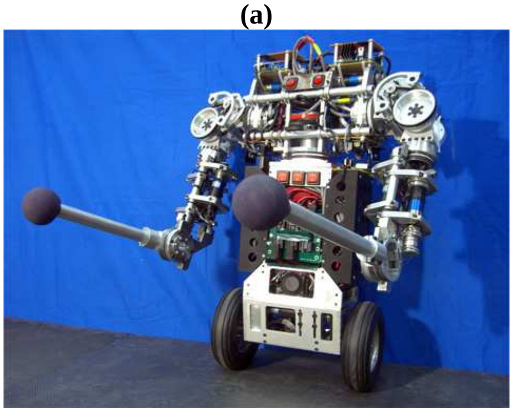

(c)

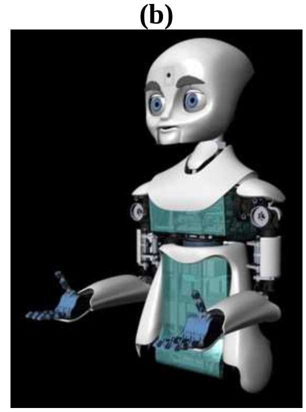

(d)

Figure 9: Some mobile manipulator prototypes

The uBot-4, shown in Figure 9 (c), is a two-wheeled dynamically stable bimanual mobile manipulator. It was designed to combine manipulation and mobility into a small and cost effective, yet very capable platform. It has been used to study a number of different robotic manipulation tasks including pushing, pulling, digging, grasping, single robot transport, and cooperative transport (using multiple copies of the platform).

MIT Media Lab is developing a team of 4 small mobile humanoid robots basing on the UMass mobile base. The purpose of this platform is to support research and education goals in human-robot interaction, teaming, and social learning. We can make the analogy between human and mobile manipulator, in the sense that human feet can be considered as mobile base and human arm can be considered as mounted manipulator, and human can be modeled as redundant spatial mobile manipulator to some degree. So it is not amazing to see that some researchers of mobile manipulators are also focusing on the study of humanoid robot.

(a) (b)

Figure 10: Cooperative mobile manipulators

In parallel with the development of mobile manipulators, some researchers have begun to take advantage of the cooperative manipulation ability of mobile manipulators. As seen in Figure 10, a group of research scientists at Stanford University leading by

Oussama Khatib have built up spatial wheeled mobile manipulator (for short, we will note this as WMM) with holonomic motion base. The end-effector of these developed WMMs has compliant motion capability to work with human in a safety guaranteed environment. NASA is also a pioneer in WMM development, and two WMMs SRR and SRR2K acting as the Robot Work Crew can cooperatively transport an extended beam (2.5 meters long) in a sandy soil terrain with an average slope of 9-degrees. The cooperative WMMs in this thesis are substantially different from the prior work and would be detailed below.

1.3 Problem Statement and Our System

Cooperation is one of the key desirable characteristics of next generation robotic systems. Though much research effort is devoted to this area, less attention is paid to physically interconnected robotic systems which have many applications that make it of particular interest for study. Object transport and manipulation by cooperative multi-robot systems, like multiple planetary rovers [4] and human-supervised multiple mobile robots [5], is proved to be an effective way to handle complex and heavy payloads in unknown and dynamic environments.

The goal of our research is to propose a motion/force control law for payload transport by multiple nonholonomic wheeled mobile manipulators. A decentralized structure is preferable for scalability and implementation. In the very practical scenario, it is desirable for the mobile agents to be imposed with avoidance collision capability.

For our system, we consider multiple wheeled mobile robots operating cooperatively on a common payload. The robots we consider consist of a two-wheel differentially driven mobile base with a two revolute manipulator mounted on top of the base. Figure

11 depicts two of these robots operating on a common payload.

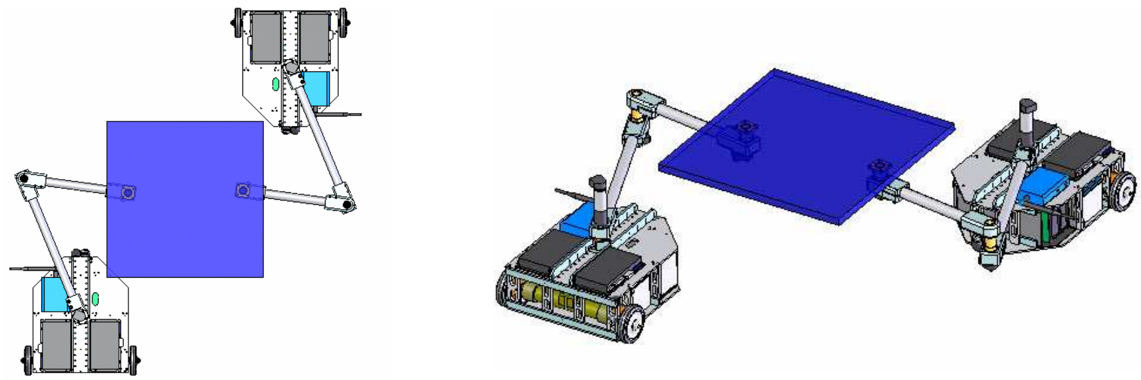

(a) (b)

Figure 11: Wheeled mobile manipulator collective with payload: (a) Top view, (b) Side view.

1.4 Literature Survey

1.4.1 Cooperative Articulated Mechanical Systems

Deploying multiple robots to cooperatively manipulate common payload creates redundancy, the resolution of which has posed longstanding yet vital challenge to the robotics community. Examples of cooperative multi-robot systems, ranging from multiple mobile robots [1], multi-fingered hands [6], and multi-legged vehicles [7] have been extensively studied in a variety of contexts. Early literature in this field addressed redundancy resolution in cooperating system from a centralized perspective, i.e., all the measurements and control signals are generated from a central point.

Under the assumption of perfect knowledge of the system parameters and rigid grasping of the payload, some control approaches have been proposed. Rigid grasping means that there is no relative motion between the payload and the manipulator end-effectors. Arimoto et al. considered the leader-follower scheme in [8] , where one manipulator acts as a leader controlling the motion of the payload, and other manipulators act like a followers. The followers' position is controlled by the motion of the leader in terms of a virtual spring like mechanism to provide certain compliance. Khatib [9] studied the dynamic properties of redundant manipulators and proposed the augmented object model for multi-arm cooperation. By considering the parameter uncertainty in the grasp system, dynamic parameters estimation by least square method is studied in [10] with an adaptive control law for the motion/force control.

In a later stage, researchers realized the vulnerability of centralized controller which limits the performance when robot numbers increase. The decentralized version of leader-follower algorithm is proposed in [11]. Motion/force control of two robots handling a common payload is implemented therein, and one of the robots is designated as leader with position control while the other robot is guided as a follower with desired impedance control. The general multiple manipulation case in [12] presented the concept of virtual leader, where each individual follower would perceive the rest of the system as a virtual leader. Later, Liu and Arimoto [13] addressed the adaptive control problem of multiple redundant manipulators cooperatively handling an object in a decentralized manner while optimizing a performance index. Szewczyk et al. [14] presented a distributed impedance approach for multiple robot system control which is scalable with increased robot modules. More recently, the nominal exponential stability of collaborative load transport by multiple robots is proved by Montemayor and Wen [15].

1.4.2 Cooperative System of Mobile Manipulators

Interest has grown in mobile manipulation to achieve cooperative payload manipulation since the workspace is significantly increased. Again, while the early work mainly focused on a centralized way, such as Desai et al. [16] studied optimal motion planning for nonholonomic cooperating mobile manipulators grasping and transporting objects and Tanner et al. [17] presented a motion planning methodology for articulated, nonholonomic robots with guaranteed collision avoidance. But decentralized approaches appear to show the greater potential for scalability since a centralized architecture is not capable of handling increased number of modules. Hirata et al. [18, 19] presented the extension of their previous 2D case work in [20]. The load is manipulated without accurately knowing the geometric relationship among the robots when using a virtual 3-D caster in a leader-follower coordination scheme. This algorithm is basically a coordination method and controls the position of the followers, and the internal force regulation is not considered therein. While early efforts deal with holonomic mobile bases [21, 22], the attention to nonholonomic chained form system permits the ability to deploy on real world vehicles. In forming such composite systems, it is important to first ensure capability of various kinematic constraints, both at individual module and system level. Bhatt et al. [23] established a systematic framework for formulation and evaluation of system-level performance on the basis of the individual-module characteristics and affiliated kinematic constraints. A kinematically compatible framework for cooperative payload transport by nonholonomic mobile manipulators is proposed by Abou-Samah et al. [24]. Having satisfied kinematic capability, there exits the potential to further optimize the performances by taking into account of dynamic consideration, such as interaction forces on actuation level. To facilitate the maintenance of holonomic and nonholonomic constraints within the system, dynamic controller could achieve better physical performance and improvement in the actuation input profiles.

1.5 Research Issues

While some researchers have attempted to investigate some kinds of mobile manipulation schemes, in this thesis we will specifically focus on the use of nonholonomic wheeled mobile manipulators for cooperative payload transport in a decentralized manner, in addition to this, one pertinent problem is formation control and obstacle avoidance for multi-agent nonholonomic systems. On this basis, this thesis can be separated into two parts. In the first part, we will look at how to achieve decentralized dynamic motion/force control of NH-WMM cooperative manipulation, while the second part would consider the incorporation of formation control within obstacle avoidance framework for multiple nonholonomic mobile robot motion planning. Three principal research questions may be posed and the intimate coupling between these two parts is illustrated in the posing of these questions.

Research Question 1: What kind of control structure is more suitable for use in multi-robotic systems?

> As noted at the beginning of this section, a decentralized control structure is usually superior to its centralized counterpart. But how to "divide" the how complex system into "pieces" and control them individually is not a trivial task.

Research Question 2: How to resolve the various kinematic constraints (holonomic and nonholonomic) and deal with them in the control algorithm? How to resolve the multiple levels of redundancies in the modular level which manifests as dynamic actuation redundancy and in the system level which manifests as grasp force *regulation?*

The entailed research challenges with respect to this question come from two aspects. First, the disk-like wheeled mobile bases are subjected to nonholonomic constraints, and it is well identified by Brockett [25] that nonholonomic systems as a class of systems that cannot be stabilized via smooth time-invariant state feedback law. This implies that motion planning and control of such systems deserves more special treatment. Secondly, the increased workspaces, mobility and manipulability could be obtained in the cost of considerable redundancy which needs to be suitably resolved in a dynamic level. With this system structure, it is worthy to note that three levels of redundancy come into it. First, when given a starting point and destination point, the nonholonomic motion planning should be used to solve the indeterminacy. In addition, for individual agent, the mobile manipulator is kinematically redundant in the sense that the surplus of articulated degrees of freedoms than the required tasks, and also dynamically redundant because of the surplus of actuation than the control outputs. The end-effector motion could be decomposed into displacements of the joints of the manipulator and rotations of the wheels of the mobile base. Finally, the payload transport is a planar version of grasp problem, the force distribution and internal force control should be well resolved in an optimized fashion. After designing a suitable motion/force controller for the collective, the third research issue immediately becomes obvious:

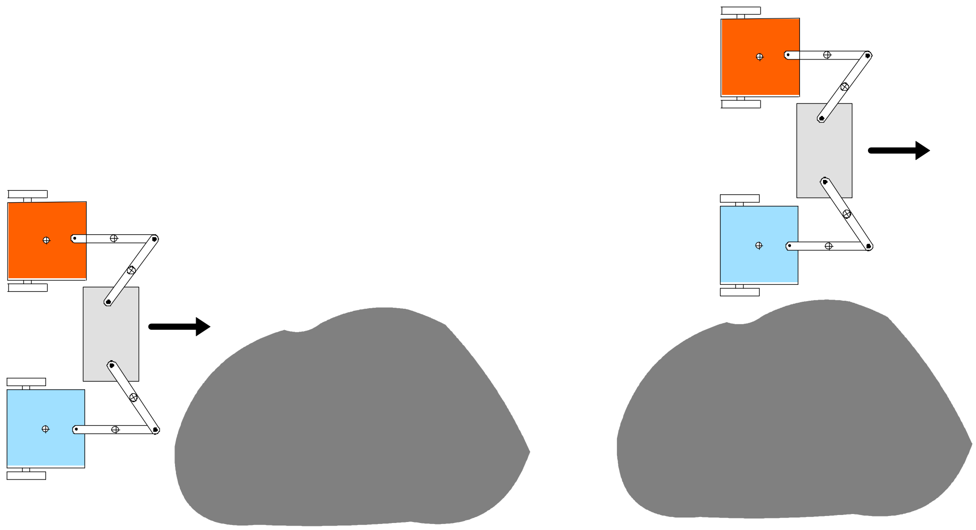

Figure 12: Wheeled mobile manipulator collective with payload makes an ideal paralel parking manuver

Research Question 3: Which kind of formation control algorithm would be in accordance with the previous developed decentralized motion/force control law? How to incorporate obstacle avoidance within all of these control frameworks?

As observed in question 2, for nonholonomic motion planning, even if this trajectory is *a priori* specified, it may have to be modified to avoid obstacles as shown in Figure 12. On a higher level, we notice that the formation control is of a paramount significance for many engineering and military task. A resolution of these pertinent problems is indispensable for a diverse array of applications.

All the above mentioned challenges can be seen in Figure 13 where a hierarchical structure of control problems is illustrated.

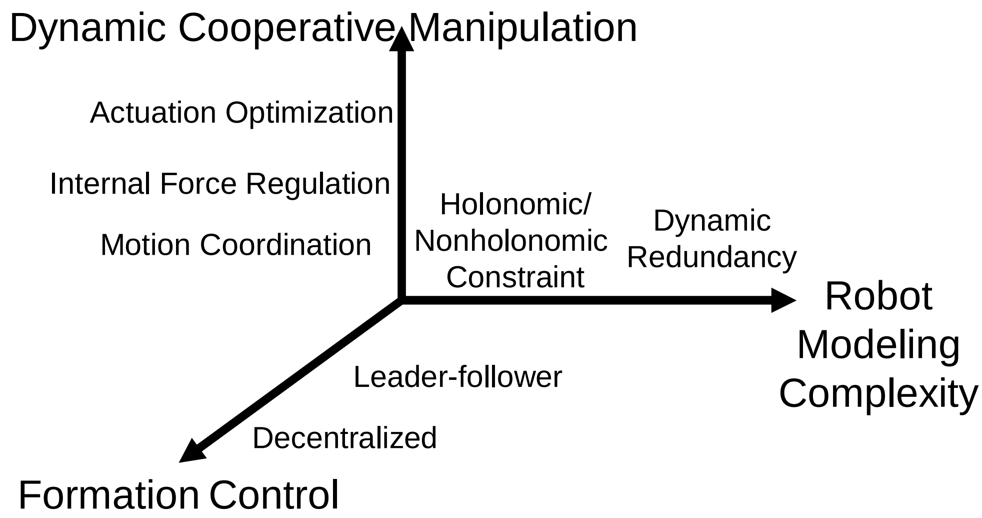

Figure 13: Difficulties of payload transport with NH-WMM

1.6 Thesis Organization

The remainder of this thesis is organized as follows:

Chapter 2 provides an overview of a variety of preliminary knowledge on modeling and control of constrained mechanical systems. Some detailed background theory includes operational space dynamics and control, constrained Lagrange dynamics.

Since the focus of this thesis is on force control of manipulators, we will introduce and categorize some popular force control schemes developed since three decades ago in Chapter 3. We will also highlight the benefits and limitations of some approaches and show some empirical and visionary perspective basing on the existing experiment results and some related literature.

Chapter 4 focuses on the modeling and control of WMMs. We begin by investigating the kinematic and dynamic model of WMR since it's a sub-system of WMM and many similar problems of WMMs would be encountered therein, like nonholonomic motion planning, kinematic and dynamic motion control of nonholonomic systems. Then the similar analysis would be performed in the WMM system with a focus on task space consistent dynamic control method. As a main body of this thesis, the multiple grasp modeling would be investigated therein and the decentralized control of WMM collectives would be presented in this chapter.

To further the theoretical study of WMM control, the formation control of a group of WMMs would be presented in Chapter 5. The mobile robot formation problem is investigated first for a basic study, and this problem is split into trajectory tracking and static obstacle avoidance, formation control and cooperative obstacle avoidance. All of these results are generalized to mobile manipulator cases.

Chapter 6 presents simulation results for various interesting cases studies using the dynamic equation formulated in Chapter 3. In particular, the first two case studies were performed for the dynamic payload transport scenario. The subsequent two cases were targeted at mobile manipulator collective formation control.

Chapter 7 introduces the experimental setup and verification procedure. This chapter presented a detailed hardware and software setup basing on the ATI force/torque sensor, xPC Target and PC/104 platform. A force sensor calibration and manipulator torque calibration method is proposed therein.

Chapter 8 summarizes the contributions in this work, and concludes with providing suggestions for future research.

2 Background

2.1 The Operational Space Dynamics Formulation

2.1.1 Manipulator Dynamics with Environment Interaction

Before analyzing the dynamic behavior of multiple manipulators, it is necessary to examine the dynamics of individual module with n degree of freedoms. The dynamics of an open chain manipulator can be described in the joint space as

$$M(\underline{q})\underline{\ddot{q}} + \underline{C}(\underline{q},\underline{\dot{q}}) + \underline{G}(\underline{q}) = \underline{\tau} \qquad [2.1]$$

where $\underline{q} \in \mathbb{R}^n$ is the full set of generalized coordinates, $M(\underline{q}) \in \mathbb{R}^{n\times n}$ is the inertia matrix expressed in terms of the extended coordinate set, $\underline{C}(\underline{q},\underline{\dot{q}}) \in \mathbb{R}^n$ denotes the Coriolis, centrifugal forces, and $\underline{G}(\underline{q}) \in \mathbb{R}^n$ denotes the gravity force. $\underline{\tau} \in \mathbb{R}^n$ is the generalized control torque.

The forward kinemics of the manipulator with respect to the end-effector position and orientation, is given by

$$\underline{x} = \underline{\phi}(\underline{q}) \qquad [2.2]$$

Differentiating the above equation, we can get the mapping between joint space velocity and end-effector velocity by

$$\underline{\dot{x}} = J(\underline{q})\underline{\dot{q}} \qquad [2.3]$$

where $J(\underline{q})$ is the manipulator's Jacobian matrix.

When the manipulator end-effector is in contact with the environment, the constrained dynamic equation of motion would become

$$M(\underline{q})\underline{\ddot{q}} + \underline{C}(\underline{q},\underline{\dot{q}}) + \underline{G}(\underline{q}) + J^T(\underline{q})\underline{F_c} = \underline{\tau} \qquad [2.4]$$

where F_c is the contact forces at the end-effector.

For redundant manipulators that not in static equilibrium, the mapping from the task space forces to the joint space forces is surjective. The null space joint torque would not affect the resulting forces at the end-effector, and the relationship between task space forces and joint space forces is characterized by

$$\underline{\tau} = J^T(\underline{q})\underline{F} + (I - J^T(\underline{q})J^{T\#}(\underline{q}))\underline{\tau}_0 \qquad [2.5]$$

where I is the $n \times n$ identity matrix, $J^{\#}$ is the generalized inverse of J, and $\underline{\tau}_0$ is an arbitrary generalized joint torques which is projected to the null space of $J^{T\#}$.

To establish the operational space dynamics, we first use the relationship between task space acceleration and joint space acceleration $\underline{\ddot{x}} = J(\underline{q})\underline{\ddot{q}} + \dot{J}(\underline{q})\underline{\dot{q}}$, which is obtained by differentiating $\underline{\dot{x}} = J(\underline{q})\underline{\dot{q}}$. Then we multiply the first equation by the matrix $J(\underline{q})M(q)^{-1}$ and use the acceleration relationship

$$\begin{gathered}\underline{\ddot{x}} + (J(\underline{q})M^{-1}(\underline{q})C(\underline{q},\underline{\dot{q}}) - \dot{J}(\underline{q})\underline{\dot{q}}) + J(\underline{q})M^{-1}(\underline{q})G(\underline{q}) + J(\underline{q})M^{-1}(\underline{q})J^T(\underline{q})\underline{F}_c = \\ (J(\underline{q})M^{-1}(\underline{q})J^T(\underline{q}))\underline{F} + J(\underline{q})M^{-1}(\underline{q})(I - J^T(\underline{q})J^{T\#}(\underline{q}))\underline{\tau}_0\end{gathered} \qquad [2.6]$$

The inverse of the matrix that multiplies $\underline{F}$ is defined as the task space inertia matrix $H(\underline{q}) = (J(\underline{q})M^{-1}(\underline{q})J^T(\underline{q}))^{-1}$. To make the task space acceleration is not affected by $\underline{\tau}_0$, we can set the term involving $\underline{\tau}_0$ zero, and this results to

$$J(\underline{q})M^{-1}(\underline{q})(I - J^T(\underline{q})J^{T\#}(\underline{q}))\underline{\tau}_0 = \underline{0} \qquad [2.7]$$

The joint space inertia weighted generalized inverse of $J(\underline{q})$, defined by $\overline{J}(\underline{q}) = M^{-1}(\underline{q})J^T(\underline{q})(J(\underline{q})M^{-1}(\underline{q})J^T(\underline{q}))^{-1}$, and is the unique dynamically consistent generalized inverse which guarantees the above equation holds.

With this dynamically consistent generalized inverse, it can be shown that the dynamics of the end-effector can be obtained by projecting the joint space dynamics into an operational space specified as the end-effector space. This yield

$$H(\underline{q})\ddot{\underline{x}} + \underline{B}(\underline{q}, \dot{\underline{q}}) + \underline{P}(\underline{q}) + \underline{F}_c = \underline{F} \qquad [2.8]$$

where $B(\underline{q}, \dot{\underline{q}}) = \overline{J}^T(\underline{q})C(\underline{q}, \dot{\underline{q}}) - H(\underline{q})\dot{J}(\underline{q})\dot{q}$ and $P(\underline{q}) = \overline{J}^T(\underline{q})G(\underline{q})$.

2.1.2 Task/Null Space Decoupled Control

Any manipulator dynamic equation described in joint space, like Equation[2.9], can always be transformed into the operational space, and motion control can be implemented thereafter basing on the task/null space decoupling. The generalized torque/force relationship provides the decomposition of the total control torque in Equation [2.10] into two parts of dynamically decoupled control torque: the one corresponding to the task behavior and the one that only affects the configuration space behaviors [25, 26]:

$$\underline{\tau} = \underline{\tau}_{task} + \underline{\tau}_{config} \qquad [2.11]$$

Or the above equation can be explicitly written as

$$\underline{\tau} = J^T(\underline{q})\underline{F} + N^T\underline{\tau}_0 \qquad [2.12]$$

where $N^T = (I - J^T(\underline{q})\overline{J}^T(\underline{q}))$.

The dynamically consistent inverse is a generalized inverse that when task space d.o.f is smaller than the configuration space d.o.f., i.e. an underconstrained case. The dynamically consistent inverse is weighted by the joint space inertia matrix. It is important to note that the task space force and the null space force are "orthogonal", which means that the null space torque would not generated motion in the task space. To see this point, we calculate (from now on, we would not show the parameter dependence in the parenthesis for simplicity reason)

$$(J^T \underline{F})^T (N^T \underline{\tau}_0) = \underline{F}^T J (I - J^T \overline{J}^T) \underline{\tau}_0 \qquad [2.13]$$

Using the symmetry of $I - J^T \overline{J}^T$, Eqn [2.13] can be rewritten as

$$(J^T \underline{F})^T (N^T \underline{\tau}_0) = \underline{F}^T J (I - J\overline{J}) \underline{\tau}_0 \qquad [2.14]$$

Noting that $J(I - J\overline{J}) = \underline{0}$, Eqn [2.14] would show the "orthogonality" between task space force and the null space force.

The task space control force, can be selected to provide a decoupled control structure by choosing

$$\underline{F} = \tilde{H} f^* + \tilde{\underline{B}} + \tilde{\underline{P}} + \tilde{\underline{F}}_c$$

where the symbol $\tilde{*}$ denotes the estimation of the quantities. Khatib proposed a generalized selection matrix as presented in [26]. The force selection matrix is denoted as Ω_f to get the force controlled direction signal, whereas Ω_m is used to denote the motion control direction. The sub-control force is designed as

$$f^* = \Omega_m f_m^* + \Omega_f f_f^* \qquad [2.15]$$

With appropriate selection matrix, the resulting dynamics would become

$$\ddot{x}_m = f_m^* \qquad [2.16]$$

$$\ddot{x}_f = f_f^* \qquad [2.17]$$

The motion control input f_m^* can be designed in terms of the linear system pole placement method, while the force control input f_f^* is usually designed based on the relation between motion and contact forces. The overall control framework is shown in Figure 14.

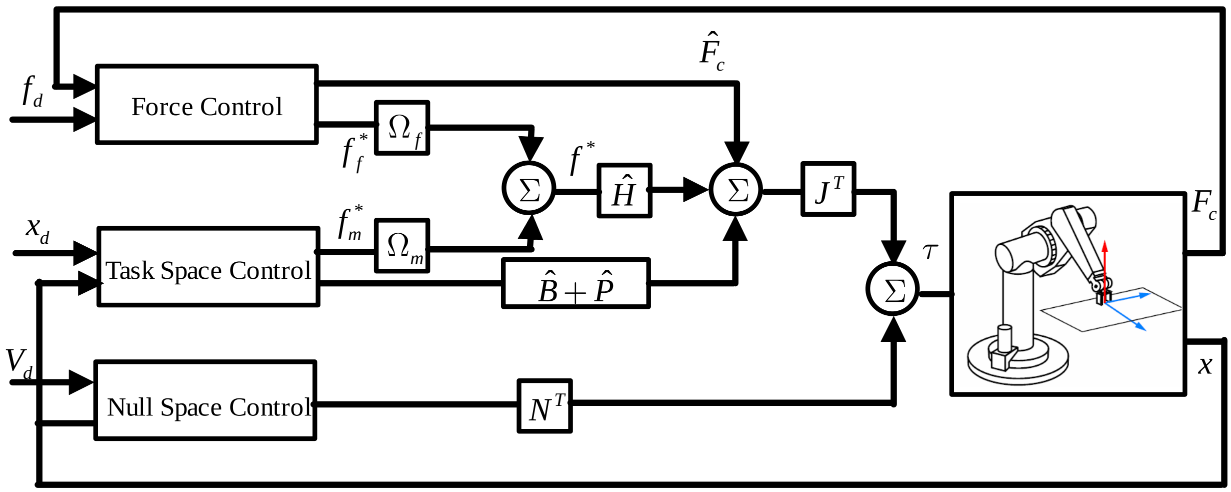

Figure 14: Operational space motion/force control architecture(modified from [26, 27])

2.2 Constrained Lagrange Dynamics

2.2.1 Multiplier Form

De Sapio et al. [28] presented an operational space control approach for the general class of holonomically constrained multibody system. For a more general holonomic constrained mechanical system, the set of m constraint equations can be written as

$$\underline{\phi} = \underline{0} \qquad [2.18]$$

The configuration space is constrained on a $c = n - m$ dimensional manifold Q^c. By taking the gradient of the constraint function, we get the constraint matrix

$$A = \frac{\partial \underline{\phi}}{\partial \underline{q}} \qquad [2.19]$$

The constrained dynamic equation can be modified in terms of [2.4] as

$$M\ddot{\underline{q}} + \underline{C} + \underline{G} = \underline{\tau} + \underline{\tau}_c \quad [2.20]$$

where $\underline{\tau}_c$ is the generalized constrained forces.

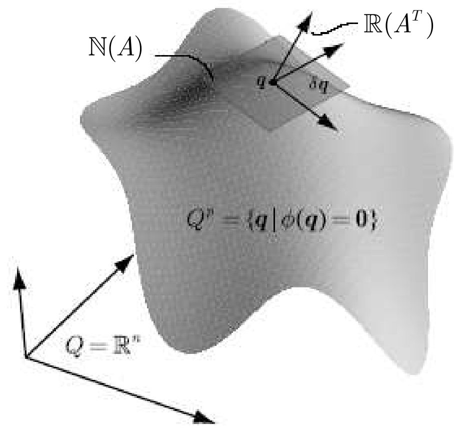

Figure 15: Visualization of constrained space [28]

Since the constraints do no virtual work under virtual displacement that is consistent with the constraint equations, we have $\underline{\tau}_c \perp \delta\underline{q}$ for all $\delta\underline{q} \in \mathbb{N}(A)$. The symbol $\mathbb{N}(A)$ represents the tangent space of the constraint manifold Q^c at some point in the configuration space $Q \in \mathbb{R}^n$. The generalized constraint forces $\underline{\tau}_c$ are orthogonal to the constraint consistent variations $\delta\underline{q}$. This geometric relation is visualized in Figure 15. With these derivations, it is easy to see that

$$\underline{\tau}_c \in \mathbb{N}(A)^{\perp} = \mathbb{R}(A^T) \quad [2.21]$$

So the generalized constraint force can be represented as a linear combination of the columns of A^T, i.e. $\underline{\tau}_c = A^T\underline{\lambda}$, where $\underline{\lambda}$ is an unknown Lagrangian multiplier. Then the dynamic equation of constrained mechanical system can be expressed in the multiplier form as

$$M\ddot{\underline{q}} + \underline{C} + \underline{G} = \underline{\tau} + A^T\underline{\lambda} \quad [2.22]$$

2.2.2 Solution of the Constrained Dynamics Problem

To solve the forward dynamics which is usually used in robotic dynamic simulation, we can assume the Lagrangian multipliers are known, thus the acceleration can be written as

$$\underline{\ddot{q}} = M^{-1}(\underline{\tau} + A^T\underline{\lambda} - \underline{C} - \underline{G}) \qquad [2.23]$$

By differentiating the constraint equation twice, we can get

$$\dot{A}\,\underline{q} + A\,\underline{\ddot{q}} = \underline{0} \qquad [2.24]$$

Thus it is easy to find the explicit form of the Lagrangian multipliers as

$$\underline{\lambda} = (AM^{-1}A^T)^{-1}(-\dot{A}\,\underline{\dot{q}} + AM^{-1}(\underline{C} + \underline{G} - \underline{\tau})) \qquad [2.25]$$

Following the notation in [29], we can rewrite Equation [2.25] as

$$\underline{\lambda} = -\tilde{A}\dot{A}\,\underline{\dot{q}} + M^{-1}P_u(\underline{\tau} - \underline{C} - \underline{G})) \qquad [2.26]$$

where $\tilde{A} = M^{-1}A^T(AM^{-1}A^T)^{-1}$ and $P_u = I - A^T(AM^{-1}A^T)^{-1}AM^{-1}$. The first term represents the accelerations due to constraint forces $-\tilde{A}\dot{A}\,\underline{\dot{q}}$. The projection matrix P_u projects the generalized forces to those that do work on the system, or to say, the forces in the unconstrained directions. Thus, the joint accelerations come from the contribution of $-\tilde{A}\dot{A}\,\underline{\dot{q}}$ and $M^{-1}P_u(\underline{\tau} - \underline{C} - \underline{G}))$ which are in the constrained and unconstrained directions respectively.

2.2.3 Energy Minimization Perspective of Dynamic Consistent Matrix

In the first part of this section, we show the derivation dynamically consistent generalized inverse in the operational space control framework, it is interesting to perceive this mathematical relation from an emery minimization perspective. Recall that the operational space velocity and joint space velocity is related by the Jacobian matrix as

$$\underline{\dot{x}} = J\underline{\dot{q}} \qquad [2.27]$$

We would try to find out a solution of Equation [2.27] which minimizes the kinetic energy of the system

$$T = \frac{1}{2}\underline{\dot{q}}^T M\underline{\dot{q}} \qquad [2.28]$$

The solution of this constrained optimization problem can be found straightforwardly as

$$\underline{\dot{q}} = M^{-1}J^T(JM^{-1}J^T)^{-1}\underline{\dot{x}} \qquad [2.29]$$

Noting that the dynamically consistent matrix is given by

$$\overline{J} = M^{-1}J^T(JM^{-1}J^T)^{-1} \qquad [2.30]$$

We have that $\underline{\dot{q}} = \overline{J}\underline{\dot{x}}$ yields the kinetic energy minimizing the solution of [2.27].

By the same token, we notice that the acceleration relation of operational space and joint space are related by

$$J\underline{\ddot{q}} = \underline{\ddot{x}} - \dot{J}\underline{\dot{q}} \qquad [2.31]$$

We would like to find the solution which minimize the acceleration energy, defined as the joint space inertia mass matrix weighted quadratic form

$$E = \frac{1}{2}\underline{\ddot{q}}^T M\underline{\ddot{q}} \qquad [2.32]$$

This solution is obtained as

$$\underline{\ddot{q}} = M^{-1}J^T(JM^{-1}J^T)^{-1}(\underline{\ddot{x}} - \dot{J}\underline{\dot{q}}) \qquad [2.33]$$

It is just in the form of $\underline{\ddot{q}} = \overline{J}(\underline{\ddot{x}} - \dot{J}\underline{\dot{q}})$ that the acceleration energy minimizing solution of Equation[2.31].

3 Force Control of Manipulators

Motion control is imperative for a variety of robotic tasks, but for the accomplishment of more complex robot tasks, motion/force control is more desirable. For example, one of the most import tasks of mobile robots is localization and mapping, and belongs to the motion control category. But for mobile manipulator systems, the capability of manipulation becomes more crucial with the combination of mounted manipulator and mobile base. With some appropriate control algorithm, it is possible to decouple the manipulator subsystem apart from the mobile manipulator system, and with some further modification, it is possible to apply the force control algorithms of general serial chain manipulators to this new subsystem. To this end, we would take a look at a diverse array of force control approaches developed since 1980s.

When interaction occurs, the dynamic coupling between the end-effector and the environment are becoming important. In a motion and force control scenario, interaction affects the controlled variable, introducing error upon which the controller must act. Even though it is usually possible to get a reasonably accurate dynamic model of the manipulator, the main difficulty comes from the dynamic coupling with the environment, while the later is usually impossible to model or the model is time-varying. A stable manipulator system could usually destabilized by the environment coupling.

A number of control approaches of robot interaction have been developed in the last three decades. The robot compliant motion control can be categorized as the one that performing indirect force control and direct force control. The distinguished difference of these two approaches is that the former achieve force control via motion control without explicit force feedback loop, and the later, instead, can regulate the contact force to a desired value because of the explicit force feedback loop.

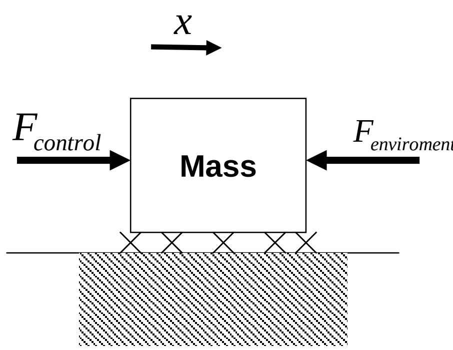

Figure 16: One d.o.f impedance control

To show the challenge force control, we can see a simple example as shown in Figure 18. One rigid mass object is placed on a horizontal friction plane, and the equation of motion of the system is

$$m\ddot{x} + b\dot{x} = F_{control} + F_{enviroment} \quad [3.1]$$

A proportional integral motion controller is applied as

$$F_{control} = K_p(x_d - x) + \frac{K_i}{s}(x_d - x) \quad [3.2]$$

If there is no environmental interaction, that is $F_{enviroment} = 0$, the closed loop system would be

$$\frac{x}{x_d} = \frac{K_p s + K_i}{ms^3 + bs^2 + K_p s + K_i} \quad [3.3]$$

In terms of the Routh-Hurwitz stability criterion, a condition for the motion control system is

$$K_i < \frac{bK_p}{m} \quad [3.4]$$

But when the robot is in interaction with the enrivoment, or simply coupled to a mass $m_{enviroment}$, this condition would become as

$$K_i < \frac{bK_p}{m + m_{enviroment}} \qquad [3.5]$$

When the coupled mass is large enough, this condition would not be satisfied, especially when the environment is a varying system, which is usually not possible for a constant coefficient controller. So a stable isolated controller does not necessarily work in contact, even it is just a simple inertia environment.

3.1 Impedance Control

The indirect force control includes compliance (or stiffness) control and impedance control [30] with the regulation of the relation between position and force (related to the notion of impedance or admittance). The manipulator under impedance control is described by an equivalent mass-spring-damper system with the contact force as input. With the availability of force sensor, the force signal can be used in the control law to achieve linear and decoupled impedance.

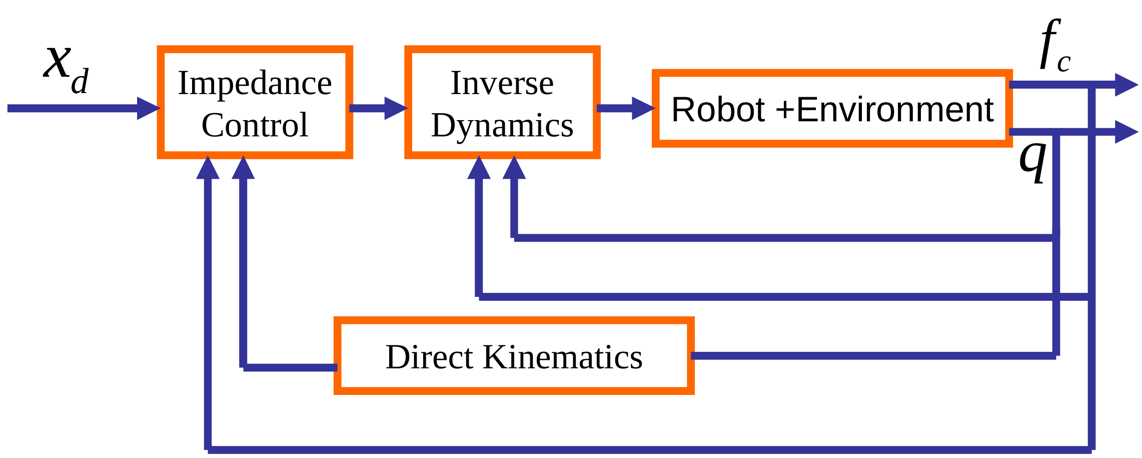

Figure 17: Impedance control diagram

One simple illustrative example (Mark Spong) of impedance control can be seen in a one d.o.f system as shown in Figure 18. One rigid mass object is placed on a horizontal frictionless plane, and the equation of motion of the system is

$$M\ddot{x} = F_{control} + F_{enviroment} \quad [3.6]$$

When the control input is zero, the system is a pure inertia with mass M. If the force control is chosen as $F_{control} = mF_{enviroment}$, the closed loop system is then

$$M\ddot{x} = (m+1)F_{enviroment} \Rightarrow \frac{M}{(m+1)}\ddot{x} = F_{enviroment} \quad [3.7]$$

Hence the object now appears to the environment as a modified inertia with mass $\frac{M}{(m+1)}$. Thus the force feedback has the effect of changing the apparent inertia of the system.

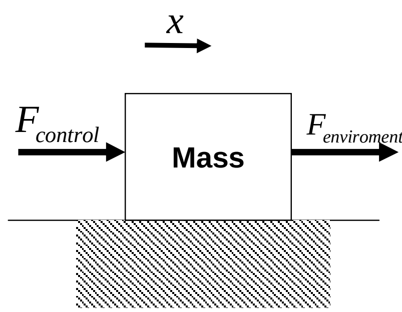

Figure 18: One d.o.f impedance control

Impedance control aims at the realization of a suitable relation between the forces and motion at the point of interaction between the robot and the environment. This relation is posed as impedance, i.e. describes the velocity as a result of imposed force. The actual motion and force is then a result of the imposed impedance, reference signals and the environment admittance (which is the opposite of impedance, i.e. describes the force as a result of imposed velocity). It is found that impedance control is superior over explicit force control methods (including hybrid control) in its stability characteristics and generality, however at the price of accurate force tracking which is better achieved by explicit force control. It is also shown that some particular formulations of hybrid control appear as special cases of impedance control, and hence the impedance control method is selected for further investigation.

As mentioned previously, impedance control is based on the recognition of a two way coupling between manipulator and environment. This coupling may lead to an exchange of energy between the manipulator and the environment, which has to be managed properly. In the following a derivation of the impedance control law will be given, and an attempt to unify impedance control and hybrid control will be given. This will clearly illustrate that impedance control just as well allows a conceptual separation of constrained and unconstrained directions, but within one single control law, and without the stability problems of hybrid control.

The derivation of the standard impedance control law is relatively straightforward, as it is based on the rigid body equations of the robot

$$M\ddot{\underline{q}} + \underline{C} + \underline{G} + J^T \underline{F}_c = \underline{\tau} \qquad [3.8]$$

The goal of impedance control is to transform the robot dynamics by appropriate selection of the actuator torque $\underline{\tau}$, into desired impedance, relating the tip movement to the external forces.

$$\bar{M}\ddot{\underline{x}} + \bar{B}\dot{\underline{x}} + \bar{K}\underline{x} = \underline{F}_e \qquad [3.9]$$

where $\underline{x}$ is the end-effector coordinates in a suitable coordinate frame (usually in Cartesian coordinates). The matrices $\bar{M}$, $\bar{B}$ and $\bar{K}$ are respectively the target mass, damping and spring stiffness, which are chosen by the user. Because of simplicity the target matrices are usually chosen to be constant and diagonal, but the choice is not limited to this.

Recall the task space and joint space mapping

$$\underline{x} = \underline{\phi} \qquad [3.10]$$

$$\dot{\underline{x}} = J\dot{\underline{q}} \qquad [3.11]$$

$$\underline{\ddot{x}} = J\underline{\ddot{q}} + \dot{J}\underline{\dot{q}} \qquad [3.12]$$

In principle the two equations [3.8] and [3.9] have only one unknown: the actuator torque $\underline{\tau}$, which means that one variable, can be eliminated.

The control law that achieve the target impedance is

$$\begin{aligned}\underline{\tau} &= \underline{C} + \underline{G} + J^T \underline{F}_c + \\ &MJ^{-1}\bar{M}^{-1}(F_c - \bar{M}\dot{J}\underline{\dot{q}} - \bar{B}J\underline{\dot{q}} - \bar{K}\underline{x})\end{aligned} \qquad [3.13]$$

The first line of Equation [3.13] eliminates the existing rigid body dynamics, while the second line inserts the target impedance.

3.2 Hybrid Motion/Force Control

If a detailed model of the environment is available, like the geometry, a widely adopted strategy is the hybrid motion/force control, which is aimed at explicit position control in the unconstrained task direction and force control in the constrained task direction. Usually, a selection matrix is used to filter the direction of position or force that to be controlled.

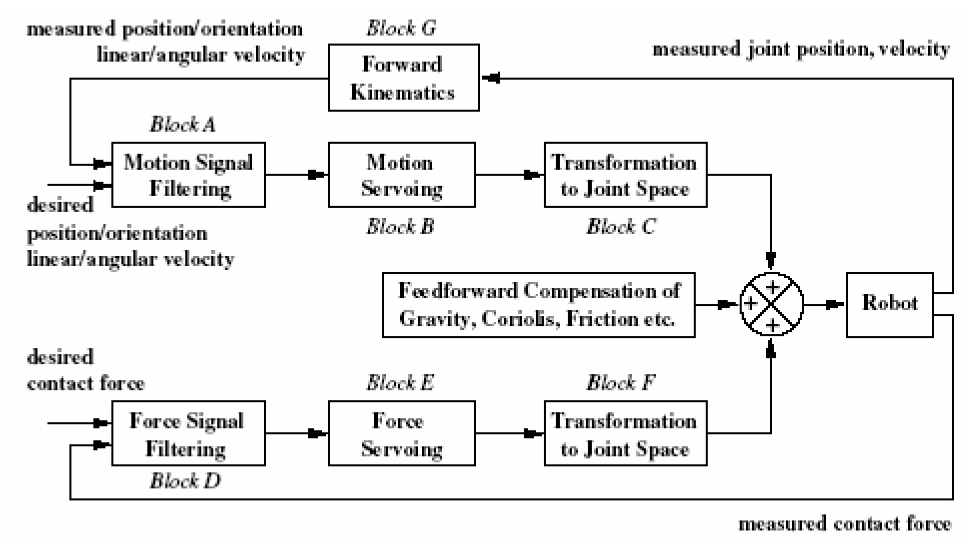

Figure 19: A generic structure of hybrid force control [31]

Figure 19 illustrates the generic structure for most of the existing hybrid motion/force control schemes, which are further roughly divided into four categories as shown in [31]: joint space servoing without inverse dynamics, operational space servoing without inverse dynamics, operational space servoing with inverse dynamics and constraint space servoing with inverse dynamics.

. In [32], Raibert and Craig presented the theory, simulation and experiments of hybrid position force control, and the control diagram can be seen in Figure 20. The most important characteristic of all hybrid control methods is the complete separation of the tasks space into two orthogonal subspaces. The constraint surfaces can be quite complex, such as in case of turning a crank or inserting a screw, or simple as in case of motion along a plane surface.

The geometric constraint can be expressed by a compliance selection matrix *S*, which is generally a diagonal matrix with zeros and ones on the diagonal. A one corresponds to a position controlled direction, a zero to a force controlled direction. The combination of position control and force control is then simply an addition of the two controller parts.

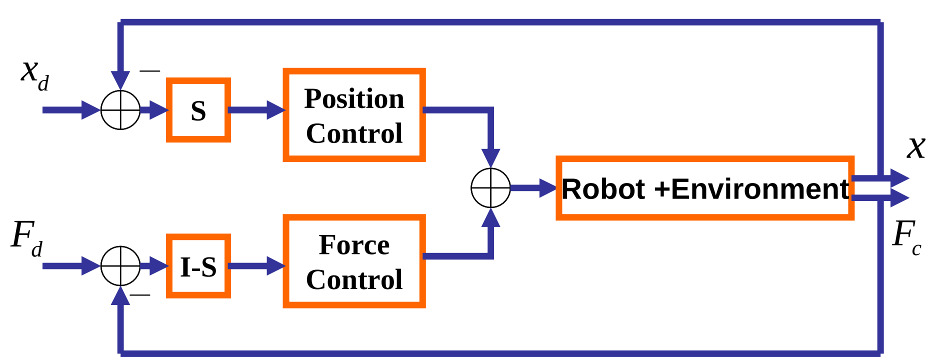

Figure 20: Original structure of hybrid force control

$$\tau = \tau_p + \tau_f \qquad [3.14]$$

where τ_p and τ_f are suitable control torques for position and force control respectively. In the original formulation by Raibert and Craig, the position control law was chosen to be a PID type controller:

$$\tau_p = K_{pp}e_q + K_{pi}\int e_q dt + K_{pd}\dot{e}_q \tag{3.15}$$

While the force control law was chosen as a saturation type PI controller:

$$\tau_f = \tau_{ff} + K_{fp}\tau_e + K_{fi}\int \tau_e^{'} dt \tag{3.16}$$

The definition of the variables follows from Figure 20. It is well known that in case of revolute joints this scheme may suffer from kinematic instability as recognized by An and Hollerbach [33]. A well known disadvantage of this method is the possibility of the possibility of kinematic instability, and several remedies have been proposed. Due to the separation into a position controlled loop and force controlled loop the same control laws as in case of respectively pure position control and explicit force control method can be applied.

Another formulation of hybrid position-force control is the operational space formulation by Khatib as showed in Chapter 2. Now that hybrid motion/force control has been presented, the explicit control of force should be considered.

$$\ddot{x}_f = f_f^* \tag{3.17}$$

The main difficulty of the force control is because of the explicit force control loop. A significant amount of literature is targeted at resolving this problem, but it is still not fully addressed. Many proposed explicit force controllers are modified versions of the PID control law. The most commonly applied method is damped proportional force control with force feed-forward:

$$f_f^* = F_d + K_f(F_d - F) - K_v\dot{x} \qquad [3.18]$$

which is also applied in a similar fashion in the operational space formulation as presented above. Another popular approach is damped integral force control:

$$f_f^* = K_{fi}\int(F_d - F)dt - K_v\dot{x} \qquad [3.19]$$

Finally, an often proposed method is PD or lead control:

$$f_f^* = F_d + (K_{fp} + K_{fd}\frac{sa}{s+a})(F_d - F) \qquad [3.20]$$

where s is the Laplacian operator. Experiments and theoretical analyses have shown that all of the above methods may suffer from inadequate performance or even instability, such that it is important to consider this problem.

4 Dynamics and Control of Mobile Manipulator Collectives

4.1 Mobile Robot Kinematics and Dynamics

4.1.1 Mobile Robot Kinematics

Wheeled mobile robot (WMR) can be categorized into two basic types as holonomic and nonholonomic mechanical systems in terms of the kinematic constraints. Holonomic constraints on the configuration-space of the system can be expressed in terms of algebraic equations which can be written in the form of:

$$\Phi(\underline{q}) = 0 \qquad [4.1]$$

where $\underline{q}$ is the vector of generalized coordinates that describes the configuration of the system. Nonholonomic constraint is the one that cannot be expressed with purely configuration variables in the form of

$$\Phi(\underline{q}, \underline{\dot{q}}) = 0 \qquad [4.2]$$

Mechanical systems that contain nonholonomic constraints can be reformulated in the Pfaffian form:

$$A\left(\underline{q}\right)\underline{\dot{q}} = 0 \qquad [4.3]$$

where *A* is the constraint matrix and is a function of only $\underline{q}$. For example a rolling wheel possesses a holonomic constraint in the rolling direction and a non-holonomic constraint perpendicular to this.

Specifically, no motion velocity restriction is imposed on holonomic WMR, and holonomic WMR possesses maximal number of degree of freedoms (as in the planar, it is

3). A diverse variety of mechanisms are employed as universal wheels, omni-directional wheels, orthogonal or ball wheels to implement a holonomic motion. The distinct feature of holonomic WMR is that it permits easier motion planning comparing with their nonholonomic counterparts. Figure 21 shows a powered caster version of holonomic WMR.

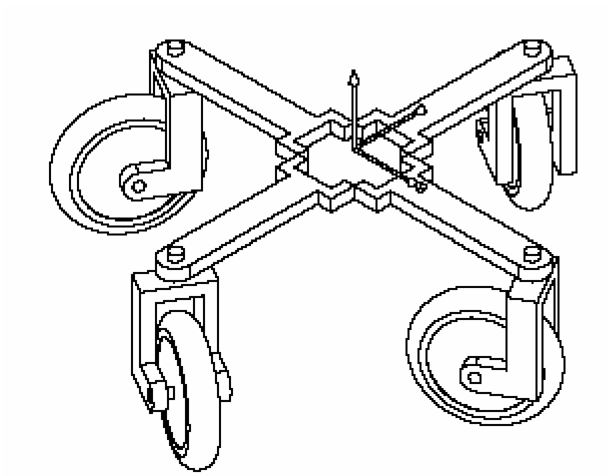

Figure 21: A holonomic mobile robot prototype [34]

Nonholonomic WMRs possess less than 3 degree of freedoms (d.o.f). They are simpler in construction and thus cheaper with less controllable axes and ensure the necessary mobility in plane. Over the millennia, the "wheeled platform design" with multiple sets of disc wheels attached to a common chassis has stayed popular for many reasons. Most importantly, the disk-wheel based design allows for sturdy and robust design implementation. While the mobility, steerability, and controllability of the overall wheeled system depend largely upon the type, nature and locations of the attached wheels, this is a reasonably well understood. See [35, 36] for a survey of some of the different design configurations possible for wheeled bases, for operation on planar terrain.

In this section, we develop the kinematic model and the terminology for the WMR and the WMM that will be used in subsequent dynamic analysis. First, we consider the WMR alone and its nonholonomic constraints. Then we consider the addition of the manipulator and develop all necessary kinematic relationships. Finally, we assemble the constraint matrix, the nullspace matrix, and construct a Jacobian matrix which relates the task-space to the joint space.

The WMR in our research is composed of three distinct rigid bodies: mobile base, left and right wheels. A body fixed frame $\{M\}$ attached at the center of mass of the WMR determines the pose with respect to the fixed ground frame $\{F\}$. The mobile base is actuated by two independently driven wheels of radii r located at an equal distance b on either side of the midline. The wheel axes are collinear and are located at a perpendicular distance $d \geq 0$ from the center of mass. The instantaneous WMR configuration can be fully described by the extended set of generalized coordinates:

$$\underline{q}_a = \left[x_c \;\; y_c \;\; \phi \;\; \theta_R \;\; \theta_L \right]$$

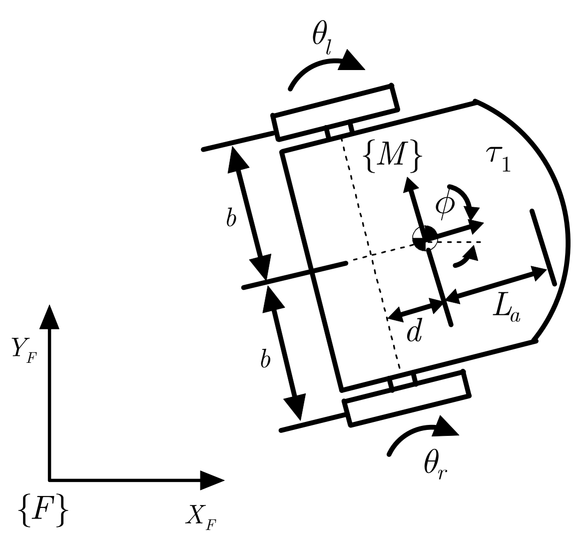

Figure 22: Nonholonomic mobile robot kinematics

where (x_c, y_c) is the Cartesian coordinates of the center of mass, and ϕ is the orientation of the WMR, θ_R and θ_L are the angular positions of the left and right wheels, respectively. For later reference, we note here that the first revolute joint is located at the look-ahead point which is located at a perpendicular distance L_a.

At the velocity level, the kinematics of the mobile robot can be simply expressed as:

$$\begin{aligned} \dot{x} &= v\cos\phi \\ \dot{y} &= v\sin\phi \\ \dot{\phi} &= \omega \end{aligned} \qquad [4.4]$$

where (x, y) is the Cartesian position of the center of the axle of the robot, ϕ is the orientation of the robot, v and ω are the linear and angular velocities of the robot. In a kinematic control scheme, the linear and angular velocities are used as the input to the system. With the kinematic relation of the mobile platform, the mapping from the wheel angular velocity to the mobile base linear and angular velocities is

$$\begin{bmatrix} v \\ \omega \end{bmatrix} = \begin{bmatrix} \frac{r}{2} & \frac{r}{2} \\ \frac{r}{2b} & -\frac{r}{2b} \end{bmatrix} \begin{bmatrix} \dot{\theta}_R \\ \dot{\theta}_L \end{bmatrix} \qquad [4.5]$$

Similarly, we can find the reverse relation of the two vectors as:

$$\begin{bmatrix} \dot{\theta}_R \\ \dot{\theta}_L \end{bmatrix} = \begin{bmatrix} \frac{1}{r} & \frac{b}{r} \\ \frac{1}{r} & -\frac{b}{r} \end{bmatrix} \begin{bmatrix} v \\ \omega \end{bmatrix} \qquad [4.6]$$

The system is subjected to 3 nonholonomic constraints. The first constraint of the mobile base comes from the nonholonomic behavior of the wheels and restricts the velocity of the WMR in the lateral directions to be zero as

$$-\dot{x}_c \sin\phi + \dot{y}_c \cos\phi - \dot{\phi} d = 0 \qquad [4.7]$$

The other two constraints, relating the base velocities and the wheel velocities, ensure the no-slip condition at each rolling wheel in the forward directions.

$$\dot{x}_c \cos\phi + \dot{y}_c \sin\phi + b\dot{\phi} = r\dot{\theta}_R \qquad [4.8]$$

$$\dot{x}_c \cos\phi + \dot{y}_c \sin\phi - b\dot{\phi} = r\dot{\theta}_L \qquad [4.9]$$

The set of m (=3) constraints can be written in Pfaffian form as:

$$A_a(\underline{q}_a)\underline{\dot{q}}_a = \underline{0} \text{ and } A_a(\underline{q}_a) = \begin{bmatrix} -S_\phi & C_\phi & -d & 0 & 0 \\ -C_\phi & -S_\phi & -b & r & 0 \\ -C_\phi & -S_\phi & b & 0 & r \end{bmatrix} \qquad [4.10]$$

where $S_\phi = \sin\phi$ and $C_\phi = \cos\phi$. By taking the independent joint velocities of $\underline{\dot{z}}_a = \begin{bmatrix} \dot{\theta}_R & \dot{\theta}_L \end{bmatrix}^T$, the corresponding null-space matrix that annihilates the constraint matrix can be determined as:

$$\underline{\dot{q}}_a = S_a \underline{\dot{z}}_a \text{ and } S_a = \begin{bmatrix} c\left(bC_\phi - dS_\phi\right) & c\left(bC_\phi + dS_\phi\right) \\ c\left(bS_\phi + dC_\phi\right) & c\left(bS_\phi - dC_\phi\right) \\ c & -c \\ 1 & 0 \\ 0 & 1 \end{bmatrix} \qquad [4.11]$$

where $c = \dfrac{r}{2b}$. We define a look-ahead point P_a with Cartesian coordinates of $\underline{x}_a = (x_a, y_a)$, and

$$\begin{aligned} x_a &= x_c + L_a C_\phi \\ y_a &= y_c + L_a S_\phi \end{aligned} \qquad [4.12]$$

where L_a is the distance from the center of mass to P_a. The corresponding Jacobian that relates independent joint velocities to velocity of the look-ahead point can be determined as:

$$\underline{\dot{x}}_a = J_a S_a \underline{\dot{z}}_a = \Phi \underline{\dot{z}}_a \quad \text{and} \quad J_a = \begin{bmatrix} 1 & 0 & -L_a \sin\phi & 0 & 0 \\ 0 & 1 & L_a \cos\phi & 0 & 0 \end{bmatrix} \qquad [4.13]$$

where $L_d = d + L_a$. J_a relates the base velocities $\underline{\dot{x}}_a$ to the generalized base velocities $\underline{\dot{q}}_a$.

4.1.2 Mobile Robot Dynamics

The dynamics of a mechanical system can be modeled using a variety of different techniques. For this thesis we will use the energy-based Lagrange method because of its simplicity, as outlined by Angeles [37]. Like other energy-based methods, the Lagrange method only considers external forces acting on the system and neglects all internal forces. Therefore, the resulting equations of motion are greatly simplified and internal forces are already factored out.

The energy-based Lagrange method is based on the principle of virtual work. By accounting for all sources of power entering the system, present in the system, and leaving the system, the equations of motion can be found. Because joint forces internal to the system have no accompanying displacements, they do no work and are therefore not included in the final equations of motion. Angeles [37] has outlined the following systematic method for finding the unconstrained equations of motion.

1. Introduce a set of generalized coordinates $\underline{q} = [q_1, \ldots, q_n]^T$ and their time rates of change $\underline{\dot{q}} = [\dot{q}_1, \ldots, \dot{q}_n]^T$, defining the state of the system.

2. Evaluate $T = T(\underline{q}, \dot{\underline{q}})$, the kinetic energy of the whole system, as the sum of the individual kinetic-energy expressions.

3. Evaluate $V = V(\underline{q})$, the potential energy of the whole system, as the sum of the individual expression, for every element storing potential energy.

4. Evaluate $L \equiv T - V$, the Lagrangian of the whole system: $L = L(\underline{q}, \dot{\underline{q}})$.

5. Evaluate $\Pi = \Pi(\underline{q}, \dot{\underline{q}})$, the power supplied to the system from external sources $(\Pi \geq 0)$. Evaluate its partial derivative $\partial \Pi / \partial \dot{\underline{q}}$.

6. Evaluate $\Delta = \Delta(\underline{q}, \dot{\underline{q}})$, the sum of the dissipation functions of all dissipative elements of the system $(\Delta \geq 0)$, as well as its partial derivative $\partial \Delta / \partial \dot{\underline{q}}$.

7. Write the governing equation using the foregoing partial derivatives:

$$\frac{d}{dt}\left(\frac{\partial L}{\partial \dot{\underline{q}}}\right) - \frac{\partial L}{\partial \underline{q}} = \frac{\partial \Pi}{\partial \dot{\underline{q}}} - \frac{\partial \Delta}{\partial \dot{\underline{q}}}$$

The resulting equations of motion can then be put in the following matrix form:

$$M(\underline{q})\ddot{\underline{q}} + \underline{V}(\underline{q}, \dot{\underline{q}}) = E\underline{\tau} \qquad [4.14]$$

where M is the mass matrix and contains the inertia terms, $\underline{\tau}$ is the input vector, E maps the input, $\underline{\tau}$, to joint-space, and $\underline{V}$ contains all other position and velocity terms.

Constraints can then be added very easily to the unconstrained dynamics to further describe the behavior of the system. These could include any combination of holonomic or nonholonomic constraints. We also note that constraints are the only way to incorporate nonholonomic behavior into the equations of motion. In either case, the constraints will be incorporated on the velocity level in the following standard form:

$$A\left(\underline{q}\right)\dot{\underline{q}} = 0 \qquad [4.15]$$

The constraint forces can then be added to the unconstrained equation of motion[4.14], by

$$M(\underline{q})\underline{\ddot{q}} + V(\underline{q},\underline{\dot{q}}) = E\underline{\tau} - A^T\underline{\lambda} \qquad [4.16]$$

where $\underline{\lambda}$ is the constraint force and A^T maps the constraint force to joint-space.

Specifically, with the help of the null-space matrix, the constrained dynamics of the WMR can be determined as:

$$M_a\left(\underline{q}_a\right)\underline{\dot{q}}_a + \underline{c}_a\left(\underline{q}_a,\underline{\dot{q}}_a\right) = E_a\left(\underline{q}_a\right)\underline{\tau}_a - A_a{}^T\underline{\lambda}_a \qquad [4.17]$$

where $\underline{q}_a$ are the generalized coordinates of the mobile base. M_a is the configuration dependent inertial matrix, $\underline{c}_a$ includes all the Coriolis/centrifugal/damping term, and E_a is the actuation transformation matrix that maps the joint torques to the corresponding independent joint coordinates. $\underline{\lambda}_a$ is the Lagrange multiplier corresponding to the constraints.

4.2 Mobile Manipulator Kinematics and Dynamics

4.2.1 Mobile Manipulator Kinematics

Kinematic analysis, including forward kinematic and inverse kinematics, is the essential basis for dynamitic analysis and control. Particularly, the wheeled locomotion systems possess the nonholonomic characteristics which make the kinematic relation deserving precautious focus and treatment. From the mechanical perspective, a manipulator can be schematically represented as an open kinematic chain of rigid bodies connected by means of (generally revolute or prismatic) joints. The kinematics of a robot manipulator describes the relationship between the motion of the joints of the manipulator and the resulting motion of the rigid bodies which from the robot. Moreover, wheeled systems, because of the rolling contact between the wheel and ground, are subject to nonholonomic constraints. These constraints can be represented at velocity level and thus becomes an essential element of kinematic analysis of a WMM of the type shown in Figure 22.

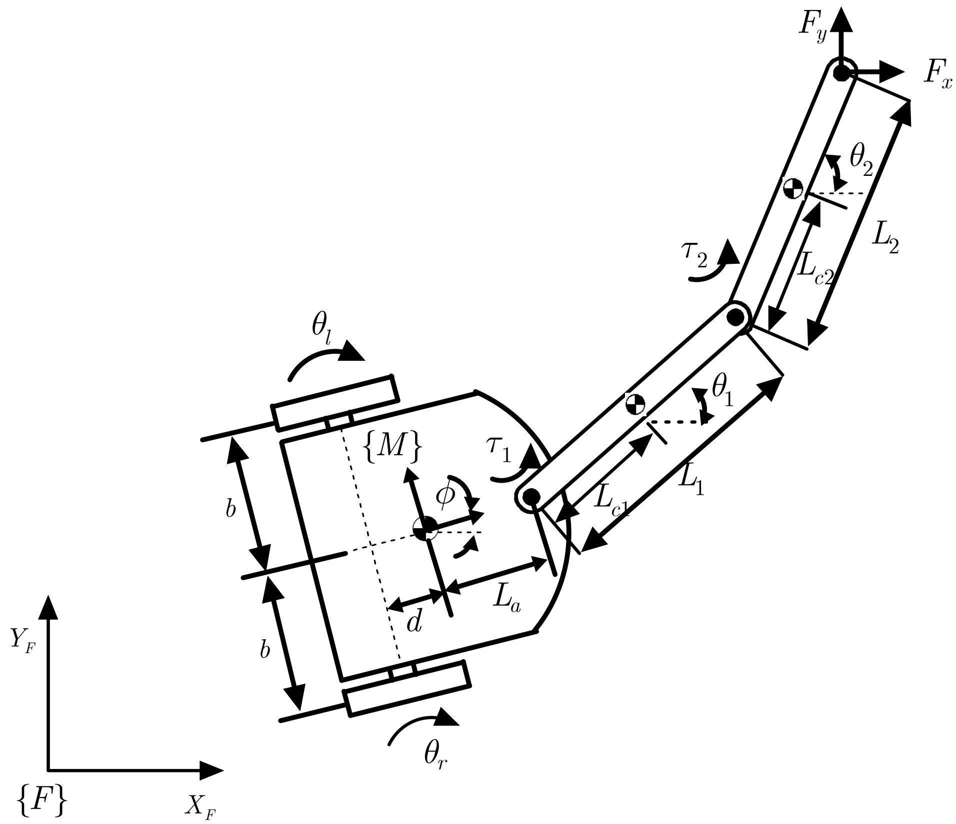

Figure 23: Nomenclature of mobile manipulator kinematics and dynamics

The full configuration of the base of WMM at any time can be fully described by five generalized coordinates. These are the three variables that describe the position and orientation of the platform and two variables that specify the angular positions for the driving wheels.

$$\underline{q}_a = \left[x_c \;\; y_c \;\; \phi \;\; \theta_R \;\; \theta_L \right] \qquad [4.18]$$

The full configuration vector of the WMM can thus by given by augmenting the base configuration vector with the angles θ_1 and θ_2.

$$\underline{q} = \begin{bmatrix} x_c & y_c & \phi & \theta_R & \theta_L & \theta_1 & \theta_2 \end{bmatrix} \qquad [4.19]$$

The detailed derivation of homogeneous transform matrices are referred to the Appendix. Briefly, in terms of the successive homogeneous transform matrices, the position vectors $\underline{r}_{c1}$ and $\underline{r}_{c2}$ are given as

$$\underline{r}_{c1} = \begin{bmatrix} x_c + L_a c_0 + L_{c1} c_{01} & y_c + L_a s_0 + L_{c1} s_{01} \end{bmatrix}^T \qquad [4.20]$$

$$\underline{r}_{c2} = \begin{bmatrix} x_c + L_a c_0 + L_1 c_{01} + L_{c2} c_{012} & y_c + L_a s_0 + L_1 s_{01} + L_{c2} s_{012} \end{bmatrix}^T \qquad [4.21]$$

The position vector of the end-effector $\underline{r}_e$ is given as

$$\underline{r}_e = \begin{bmatrix} r_{xb} + L_a c_0 + L_1 c_{01} + L_2 c_{012} & r_{yb} + L_a s_0 + L_1 s_{01} + L_2 s_{012} \end{bmatrix}^T \qquad [4.22]$$

One can now determine the velocity forward kinematics for each of the different points of interest (for which we developed the position forward kinematics) using the twist-based mathematics. We show the process for one case of the location of joint 1 on the base and present the results for the rest of the cases.

We determine the body fixed twist of the frame using body fixed twist matrix and then extract the twist vector. The velocity of joint 1 expressed in the inertial frame is given as

$$\vec{v}_{0_1} = \begin{bmatrix} \dot{x}_c - L_a s_0 \dot{\phi} & \dot{y}_c + L_a c_0 \dot{\phi} \end{bmatrix}^T \qquad [4.23]$$

Following a similar procedure, we can determine the expressions for velocities of any point of interest. The resulting expressions are given below as

$$\vec{v}_{0_{c1}} = \begin{bmatrix} \dot{x}_c - (L_a s_0 + L_{c1} s_{01})\dot{\phi} - L_{c1} s_{01} \dot{\theta}_1 \\ \dot{y}_c + (L_a c_0 + L_{c1} c_{01})\dot{\phi} + L_{c1} c_{01} \dot{\theta}_1 \end{bmatrix} \qquad [4.24]$$

$$\vec{v}_{0_{c2}} = \begin{bmatrix} \dot{x}_c - (L_a s_0 + L_1 s_{01} + L_{c2} s_{012})\dot{\phi} - (L_1 s_{01} + L_{c2} s_{012})\dot{\theta}_1 - L_{c2} s_{012}\dot{\theta}_2 \\ \dot{y}_c + (L_a c_0 + L_1 c_{01} + L_{c2} c_{012})\dot{\phi} + \left(L_1 c_{01} + L_{c2} c_{012}\right)\dot{\theta}_1 + L_{c2} c_{012}\dot{\theta}_2 \end{bmatrix} \quad [4.25]$$

$$\vec{v}_{0_e} = \begin{bmatrix} \dot{x}_c - (L_a s_0 + L_1 s_{01} + L_2 s_{012})\dot{\phi} - (L_1 s_{01} + L_2 s_{012})\dot{\theta}_1 - L_2 s_{012}\dot{\theta}_2 \\ \dot{y}_c + (L_a c_0 + L_1 c_{01} + L_2 c_{012})\dot{\phi} + \left(L_1 c_{01} + L_2 c_{012}\right)\dot{\theta}_1 + L_2 c_{012}\dot{\theta}_2 \end{bmatrix} \quad [4.26]$$

4.2.2 Mobile Manipulator Dynamics

For the mobile manipulator system, the constraints is of the same as the mobile robot where the set of constraints can be written in Pfaffian form in terms of the configuration space of the mobile manipulator as

$$A\left(\underline{q}\right)\underline{\dot{q}} = 0 \quad [4.27]$$

where $A(\underline{q}) = \begin{bmatrix} -\sin\phi & \cos\phi & -d & 0 & 0 & 0 & 0 \\ -\cos\phi & -\sin\phi & -b & r & 0 & 0 & 0 \\ -\cos\phi & -\sin\phi & b & 0 & r & 0 & 0 \end{bmatrix}$.

Considering the nonholonomic constraints, we can now find an appropriate annihilator matrix that satisfies $AS = 0$. The set of feasible velocities could be parameterized in terms of a suitable vector of $n - m$ independent velocities, $\underline{\dot{z}} = \begin{bmatrix} \dot{\theta}_r & \dot{\theta}_l & \dot{\theta}_1 & \dot{\theta}_2 \end{bmatrix}^T$ as

$$\underline{\dot{q}} = S\underline{\dot{z}} \quad [4.28]$$

where $c = \dfrac{r}{2b}$ and $S = \begin{bmatrix} c\left(b\cos\phi - d\sin\phi\right) & c\left(b\cos\phi + d\sin\phi\right) & 0 & 0 \\ c\left(b\sin\phi + d\cos\phi\right) & c\left(b\sin\phi - d\cos\phi\right) & 0 & 0 \\ c & -c & 0 & 0 \\ 1 & 0 & 0 & 0 \\ 0 & 1 & 0 & 0 \\ 0 & 0 & 1 & 0 \\ 0 & 0 & 0 & 1 \end{bmatrix}$.

If the task space is specified by xy position of the end-effector, the Jacobian that relates the extended joint-rates, $\underline{\dot{q}}$ to the task-space velocity $\underline{\dot{x}}$, as:

$$\underline{\dot{x}} = J_q \underline{\dot{q}} \qquad [4.29]$$

where $J_q = \begin{bmatrix} 1 & 0 & -L_a \sin\phi & 0 & 0 & -L_1 \sin\theta_1 & -L_2 \sin\theta_2 \\ 0 & 1 & L_a \cos\phi & 0 & 0 & L_1 \cos\theta_1 & L_2 \cos\theta_2 \end{bmatrix}$.

In terms of the velocity dependency, we can always get the modified Jacobian with respect to the independent velocities as

$$\underline{\dot{x}} = J_q S \underline{\dot{z}} = J \underline{\dot{z}} \qquad [4.30]$$

For the dynamic modeling, we make the assumption that the interaction forces between the end-effector and the environment are considered to be pure forces (with xy components). Furthermore, it is assumed that no moment is exerted on the end-effector. With these assumptions, the Euler-Lagrange dynamic equation of motion (EOM) of the constrained WMM can be described as

$$\begin{gathered} M\underline{\ddot{q}} + \underline{V} = E\underline{\tau}_m + E_2\underline{F} - A^T\underline{\lambda} \\ A\underline{\dot{q}} = 0 \end{gathered} \qquad [4.31]$$

where $\underline{q}$ is the full set of extended generalized coordinates, including the manipulator configuration variables as mentioned above, $M\left(\underline{q}\right)$ is the inertia matrix expressed in terms of the extended coordinate set, $\underline{V}(\underline{q}, \underline{\dot{q}})$ denotes the Coriolis, centrifugal and gravity forces, E is a full rank input transformation matrix, $\underline{\tau} = \begin{bmatrix} \tau_R & \tau_L & \tau_1 & \tau_2 \end{bmatrix}^T$ consists of the four two wheels and two arms motor inputs. $\underline{F} = \begin{bmatrix} F_x & F_y \end{bmatrix}^T$ consist of the Cartesian forces applied at the end-effector. The E_2 matrix maps the task-space end-effector force, $\underline{F}$, to the joint-space. $\underline{\lambda}$ denotes the Lagrangian multiplier.

We can now project the constrained EOM into the feasible motion space by the matrix S^T as

$$S^T M\underline{\ddot{q}} + S^T V = S^T E\underline{\tau}_m + S^T E_2 \underline{F} - S^T A^T \underline{\lambda} \quad [4.32]$$

Since S lies in the null space of the constraint matrix A , the last term in the right hand side of Equation [4.32] would vanish, thus the Lagrangian multiplier would be eliminated. Also use the relationship $\underline{\dot{q}} = S\underline{\dot{z}}$ and its differentiation $\underline{\ddot{q}} = S\underline{\ddot{z}} + \dot{S}\underline{\dot{z}}$, Equation [4.32] can be written in the form

$$H\underline{\ddot{z}} + C\underline{\dot{z}} + \underline{g} = \underline{\tau} + \underline{\tau}_E \quad [4.33]$$

where $H = S^T MS$ is the symmetric positive-definite mass matrix, $C\underline{\dot{z}} = S^T M\dot{S}$ and $\underline{g} = S^T \underline{V}$ includes Coriolis, centrifugal and gravity forces, $\underline{\tau} = S^T E\underline{\tau}_m$ is a vector of independent generalized actuation forces, and $\underline{\tau} = S^T E_2 \underline{F}$ is a vector of independent generalized forces due to external forces acting on the manipulator.

To get a better insight into this system, we note that the generalized coordinate of the WMM can be decoupled as $\underline{q} = \begin{bmatrix} \underline{q}_a^T & \underline{q}_b^T \end{bmatrix}^T$, where $\underline{q}_a$ as developed previously are the generalized coordinates of the mobile base and $\underline{q}_b$ as the generalized coordinates of the manipulator. Then we can reformulate Equation [4.33] in a partitioned manner as

$$\begin{bmatrix} M_{aa}\left(\underline{q}_a\right) & M_{ab}\left(\underline{q}\right) \\ M_{ba}\left(\underline{q}\right) & M_{bb}\left(\underline{q}_b\right) \end{bmatrix} \begin{bmatrix} \underline{\ddot{q}}_a \\ \underline{\ddot{q}}_b \end{bmatrix} + \begin{bmatrix} \underline{V}_a\left(\underline{q},\underline{\dot{q}}\right) \\ \underline{V}_b\left(\underline{q},\underline{\dot{q}}\right) \end{bmatrix} = \begin{bmatrix} E_a & 0 \\ 0 & E_b \end{bmatrix} \begin{bmatrix} \underline{\tau}_a \\ \underline{\tau}_b \end{bmatrix} + \begin{bmatrix} E_{2a} \\ E_{2b} \end{bmatrix} \underline{F} - \begin{bmatrix} A_a^T \underline{\lambda} \\ 0 \end{bmatrix} \quad [4.34]$$

$$A_a\left(\underline{q}_a\right)\underline{\dot{q}}_a = 0 \qquad [4.35]$$

where $M_{aa}\left(\underline{q}_a\right)$ is the mass matrix of the mobile based, $M_{ab}\left(\underline{q}\right)$ is the inertia matrix representing the dynamic effects of the motion of the manipulator on the base, $M_{ba}\left(\underline{q}\right)$ inertia matrix representing the dynamic effects of the motion of the base on the manipulator and $M_{bb}\left(\underline{q}_b\right)$ is the inertia matrix of the manipulator. $V_a\left(\underline{q}, \underline{\dot{q}}\right)$ and $V_b\left(\underline{q}, \underline{\dot{q}}\right)$ are the vectors that include Coriolis, centrifugal and gravity forces for the mobile base and manipulators respectively.

After the observation of the partitioned form of the EOM, we notice that the matrix A in the Pfaffian form actually come from the mobile base, so we can also define the matrix S_a which takes the columns of S that only consists of constraints of mobile base. By the same token, we can similarly project the constrained equations on the space of feasible motions by pre-multiplying the partitioned EOM by S_a^T and substituting $\underline{\ddot{q}}_a = S_a\underline{\ddot{z}}_a + \dot{S}_a\underline{\dot{z}}_a$, it is simplified to

$$\left(S_a^T M_{aa} S_a\right)\underline{\ddot{z}}_a + S_a^T M_{aa}\dot{S}_a\underline{\dot{z}}_a + \left(S_a^T M_{ab} S_a\right)\underline{\ddot{q}}_b + S_a^T \underline{V}_a = \underline{\tau}_a + S_a^T E_{2a}\underline{F} \qquad [4.36]$$

4.3 Molding of Multi-Grasp Manipulation

In cooperative manipulation literature, much research effort is devoted to the internal force control. An internal force is a set of contact forces which result in no net force on the payload.

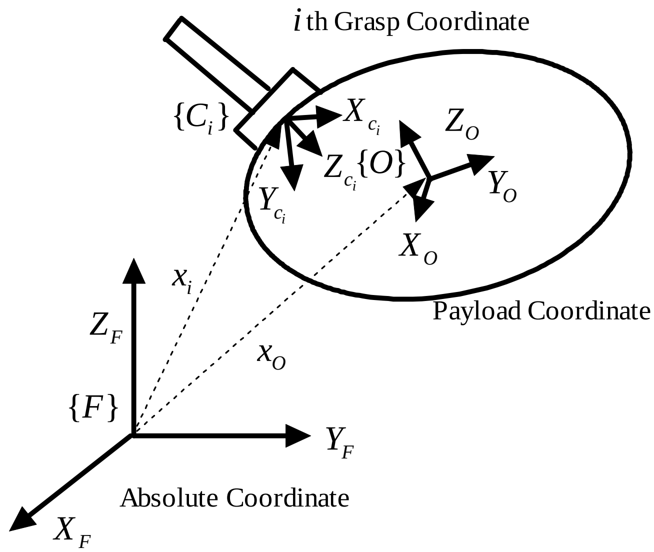

Figure 24: Payload grasp nomenclature

The first motivation is because large internal forces would usually be produced in multiple manipulator motion control, and the other reason for characterizing and controlling internal forces is the desire to satisfy frictional constraints during multiple manipulator manipulation. Internal forces are usually defined according to the null space of the relationship between applied forces and their resultant, like the force distribution work by Kumar and Waldron [7]. Kumar, Yun, Paljug and Sarkar [38] used the characterization of grasp-force redundancy to control relative motion at the contact point, and this redundancy is used to minimize internal forces during motion.

Consider N multiple manipulators rigidly grasp a common payload and each manipulator applies force/moment to the object as shown in Figure 24. For convenience, we always choose the center of mass of the payload to be the payload reference point, and we also choose the contact coordinate frame, c_i such that the z-axis of this frame points in the direction of the inward surface normal at the point of contact [39]. The world coordinate, payload coordinate and ith grasp coordinate are noted as $\{F\}$, $\{O\}$ and $\{C_i\}$ respectively. The absolute configuration of $\{O\}$ with respect to the world coordinate $\{F\}$ is given by a position vector $\underline{x}_o$ and the 3×3 rotation matrix ${}^{O}R_F$.

The generalized velocity of $\{O\}$ is expressed by a 6×1 vector

$$\underline{x}_o = \begin{bmatrix} \underline{v}^T & \underline{\omega}^T \end{bmatrix}^T \quad [4.37]$$

where $\underline{v}$ and $\underline{\omega}$ are the linear and rotational velocity vector.

The payload Newton-Euler EOM can be described

$$M_o \ddot{\underline{x}}_o + \underline{C}_o = \underline{F}_o \quad [4.38]$$

where $M_o = \begin{bmatrix} m_o I_3 & 0_3 \\ 0_3 & I_o \end{bmatrix}$, $C_o = \begin{bmatrix} -m_o g \\ \omega \times I_o \omega \end{bmatrix}$. m_o and I_o are the payload mass and inertia respectively, I_3 is the 3×3 identity matrix and 0_3 is the 3×3 null matrix. $\underline{F}_o$ is the resultant wrench vector by the multiple manipulator grasp. If we note the pure force applied to the payload at the i th contact as $\underline{F}_i$, the cascaded vector of N forces $\underline{F} = \begin{bmatrix} \underline{F}_1^T, & \dots & \underline{F}_N^T \end{bmatrix}^T$ would be mapped to the resultant wrench at the reference point by the $6 \times 3N$ grasp matrix W as

$$\underline{F}_o = W\underline{F} \quad [4.39]$$

Any component of the vector $\underline{F}$ that lies to the null space of W is the internal force. The null space approach works well to minimize internal forces during motion, however when the forces are regulated to a non-zero value, the resulting object deformation depends on the basis vectors used to describe the null space. So here we would adopt the virtual linkage model [40] proposed by Williams and Khatib, which is a physical characterization of internal forces.

In a cooperative manipulation scheme, the relationship between applied forces and their resultant and internal forces can be described by

$$\begin{bmatrix} \underline{F}_o \\ \underline{F}_{int} \end{bmatrix} = G \begin{bmatrix} \underline{F}_1 \\ \vdots \\ \underline{F}_N \end{bmatrix} \qquad [4.40]$$

where $\underline{F}_o$ represents the resultant forces at the reference point, $\underline{F}_{int}$ is the internal forces and $\underline{F}_i$ is the forces applied at the grasp point i. G is called the grasp description matrix, and relates the forces applied at every grasp point to the resultant and internal forces in the payload. G can be decomposed as

$$G = \begin{bmatrix} G_{res,1} & \dots & G_{res,N} \\ G_{int,1} & \dots & G_{int,N} \end{bmatrix} \qquad [4.41]$$

where $G_{res,i}$ is the contribution of $\underline{F}_i$ to the resultant forces in the payload and $G_{int,i}$ to the internal ones.

The inverse relationship can be obtained as:

$$\begin{bmatrix} \underline{F}_1 \\ \vdots \\ \underline{F}_N \end{bmatrix} = G^{-1} \begin{bmatrix} \underline{F}_o \\ \underline{F}_{int} \end{bmatrix} \qquad [4.42]$$

Similarly, the inverse of grasp description matrix, G^{-1}, can be written as

$$G^{-1} = \begin{bmatrix} \overline{G}_{res,1} & \overline{G}_{int,1} \\ \vdots & \vdots \\ \overline{G}_{res,N} & \overline{G}_{int,N} \end{bmatrix} \qquad [4.43]$$

4.4 Decentralized Control of Mobile Manipulator Collectives

Before presenting the control scheme for multiple WMMs, we would like to look back to some simpler cases, i.e. the human motor control and multi-finger hand robot control. A multi-finger robot can be modeled as a set of robots which are physically interconnected with the common payload by some position and velocity constraints. One of the significant challenges of controlling such systems comes from the computational consumption, and this problem becomes more important when the number of fingers scales up. Although it is conceptually simple and similar to general robotic systems, this complex system with large amounts of sensory feedback would have high computational requirement even with the state of the art hardware. In our system, each mobile manipulator module has four actuators (could be more for general spatial manipulator) and mobile base has three constraints, so the order of state space model could be substantially high even for three or four modules. Sensing the system state and computing the control torque should be accomplished with in milliseconds, and this is impossible if the system is modeled as a complete complex system.

This kind of difficulty of also recognized by the researchers of biomechanics, and the human motor control mechanism is studied under this motivation. It is shown that human uses a hierarchical control scheme for a human finger. As shown in Figure 25, the highest level is represented as sensory and motor cortex, brainstem and cerebellar structures. The lower level as expressed as spinal cord, a pair of fingers forms a composite system. The lowest level is implemented by muscles and sensory organs for each finger. This hierarchal structure shed light on the control method for multiple WMMs.

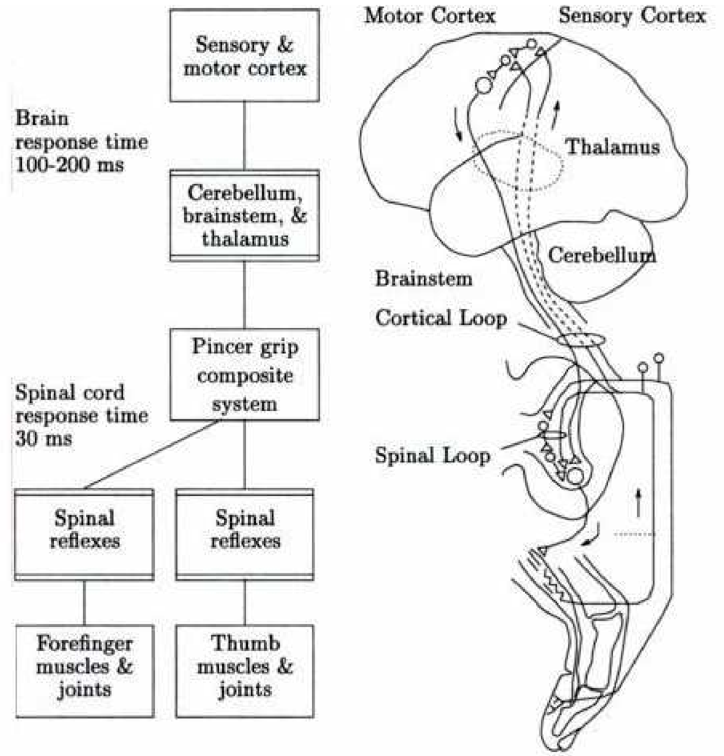

Figure 25: Hierarchical control scheme for a human finger [39]

Coordinated motion/force control of multiple serial-chain manipulators has been well studied and the coordinated control algorithms proposed as far can be categorized into five types as summarized in [41]: the master-slave type of control algorithms, the hybrid type of control algorithms, and the compliance based control algorithms, the object dynamics based control algorithms, and the augmented dynamics based control algorithms. Here we would adopt an algorithm similar to the object dynamics-based control to achieve a decentralized control.

If we specify the desired trajectory of the payload as $\underline{x}_o^d$, then the following resultant force

$$\underline{F}_o = \underline{C}_o + M_o(\ddot{\underline{x}}_o^d + K_{ov}(\dot{\underline{x}}_o^d - \dot{\underline{x}}_o) + K_{op}(\underline{x}_o^d - \underline{x}_o)) \qquad [4.44]$$

could guarantee the payload is controlled so as to satisfy the following equation

$$(\ddot{\underline{x}}_o^d - \ddot{\underline{x}}) + K_{ov}(\dot{\underline{x}}_o^d - \dot{\underline{x}}_o) + K_{op}(\underline{x}_o^d - \underline{x}_o)) = 0 \qquad [4.45]$$

where K_{ov} and K_{op} can be tuned in a pole placement fashion.

In our system, each basic module is composed of a differentially-driven WMR with a mounted planar two-d.o.f manipulator. The common payload is placed on the multiple end-effectors with passive revolute joints, and the schematic diagram of two cooperative robot modules is shown in Figure 26.

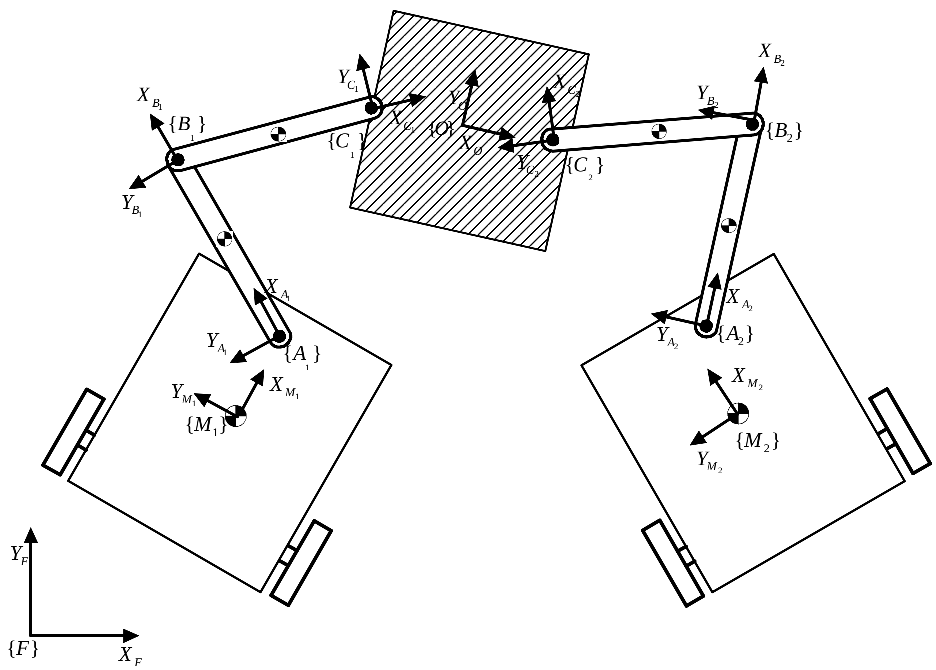

Figure 26:Schematic diagram of two cooperative robot modules with a common payload

Since the end-effector is connected to the payload by a revolute joint, this is a subclass of grasp problem where the grasp forces do not have to fall in the friction constraint cone or to be positive. From the energy consumption perspective, zero internal forces are desirable. This mechanism implies that zero internal forces are possible to be deployed in a payload transport scheme. With this in mind, we can determine the desired resultant forces and internal forces, and these forces would be distributed to individual agent by

Equation[4.42]. These distributed forces would be the desired forces for individual NH-WMM. Every NH-WMM could use the sensed local information to achieve decentralized control. The controller structure is shown in Figure 27.

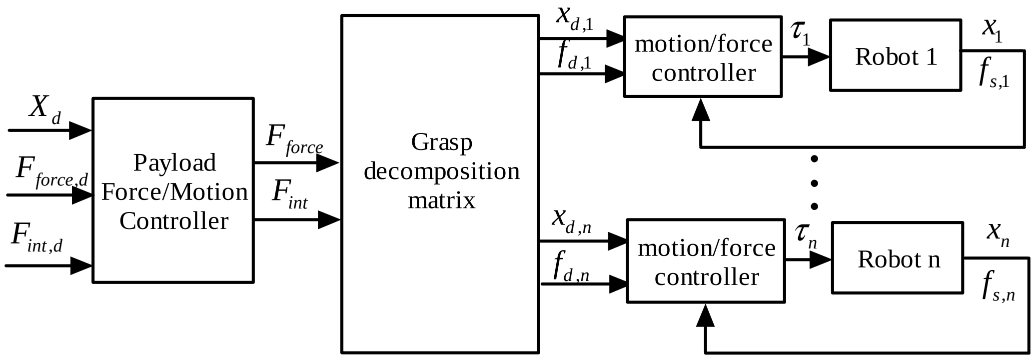

Figure 27: Decentralized controller of the cooperative payload transport system

Physically, when the payload geometry is known priori, the payload motion can be sensed by individual modules with the joint sensors. So one of the special features of this control structure is that this is a decentralized controller, which would be scalable with increased robot agents when more agents are necessary for some very complex task. Secondly, since for individual agent, the task/null space motion is completely decoupled with prioritized task accomplishment, the nonholonomic motion base would not affect the final end-effector performance, even when the task specified by the end-effector motion/force is conflicted with the base. This special feature would guarantee that multiple NH-WMM could always achieve good task performance while not getting conflicted with each other.

5 Formation Control of Mobile Manipulator Collectives

5.1 Motivation and Review

A variety of approaches have been proposed to address the problem of coordination of multiple agents and various stability criteria and many control techniques are reported recently. The behavior based approach by Balch and Arkin [42] defines an interaction law between the subsystems that leads to the emergence of a collective behavior. The leader-follower approach by Tanner [43] defines a hierarchy between the agents where one or more leaders drive the configuration scheme generating commands, while the followers follow the commands generated by the leaders. Here, we would review a systematic method of motion control for nonholonomic mobile robots proposed by Mastellone et al [44, 45]. In this framework, first, a Lyapnov-type analysis would facilitate the derivation of feedback law that guarantees tracking of reference trajectory and collision avoidance. Then this result is extended to the multiple nonholonomic mobile robot case, where formation control and leaser-follower control can be addressed within the same framework. Finally, the motion coordination problem for a group of nonholonomic vehicles is addressed. We would extend this method to motion control of mobile manipulators and show the collision avoidance and coordinated trajectory tracking capability with various simulation results.

5.2 Trajectory Tracking and Collision Avoidance of WMR

The aim of this section is to find out a controller that guarantees bounded error of a reference trajectory while avoiding collision with static objects. The special feature of this approach is that it is not only capable of collision avoidance with static objects, but also is able to perform robot avoidance, which is imperative characteristic in real world application. Much of the following derivation is modified according to [45].

Recall that the kinematics of the mobile robot can be simply expressed as:

$$\begin{aligned} \dot{x} &= v\cos\phi \\ \dot{y} &= v\sin\phi \\ \dot{\phi} &= \omega \end{aligned} \tag{5.1}$$

where (x, y) is the Cartesian position of the center of the axle of the robot, ϕ is the orientation of the robot, v and ω are the linear and angular velocities of the robot. In this method, the robot orientation ϕ is defined in the range of $[0, 2\pi)$, and the reference trajectory is defined as $\left(x^d, y^d\right)$ with bounded derivative. Correspondingly, the position error and orientation error are defined as

$$e_x = x - x^d \tag{5.2}$$

$$e_y = y - y^d \tag{5.3}$$

$$e_\theta = \theta - \theta^d \tag{5.4}$$

The coordinate of the objects to be avoided, including the regular objects and the robots, are defined as (x^o, y^o). With these definitions, a distance function is defined as

$$d = \sqrt{\left(\frac{x - x^o}{\alpha}\right)^2 + \left(\frac{y - y^o}{\beta}\right)^2} \tag{5.5}$$

where α and β are positive numbers to shape the distance function and they are usually defined as $\alpha = \beta = 1$ for general case.

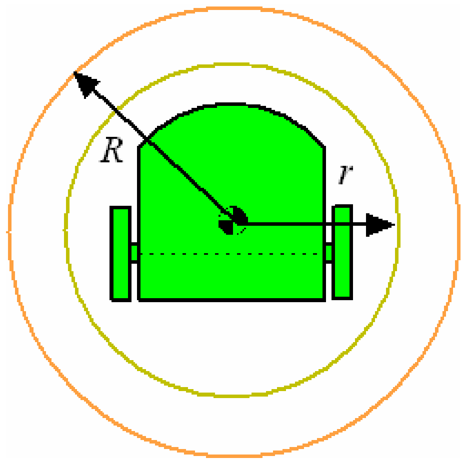

Figure 28:The detection region and avoidance region

The avoidance function proposed by Leitmann and Skowronski [46] as

$$V_a = (\min\left\{0, \frac{d_a^2 - R^2}{d_a^2 - r^2}\right\})^2 \qquad [5.6]$$

where $R > 0$, $r > 0$ and $R > r$. R and r are the radii of the avoidance and detection regions. This function blows up whenever the robot approaches the avoidance region and would be zero whenever the robot is outside the sensing region. The detection region and avoidance region can be seen in Figure 28 and the qualitative avoidance function can be seen in Figure 29. To define an asymmetric shaped avoidance function, we can choose different values for α and β.

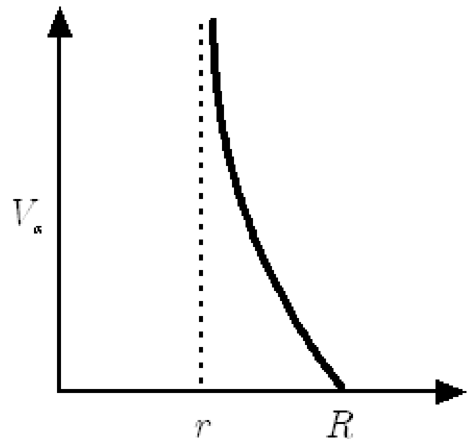

Figure 29:The Avoidance function

The partial derivative of the avoidance function can be obtained as

$$\frac{\partial V_a}{\partial x} = \begin{cases} 0 & if \;\; d_a \geq R \text{ or } d_a < r \\ 4\dfrac{(R^2 - r^2)(d_a^2 - R^2)(y - y_a)}{(d_a^2 - r^2)^3} & if \;\; r < d_a < R \end{cases} \qquad [5.7]$$

$$\frac{\partial V_a}{\partial y} = \begin{cases} 0 & if \;\; d_a \geq R \text{ or } d_a < r \\ 4\dfrac{(R^2 - r^2)(d_a^2 - R^2)(y - y_a)}{(d_a^2 - r^2)^3} & if \;\; r < d_a < R \end{cases} \qquad [5.8]$$

A set of new variables are defined as

$$E_x = e_x + \frac{\partial V_a}{\partial x} \qquad [5.9]$$

$$E_y = e_y + \frac{\partial V_a}{\partial y} \qquad [5.10]$$

The desired orientation is defined as

$$\theta_d = a\tan 2(-E_y, -E_x) \qquad [5.11]$$

It is worthy to note that θ_d defines a desired direction of motion that depends on the reference trajectory, the robot position and the obstacle to be avoided by the robot.

One of the main drawbacks of this definition comes from the fact that some configurations might lead to singular directions of the robot. In order to avoid singular cases, the following assumptions are used [44]

Assumption 1: The reference trajectory is smooth and satisfies

$$\left|e_{\theta}\right| \neq \frac{\pi}{2} \qquad [5.12]$$

This assumption on the reference trajectory implies two conditions. When the robot is outside the detection region, we have $\theta_{d} = a\tan 2(-e_{y}, -e_{x})$. The reference trajectory has the property of no initial sharp turns of 90^{o} with respect to the current orientation of the robot. When the robot is inside the detection region, we have

$$\theta_{d} = a\tan 2(-e_{y} - \frac{\partial V_{a}}{\partial y}, -e_{x} - \frac{\partial V_{a}}{\partial x}) \qquad [5.13]$$

The resultant control signal of obstacle avoidance and reference trajectory might make the robot in a singular configuration. One remedy to this problem is that when Assumption 1 is not satisfied, the reference trajectory is perturbed with small value as

$$\tilde{\theta}_{d} = \theta_{d} + \varepsilon \qquad [5.14]$$

Figure 30 shows two examples of infeasible trajectory that violates the nonholonomic constraints. In Figure 30 (a) a mobile robot is commanded to run in the horizontal direction, but since its current velocity is in the vertical direction, this motion is infeasible for violating the nonholonomic constraints. The Figure 30 (b) shows a nonholonomic agent approaching an obstacle: $\mathrm{D_t}$ is the direction required by the reference trajectory, $\mathrm{D_a}$ is the avoidance direction and $\mathrm{D_r}$ is the resulting direction which is not admissible since it violates the nonholonomic constraints.

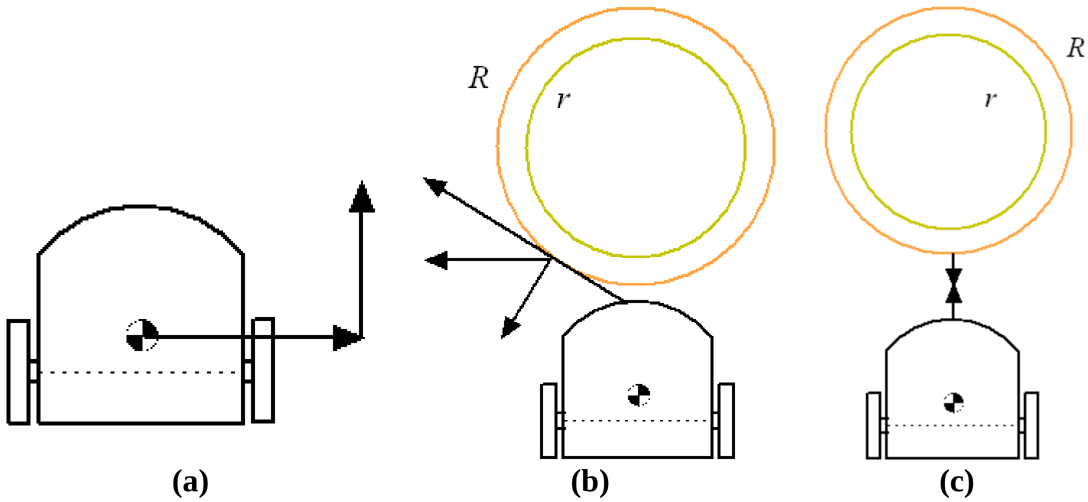

Figure 30: Some infeasible trajectories

Figure 30 (c) illustrates the dead lock scenario where the reference trajectory and avoidance direction just opposite and the commanded velocities are of the same.

Assumption 2. The reference trajectory remains constant inside the detection region, i.e. $\dot{x}_d = \dot{y}_d = 0$ for $r < d_a < R$. This assumption is based on the consideration of the priority of collision avoidance and trajectory tracking. When the robot detects an obstacle in its path, the desired reference velocity would become zero immediately and freeze the reference to the last data received. Once the robot gets out of the collision region, the reference would update to new ones.

Assumption 3. Let $\hat{\dot{\theta}}_d$ be an estimate of some measurement error of

$$\dot{\theta}_d = \frac{E_x \dot{E}_y - \dot{E}_x E_y}{E_x^2 + E_y^2} \qquad [5.15]$$

We can define $D = \sqrt{E_x^2 + E_y^2}$, and it is assumed that $\left| \hat{\dot{\theta}}_d - \dot{\theta}_d \right| < \varepsilon_\theta$.

When the object to be avoided is static, the control law to achieve reference trajectory tracking is proposed in [44] as

$$\begin{aligned} \omega &= -K_\theta e_\theta + \hat{\dot{\theta}}_d \\ v &= -K \cos e_\theta D \end{aligned} \quad [5.16]$$

This developed theorem can be extended to include multiple obstacles by defining avoidance functions for each obstacle and appending them to the total Lyapunov-like function. The total avoidance and detection regions are defined as the union of avoidance and detection regions of all of the obstacles.

To demonstrate the effectiveness of the controller, we first run the simulation of a mobile robot, and initial condition of the mobile robot is

$$x_0 = 0; y_0 = 0; \theta_0 = \frac{\pi}{3}$$

The robot is required to track a circular trajectory

$$\begin{aligned} x_r &= 6 + 6\cos(\frac{\pi}{30}t); \\ y_r &= 6 + 6\sin(\frac{\pi}{30}t); \end{aligned}$$

The tracking result is shown in Figure 31 with some initial snapshots of the robot motion. The controller can effectively compensate the initial error and enforce the robot to the reference trajectory. It is worth noting that these snapshots are taken with the same sampling time and it is easy to see that the initial driving velocity is pretty high and would jump from the initial position to the desired trajectory in high speed. Sometimes this is impossible to be achieved in the mobile robot hardware, and we can set some actuator velocity limit in the simulation for the emulation of practical case.

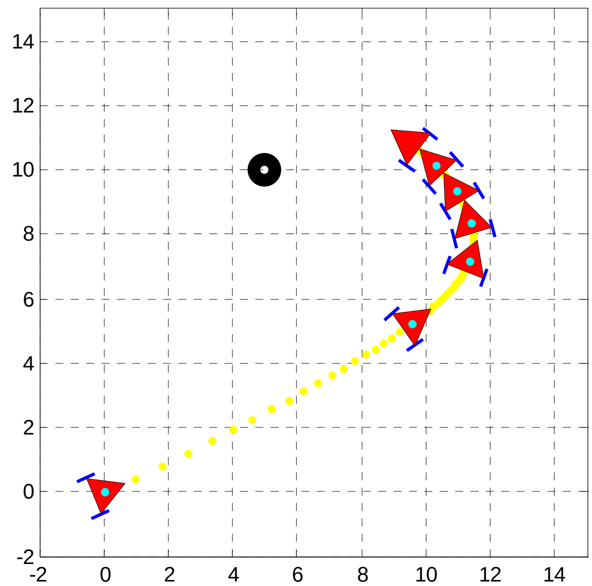

Figure 31: Snapshot of mobile robot trajectory tracking

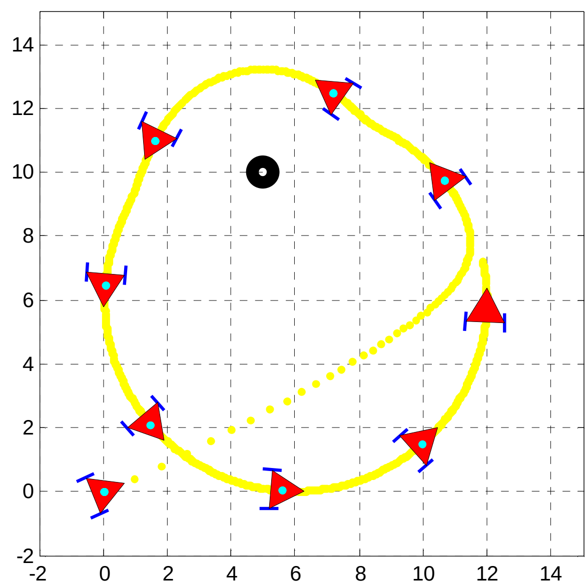

Figure 32: Snapshot of mobile robot collision avoidance

In a second simulation, an obstacle is placed at the position $(5,10)$, and the detection radius is 4 and the avoidance radius is 2. A series of snapshot of the mobile robot motion is shown in Figure 32. When the mobile robot falls into the detection region, it would prioritize the collision avoidance task and maneuvers away from the obstacle potential field. After getting away from the obstacle, the robot would resume the trajectory tracking task.

5.3 Cooperative Collision Avoidance of WMR

Two of the most important features of the controller described here is that first the obstacle is not constrained to be static obstacle, i.e. it can perform collision avoidance in a dynamic sense. So the obstacle can be general static or dynamic or the others robots in the neighbor. This feature is imperative in the practical scenarios for robot operation safety. The second feature is that this controller is performed in a decentralized manner and scales well with the number of robots.

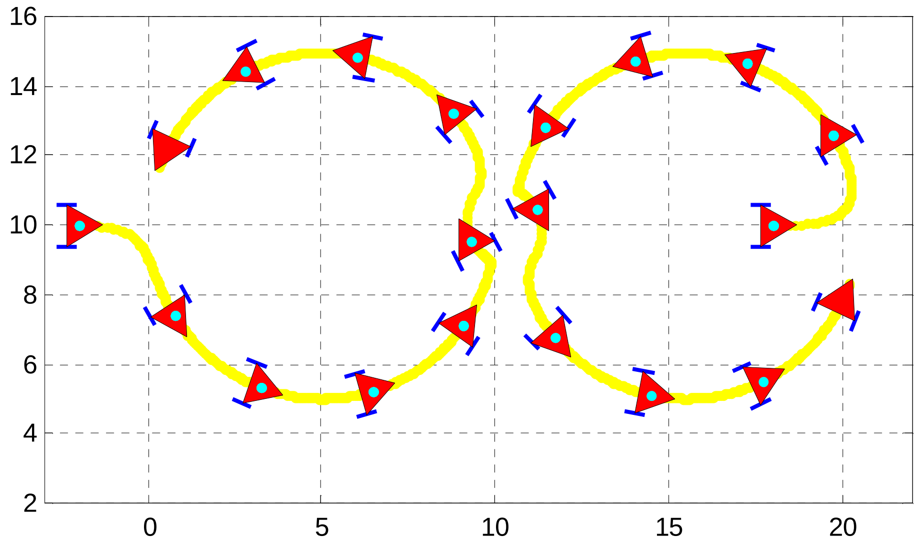

Figure 33: Two mobile robot perform collision avoidance

Figure 33 depicts a scenario that two robots are required to track circular trajectories respectively

$$x_{r_1} = 5 + 5\cos(\frac{\pi}{30}t + \pi); y_{r_1} = 5 + 5\sin(\frac{\pi}{30}t + \pi) + 10;$$
$$x_{r2} = 15 + 5\cos(\frac{\pi}{30}t); \quad y_{r2} = 5 + 5\sin(\frac{\pi}{30}t) + 10;$$

The screenshots show the trajectory tracking results and the actual trajectory is also imposed on the graph to show a continuous result. When the distance of the two robots is far enough and they can track the trajectory perfectly, but when they approach each other and a collision repulsion force is generated by the controller to separate the two robots.

5.4 Formation Control of WMR

With the developed kinematic controller, now we come to resolve the formation control problem. When a desired formation and a desired trajectory of the center of mass of the formation are prescribed, the mobile robots are required to converge to the formation and to follow the desired trajectory while maintaining the stability of the formation.

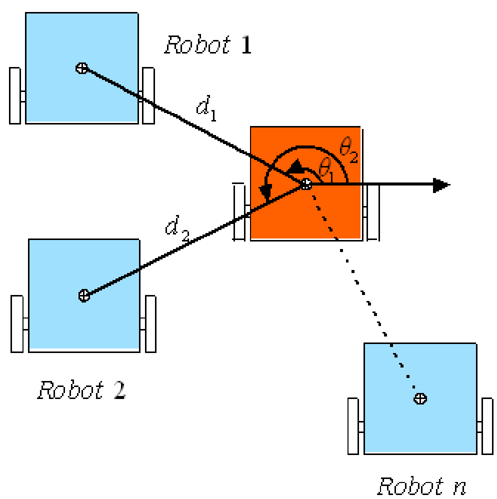

Figure 34: Notation for formation structure

As seen in Figure 34, when we specify the desired trajectory of the center of mass, then the desired motion of other robots can be determined with the geometric relation correspondingly. Consequently, we can find out the desired motion for each mobile agent. At this stage, we can continue using the previously developed control algorithm to achieve formation control in a decentralized manner.

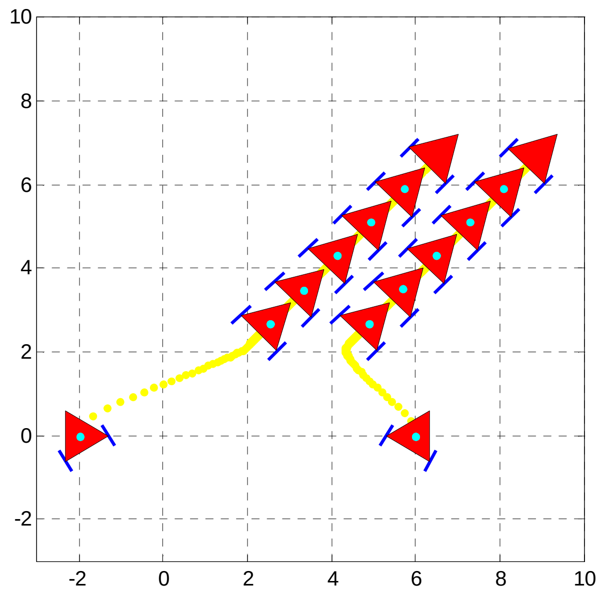

Figure 35: Two robot formation control

In the simulation shown in Figure 35, we use the leader instead of the center of mass as reference point. The objective is to first achieve a straight line formation, and then the robots would keep this formation structure to make some straight line movement. Note that the leader follower control problem is a special case of the formation control problem.

6 Simulation Results

6.1 *Cooperative Payload Transport Simulation*

In the first stage, we would employ SimMechanics and SIMULINK to rapidly create, evaluate and refine parametric models of the overall system and test various algorithms within a simulation environment. A simplified solid model of the mobile platforms and the manipulators of interest is created in SolidWorks, and exported with the corresponding geometric and material properties into SimMechanics. Figure 36 shows the dynamic model of one WMM module with payload (for space limit, the other module is not shown here).

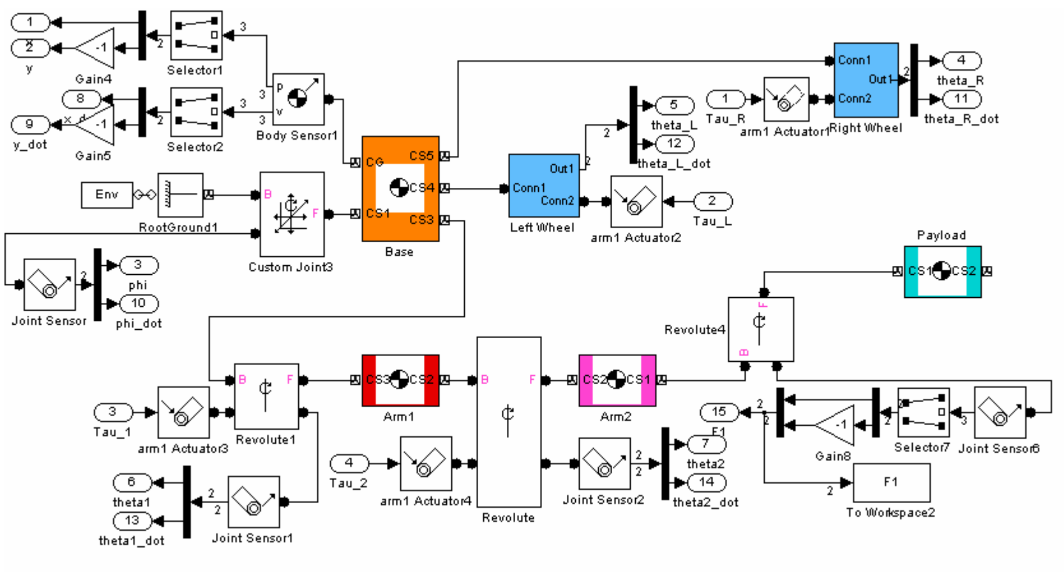

Figure 36: SimMechanics model of WMM and payload

Theoretically, from the energy consumption perspective, zero internal forces are desirable. This mechanism also implies that zero internal forces are possible to be deployed in a payload transport scheme. But practically, we still would expect to use some nonzero internal forces to guarantee the payload in some controlled equilibrium mode. With this in mind, we can determine the desired resultant forces and internal forces, and these forces would be distributed to individual agent. These distributed forces would be the desired forces for individual NH-WMM. Each NH-WMM could use the sensed local information to achieve decentralized control. The controller structure is shown in Figure 37.

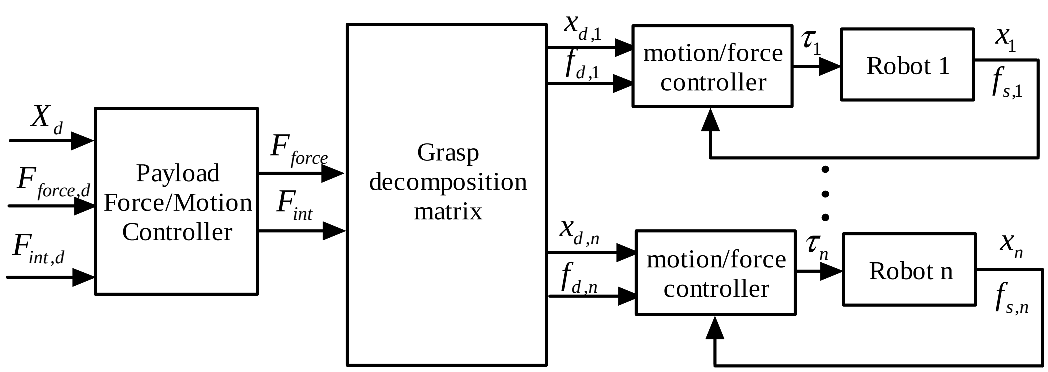

Figure 37: Overall simulation routine implementing decentralized control of the cooperative payload transport system

The controller is implemented in SIMULINK and the payload model and the NH-WMM model is build with SimMechanics. The nonholonomic model in SimMechanics is set up with the in-build velocity constraint block as shown in Figure 38 (a) and the overall simulation architecture is shown in Figure 38 (b).

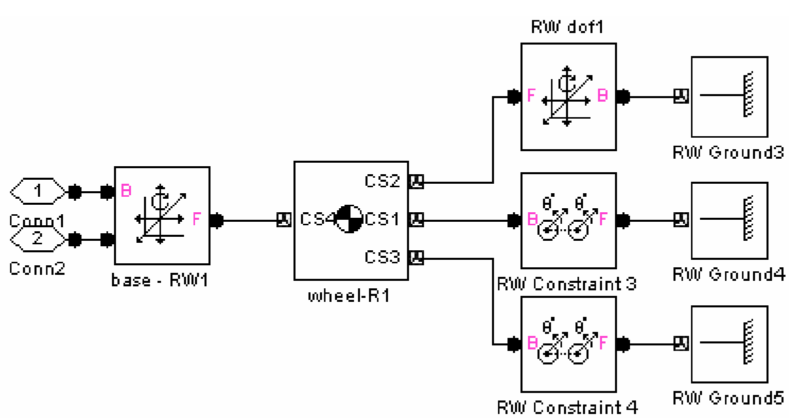

(a)

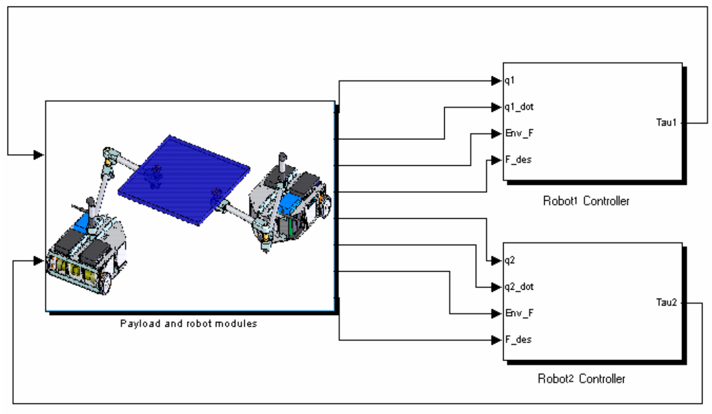

(b)

Figure 38: SimMechanics model :(a) a nonholonomic wheel; (b) the simulation architecture in SIMULINK

All the parameters of the mobile manipulator are shown in Table 1.

Table 1: Mobile Manipulator Parameters

Parameters	Values	Units
Mass of the wheel	0.159	kg
Mass of mobile base	17.25	kg
Mass of Link 1	2.56	kg
Mass of Link 2	1.07	kg
Moment of inertia of the wheels about its center of mass (CM)	2.00×10^{-4}	kg-m^2
Moment of inertia of mobile base about its CM	0.297	kg-m^2
Moment of inertia of Link 1 about its CM	0.148	kg-m^2
Moment of inertia of Link 2 about its CM	0.0228	kg-m^2
Radii of the wheels	0.0508	m
Distance from the center of the wheel axle to the CM of the mobile base	0.116	m
Distance from CM of the mobile base to the point P_a	0.100	m
Length of Link 1	0.514	m
Length of Link 2	0.362	m
Payload length	0.4	m

6.1.1 Case Study I: Without Uncertainty

We test the null-space controller with dynamic path-following along with the end-effector impedance-mode controller. Figure 39 shows the results from testing performed with a primary controller implementing a task-space impedance-mode for the end-effector and a secondary dynamic path-following controller for the WMR base. Here, the payload is 2kg and is commanded to tracking a sinusoid curve with $\underline{r}^d = \left[0.5 + 0.1t \quad 0.25\sin(0.2\pi t)\right]^T$.

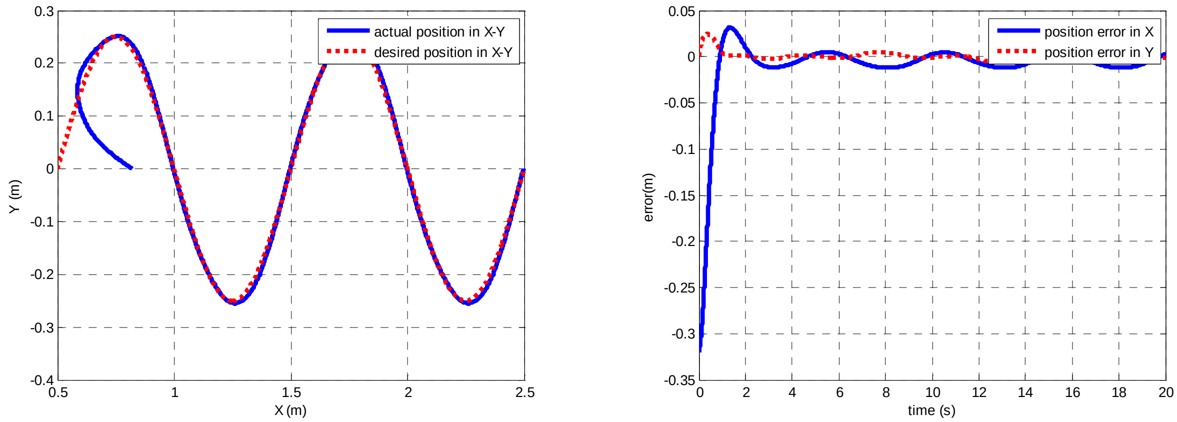

(a) **(b)**

Figure 39: Payload motion profile. (a) Desired and actual trajectory of payload, (b) tracking error in X and Y.

To facilitate the motion planning, we specify a priori designed end-effector trajectory and mobile platform for the individual robot. If we note the length of the payload as l, the desired end-effector trajectory and motion base trajectory for the first NH-WMM are

$$\underline{r}_{EE1}^d = \left[0.5 + 0.1t \quad 0.25\sin(0.2\pi t) + \frac{l}{2}\right]^T$$
$$\underline{r}_{base1}^d = \left[0.1t \quad 0.3 + \frac{l}{2}\right]^T$$

And the desired end-effector trajectory for the second NH-WMM is:

$$\underline{r}_{EE2}^{d} = \left[0.5 + 0.1t \quad 0.25\sin(0.2\pi t) - \frac{l}{2}\right]^T$$

$$\underline{r}_{base2}^{d} = \left[0.1t \quad -0.3 - \frac{l}{2}\right]^T$$

Since we only care about the translational motion of the payload, these two end-effector trajectories are kinematically consistent. It is necessary to note that since the grasp description matrix incorporates the resultant moment term, the payload rotational position can also be achieved in a similar manner.

Figure 39 (a) is the tracking performance of the payload in Cartesian space. Figure 39 (b) shows the tracking error in Cartesian space with respect to time. The payload is enforced to track the desired trajectory with the motion controller and initial deviation would decrease within 2 seconds. The controller is capable of correcting the initial error and enforcing good tracking profiles.

Figure 40 shows the tracking performance of individual agent. Figure 40 (a) shows the end-effector and base tracking results for robot 1. And the same performance for robot 2 is shown in Figure 40 (b). All the trajectories are converged to the desired position within 4 seconds. But we also note that since the end-effector is asked to maintain some desired forces, this would result in some minor position error in the task space.

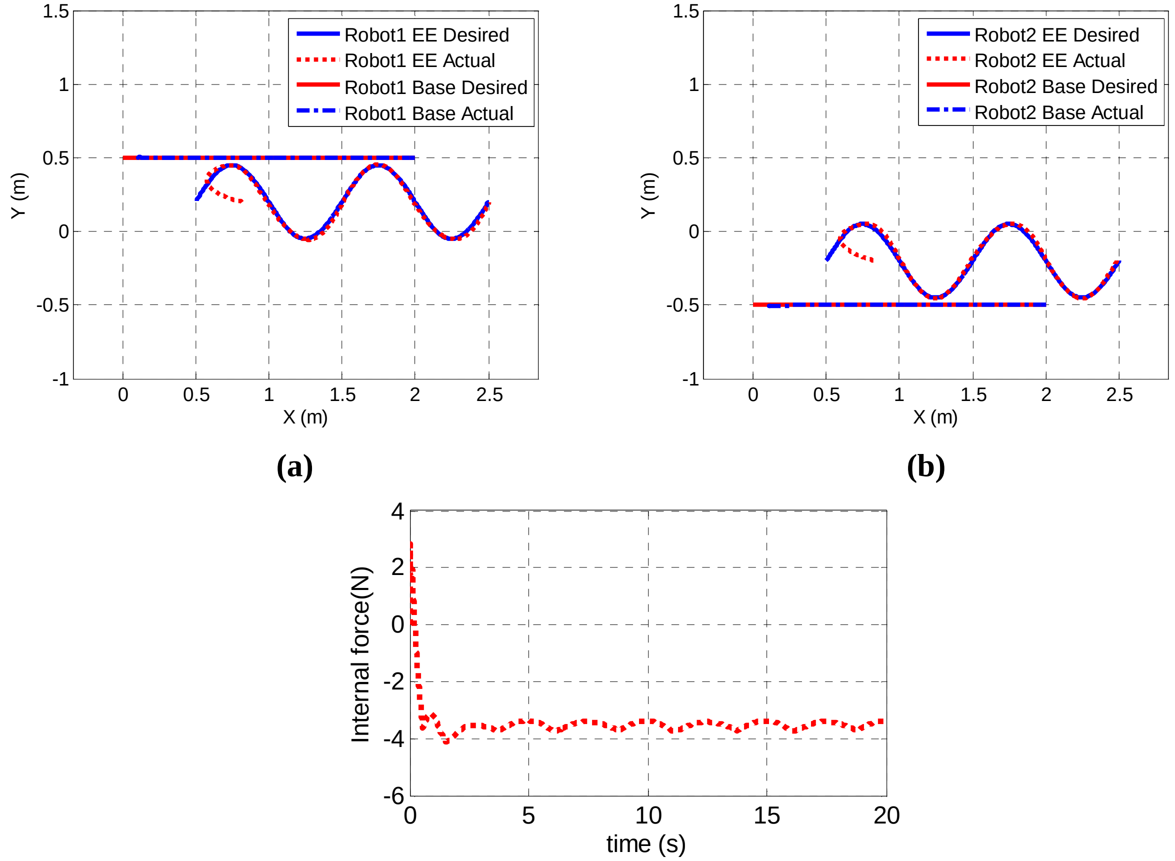

(a) **(b)**

(c)

Figure 40: The mobile platform tracking a line and end-effector tracking a sinusoid curve. (a) base and end-effector tracking results for robot1, (b) base and end-effector tracking results for robot2, (c) Internal force

Figure 40 (c) is the internal force profile of the grasped payload. We can see that after some initial oscillation, the internal force is regulated to the value around the desired ones.

6.1.2 Case Study II: With Mass Uncertainty

In a practical robot working scenario, the parameters of robotic system or working environment are always varying. In this case study, we consider the payload mass uncertainty (which is frequently encountered in real world application) in order to study the robustness and sensitivity of the controller to uncertainty.

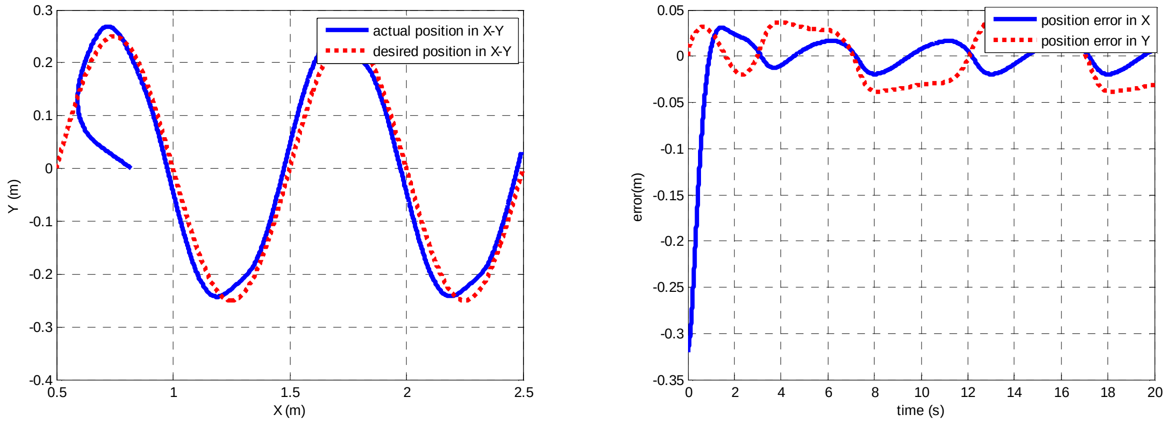

(a) **(b)**

Figure 41. Payload motion profile with mass uncertainty. (a) Desired and actual trajectory of payload, (b) tracking error in x and y.

In this case study, we underestimate the payload mass to be 1.5kg (recall that the actual payload is 2kg). Figure 41 (a) shows the tracking performance of the payload in Cartesian space. Figure 41 (b) shows the time history of Cartesian tracking error. While reflecting the degeneration in performance, due to poor estimation of the mass, the results remain nevertheless bounded.

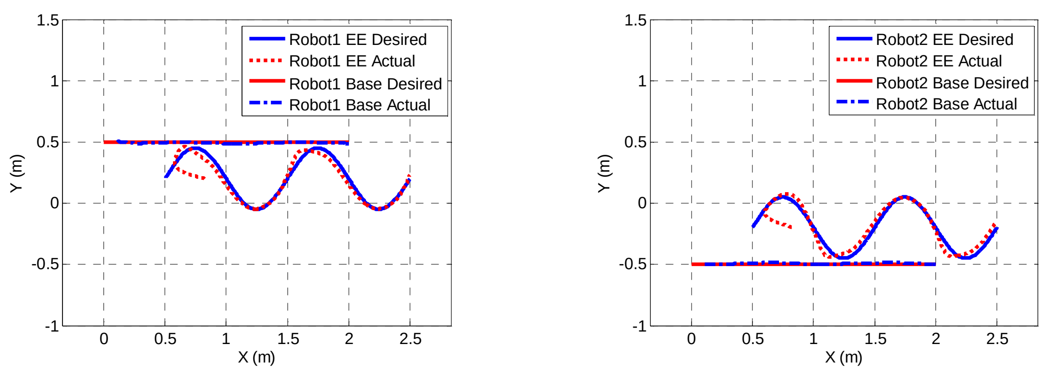

(a) **(b)**

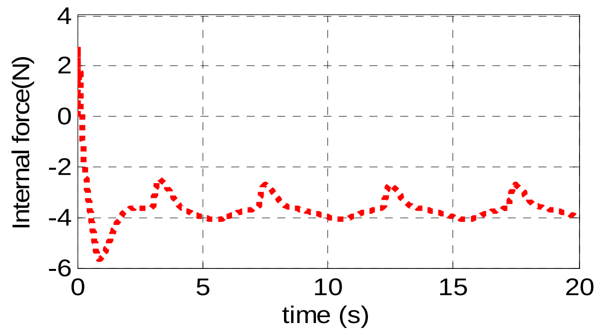

(c)

Figure 42. The mobile platform tracking a line and end-effector tracking a sinusoid curve with mass uncertainty. (a) base tracking error for robot1, (b) end-effector tracking error for robot1, (c) Internal force

Correspondingly, Figure 42 shows the tracking performance of individual agent with mass uncertainty. Figure 42 (a) and Figure 42 (b) show the end-effector and base tracking results for robot 1 and 2. Figure 42 (c) is the profile of the internal force in the grasped payload, wherein larger oscillation can be observed.

6.2 Formation Control Simulation

6.2.1 Case Study I: Mobile Base Tracking and End-Effector Perform Different Tracking

The simulation in this section would focus on the motion control of WMM, and the formation control results would be presented particularly.

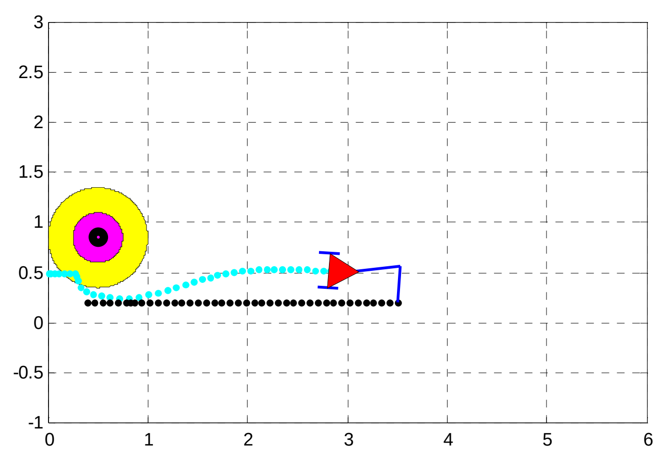

(a)

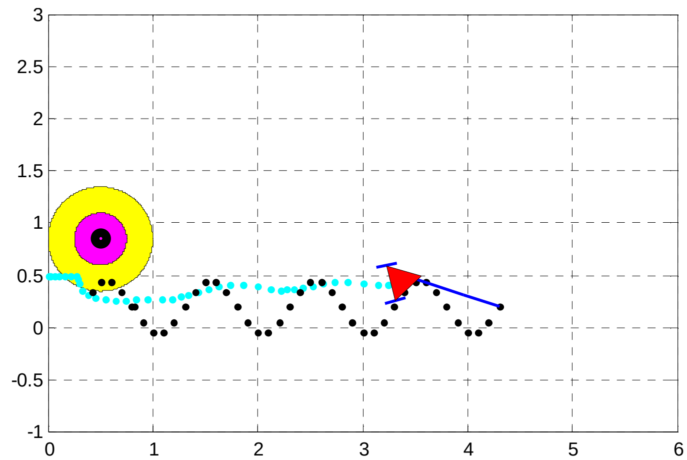

(b)

Figure 43: (a) WMM performs collision avoidance with end-effector tracking straight line and mobile base tracking straight line; (b) WMM performs collision avoidance with end-effector tracking sinusoid and mobile base tracking straight line

In the first simulation as shown in Figure 43 (a), the WMM is required to track a straight line with the end-effector while the mobile base is required to track a straight line simultaneously. The obstacle is located at the position $(0.5, 2.35)$, the detection region and avoidance radii are 1 and 0.5 respectively which are represented in the figure with filled color. The tracking results are shown in the same figure, and it is clear that the WMM can maneuver to avoid the obstacle and when it is outside of the detection region, it regains the tracking ability. Similar scenario is also shown in Figure 43 (b), where the end-effector is required to track a sinusoid line. Collision avoidance is performed pretty well, but with this kinematic controller, the base tracking results is scarified to maintain a good end-effector tracking.

6.2.2 Case Study II: WMMs Formation Control

The formation control technique can also be extended to WMM formation control. The motivation is that for each WMM module, the end-effector and mobile base four variables are to be controlled, but in practical the mobile bases would have collision with each other. In the simulation, the two WMMs are required to track a straight line (mobile base and end-effector) from different initial condition.

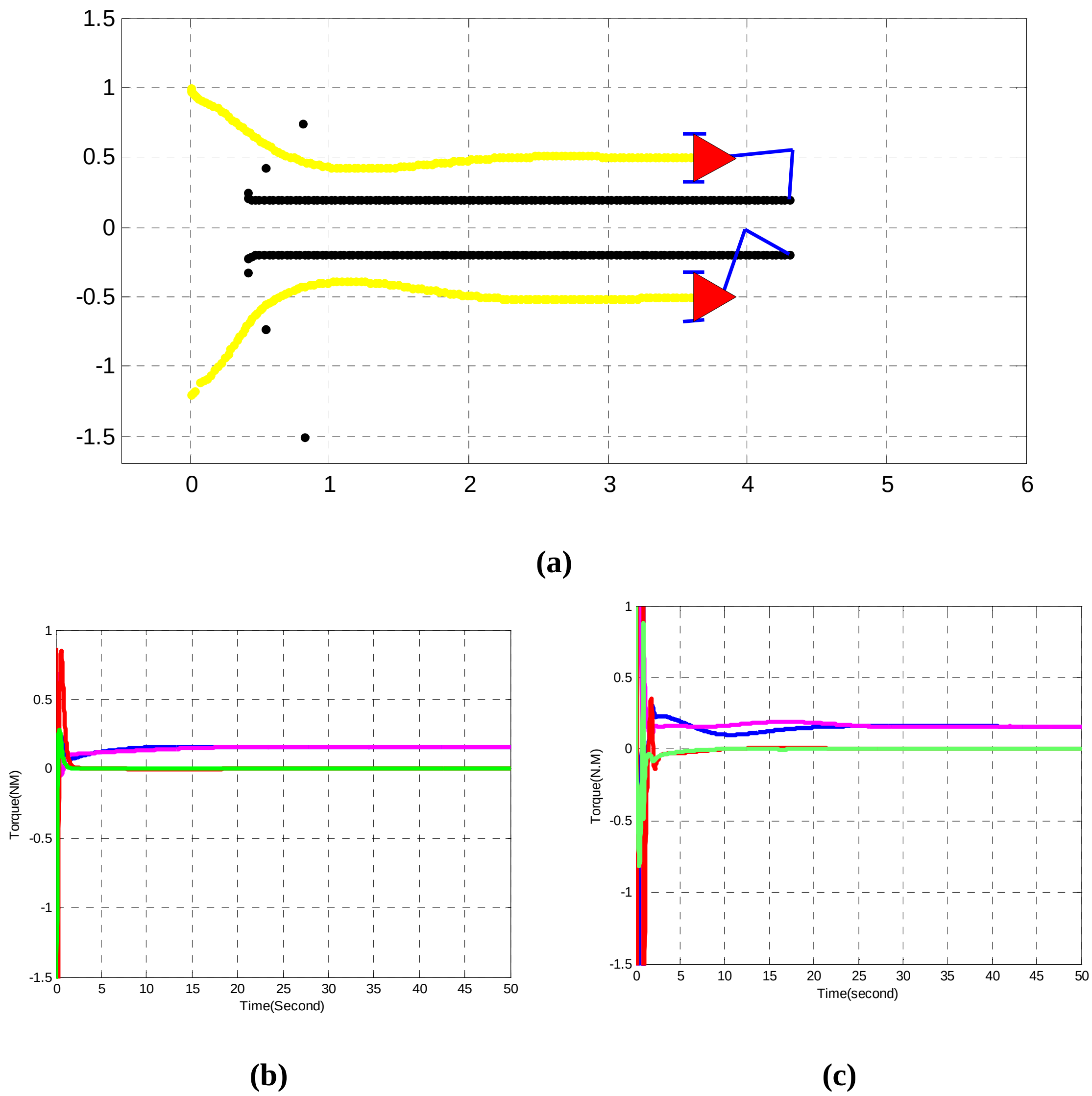

Figure 44: (a) WMMs formation result; (b) control torque of WMM 1; (c) control torque of WMM 2

The tracking result and the control torque profiles are shown in Figure 44.

7 Force Control Experiment

7.1 ATI Force *Sensor Overview*

The Network Force/Torque (Net F/T) sensor system is a six-axis force and torque sensor that simultaneously measures three-axis forces and three-axis torques. The Net F/T system provides DeviceNet^{TM}, EtherNet/IP^{TM}, a basic CAN, and Ethernet communication interfaces. The transducer is a compact, rugged, monolithic structure that converts force and torque into analog strain gauge signals for the F/T Controller. It comes fully calibrated for SI units of Newtons and Newton-meters. The Net F/T System supports the following features [47].

7.1.1 Multiple Calibrations

The Net F/T sensor can hold up to 16 different calibrations, each with a different sensing range. The different calibrations are created with different load scenarios during the calibration process at the factory and stored permanently in nonvolatile memory on the Net F/T sensor. Multiple calibrations permit to use a larger calibration for coarse adjustments and smaller calibrations for fine adjustments, or to use the same sensor in two or more very different loading regimes. The calibration information is accessible as read-only information on the integrated web server.

7.1.2 Multiple Configurations

The Net F/T sensor allows up to 16 different user configurations. Each configuration is linked to a particular calibration, and has its own tool transformation. Configurations are set up on the user configurations page of the integrated web server.

7.1.3 Force and Torque Values

The Net F/T sensor outputs engineering units, or "counts", for each force and torque axis. The number of counts-per-unit force and torque is specified by the calibration. If the user wants to use different force and torque units (i.e.; the sensor is originally calibrated to use pounds and pound-inches, but the user would like to use Newtons and Newton-meters), the user can change the output units on the user configuration page on the integrated web server and see what the counts-per-unit are for the desired units.

7.1.4 Tool Transformations

The Net F/T sensor is capable of measuring the forces and torques acting at a point other than the origin of the sensor by changing the frame of reference. This change of reference is called a "tool transformation". The user can specify tool transformations for each configuration of the sensor on the configurations page of the integrated web server.

7.1.5 Power Supply

The Net F/T system accepts power through PoE (Power-over-Ethernet) or from a DC power source with an output voltage between 11V and 24V.

7.2 ATI Force Sensor System Architecture

7.2.1 Force/Torque Transducer Working Mechanism

The complete ATI F/T sensors system includes two parts: the force/torque transducer and transducer control box.

The most basic concept of the force sensor is based on Newton's third law and the transducer reacts to applied forces and torques. In terms of Hooke's law, the transducer can be considered as a linear spring which transforms the force signal into mechanical deformation.

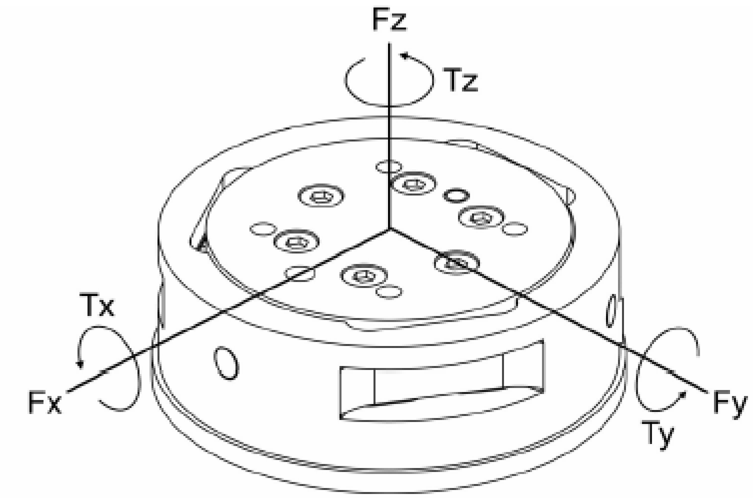

Figure 45: ATI F/T sensor

To decrease the hysteresis and increases the strength and repeatability of the structure, the transducer is monolithic structure. The beams are machined from a solid piece of metal. Semiconductor strain gauges are attached to the beams and are considered strain-sensitive resistors.

7.2.2 System Connection

The two are connected with a Controller Area Network (CAN) bus connector for high speed data transmission. All power and data calibration is handled by the control box. Also, the control box supports an integrated web server which displays output units and calibration factors about the sensor. The transducer is a compact, rugged, monolithic structure that converts force and torque into analog strain gauge signals for the F/T Controller. The main components of the Net F/T system are displayed in Figure 45.

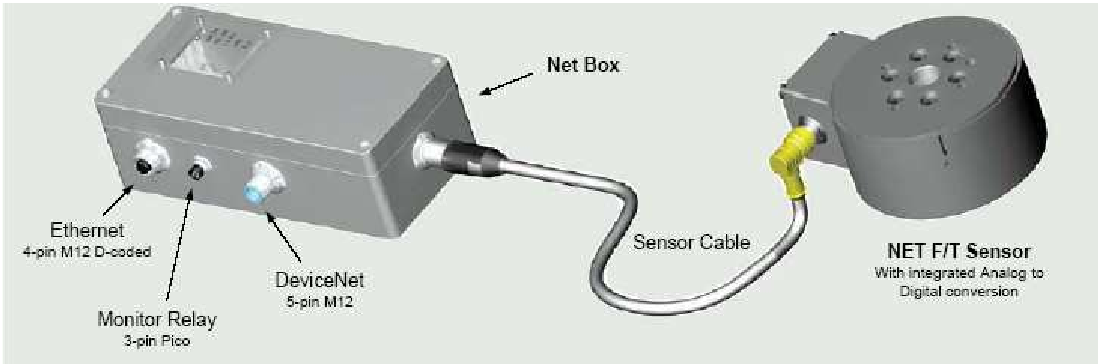

Figure 46: Net F/T System Components

The Net Analog Board converts the strain gage signals into digital data. It also stores the calibration data. The F/T sensor is commonly used as a wrist sensor mounted between a robot and a robot end-effector. Figure 46 shows a basic block diagram of the Net F/T System.

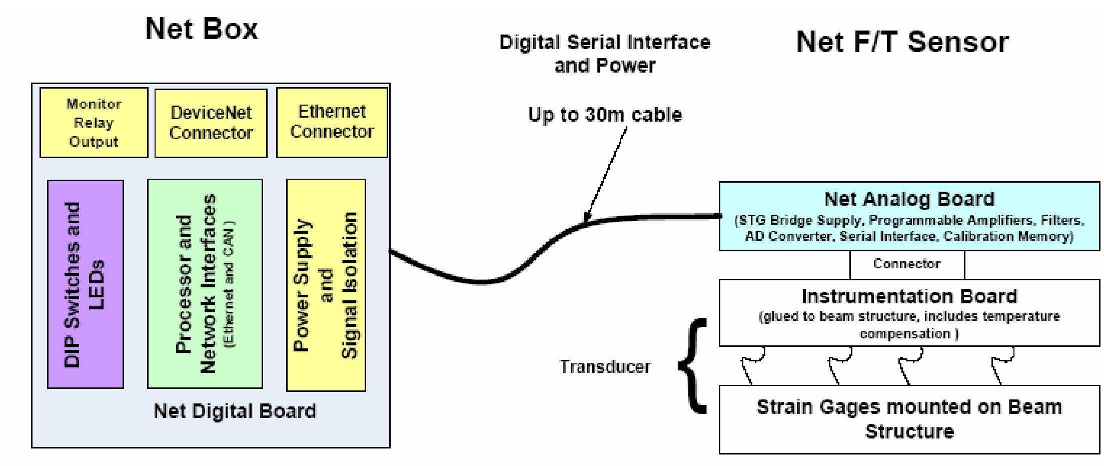

Figure 47: Net F/T System Block Diagram

The box has two main data interfaces: a Power over Ethernet (PoE) port running a UDP protocol and a DeviceNet high speed CAN interface. Our procedure will outline the setup and testing of a UDP based real time device interface using MATLAB SIMULINK.

The physical connection procedure is as following: connect the PoE switch to its external AC power supply; connect the AC power supply to the AC mains; the "PWR"

LED should turn on and glow green; connect the PoE switch to the Ethernet network and connect the Net Box via RJ45 cable to one of the PoE ports as shown in .

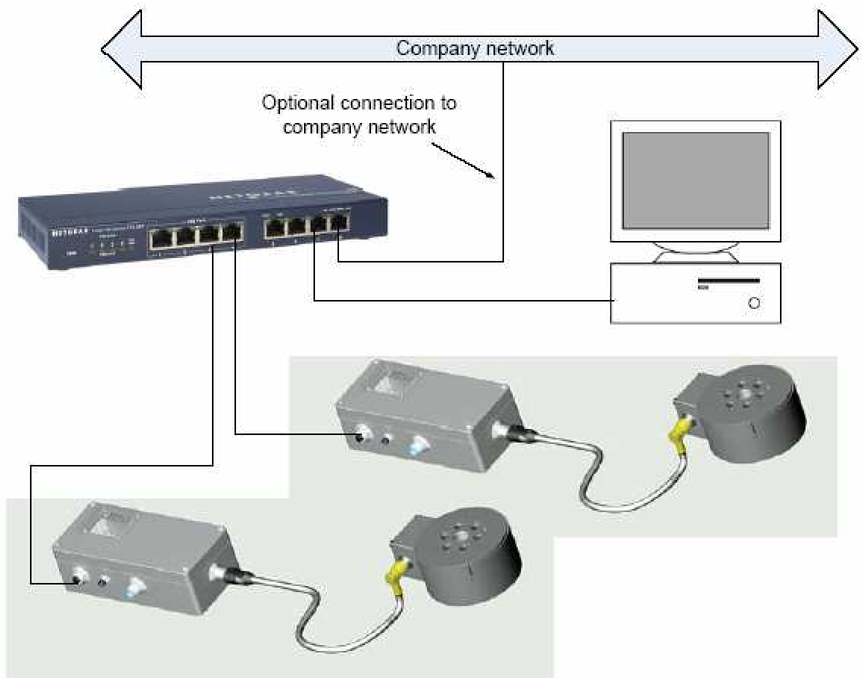

Figure 48: Force sensor network connection

7.2.3 Hardware Setup

The entire data logging system is composed of four main parts: a host development computer, a PC104 embedded computer, a power over Ethernet (PoE) switch and the ATI F/T sensor system. To develop and compile the MATLAB code a host computer with RealTime Workshop is needed. Compiled code is routed through the PoE switch and downloaded to the target computer via an Ethernet connection. The xPC PC104 target remotely also uses the PoE switch to interface with the F/T sensor. Commands are sent to the control box while force and torque data is transmitted back to the target computer. The control box is powered entirely over the PoE connection. A hardware block diagram is illustrated in Figure 49.

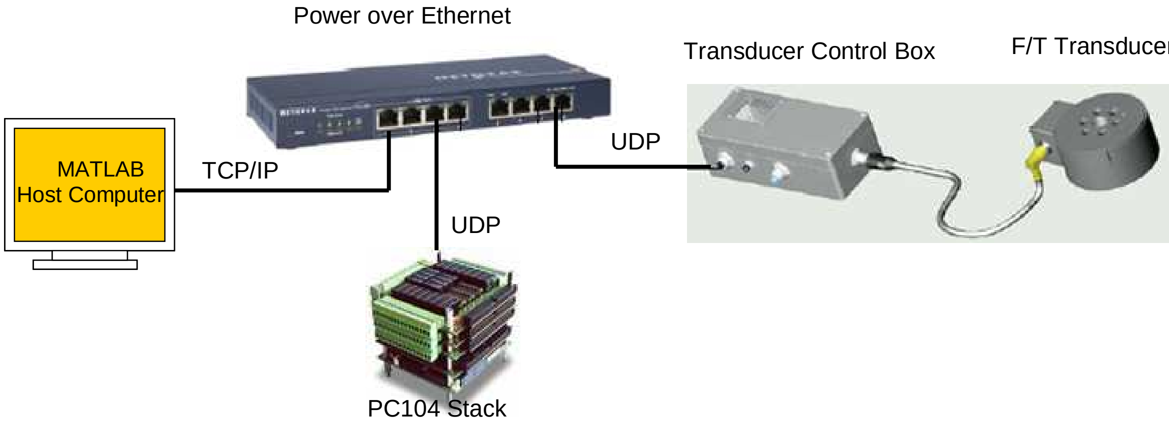

Figure 49: System setup with PC104

7.3 MATLAB Interface Setup

The Net F/T Sensor can output data at up to 7000 Hz over Ethernet using UDP. This method of fast data collection is called Raw Data Transfer (RDT). Our MATLAB code controls the interface between the xPC Target™ system and the ATI transducer control box. The specific communication protocol and message structure used to control and receive data from the ATI command box will be discussed in this section.

7.3.1 Communication Protocol

The F/T sensor provides several modes of RDT output and two commands to bias and unbias the sensor as shown in Table 2.

Table 2: Net F/T Modes

Mode	Description	Speed	Situation Best Suited To
1	Non real-time output	Slow (limit to ~333Hz)	Non-real time situations
2	High speed real-time output	Fast (up to 8000Hz)	Real-time response application
3	High-speed buffered output	Fast (up to 8000Hz), but comes in bursts (buffered)	Collecting data at high speed, but not responding in real-time
4	Multi-unit synchronization (Not yet implemented)	Slow (depending on the number of sensors involved)	Multi-unit synchronization

As previously stated the ATI command box needs a unique command structure to setup the sensor interface. To start the Net F/T outputting RDT messages, it is necessary to first send an RDT request. The Net F/T listens for RDT requests on UDP port 49152. It also sends the RDT output messages from this port. The message has three parts with a total length of 8 bytes (64 bits). All sensor commands must follow the following structure to be properly understood.

$$Header_{16} + Mode_{16} + SampleCount_{32} \qquad [7.1]$$

where the subscripts denote number of bits.

The header is a unique binary sequence identifying the message beginning. It must have a value of 0x1234 in hexadecimal (or 4660 in decimal). The next two bytes (16 bits) specify the feedback mode. The sensors comes factory ready with several feedback modes varying from one shot operation to high speed real time data streaming.

The final 4 bytes (32 bits) represent the total number of data samples to be sent back to the target computer in response to this command message. Using a zero value in this field is translated as infinity. After issuing a "non-halt" command with $SampleCount$ equal to zero, samples will continually be sent at the desired interval. To stop this looping process a "halt" command (Mode 0) should be issued to the control box.

Data samples being sent out of the control box also follow a predefined data structure. Received data packets are 36 bytes long (288 bits) with the following structure.

$$RDT_{32} + FT_{32} + Status_{32} + Fx_{32}Fy_{32}Fz_{32} + Tx_{32}Ty_{32}Tz_{32} \qquad [7.2]$$

The RDT is a number representing the current record index. This number should span 1 to $SampleCount$ and is useful for detecting if data is ever lost in transit. The FT represents the internal count of the total number of samples transmitted since the box was powered up. This number is unaffected by the “halt” command and will only reset when power is lost to the unit. The $Status$ word is a sequence of bit corresponding to the health and overall state of the sensor. Finally, the $Fx_{32}Fy_{32}Fz_{32}$ and $Tx_{32}Ty_{32}Tz_{32}$ words all represent the orthogonal forces and torques being applied to the transducer. Fx, Fy and Fz are the Cartesian forces and Tx, Ty and Tz are the Cartesian torques. All values are represented in counts per desired unit of force (engineering units). The output units can be found on the integrated web server maintained by the control box.

7.3.2 UDP Interface

The ATI control box uses a User Datagram Protocol (UDP) to transmit messages to and from the target computer. UDP unlike TCP/IP is ideally suited for real time communication because of its lacks the redundancy and error checking of TCP/IP. This compromise provides potentially faster maximum data rates but makes packets more prone to errors.

To properly communicate, the following settings must be used for the target computer and control box.

7.3.3 MATLAB Program Implementation

To program the target computer, a MATLAB SIMULINK framework was used. SIMULINK was used to create the message construction, UDP interface and data logging. The RealTime Workshop Toolbox was created the xPC compatible C code for the xPC real-time kernel. The newly created code was downloaded to the target computer from the host machine via a TCP/IP Ethernet interface. The constructed code can be broken up into two sections; message transmission and data logging.

The message transmission section creates the commands messages required to control the sensor. These messages tell the control box to transmit records in the real-time mode at once every time instant of the real-time target. The byte message in hexadecimal format is included bellow.

$$12\ 34_{16}00\ 02_{16}00\ 00\ 00\ 01_{32} \qquad [7.3]$$

Equation [7.3] represents the message transmission portion of the MATLAB code. The byte order is between the target computer and transducer control box computer. To maintain byte-wise consistency the byte order of each message word had to be reversed. Conveniently, MATLAB provides a byte reversal command box which handles this process. The next block takes the byte messages and combines them into a single UDP byte stream or packet for proper transmission. The final block transmits the packet to the transducer control box over the UDP link. This block should contain all of the UDP information specified in Table 3.

Table 3: UDP Port Settings

Parameter	Value	Description
Sensor IP	192.168.1.250	Hard coded IP port of the sensors. This value can be changed from the integrated web server.
Sensor IP Port	49152	Hard coded IP port used for receiving data at the transducer box.
Computer IP Port	22111	A user selectable IP port used for receiving data on the target computer side.
Output port width (number of bytes)	36	The total number of bytes transmitted to the target computer incoming record.

Figure 50 is the block diagram representing the data logging code. The first block contains the same information outlined in Table 3. The MATLAB unpack block takes the UDP packet and breaks it up into the predefined data structure. Once the data is properly parsed, it must be byte reversed so MATLAB can properly interpret the information.

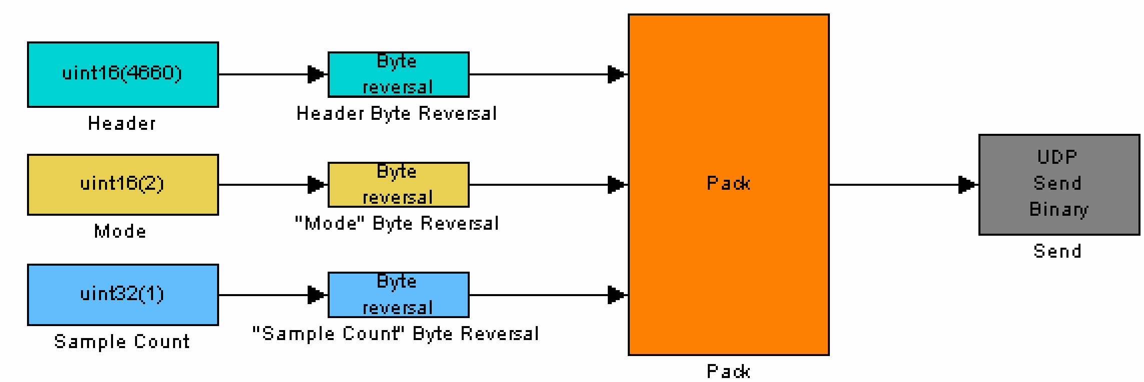

Figure 50: F/T system SIMULINK command blocks

Finally, the force and torque data is divided by there corresponding counts per unit value. For force, 80 counts represent one calibrated unit of force. 160 counts represent one calibrated unit of torque. Again it is important to stress that all units are specified on the ATI integrated web server. The resulting forces and torques can now but logged on a host computer or plotting using a MATLAB scope.

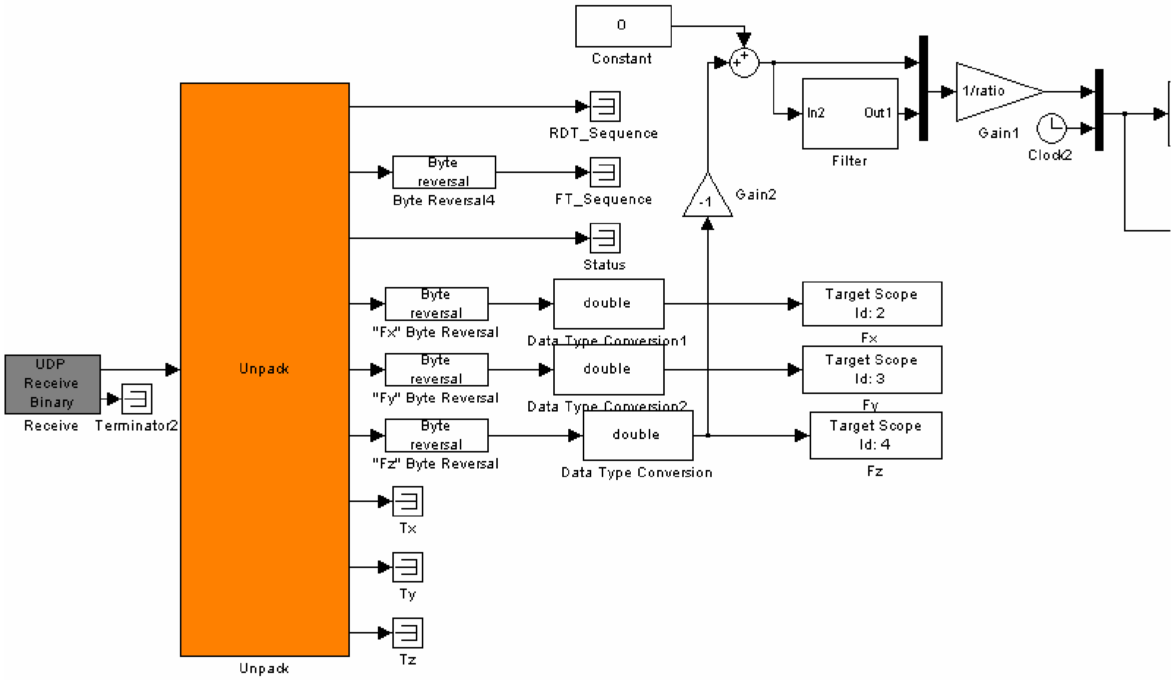

Figure 51: F/T system data reception and display blocks.

7.4 End-effector Design

Since the force transducer contains considerable mass, and it is imperative to design a delicate end-effector to fix it to the main body of the mobile manipulator. The designed manipulator arm with mounted force sensor is shown in Figure 52.

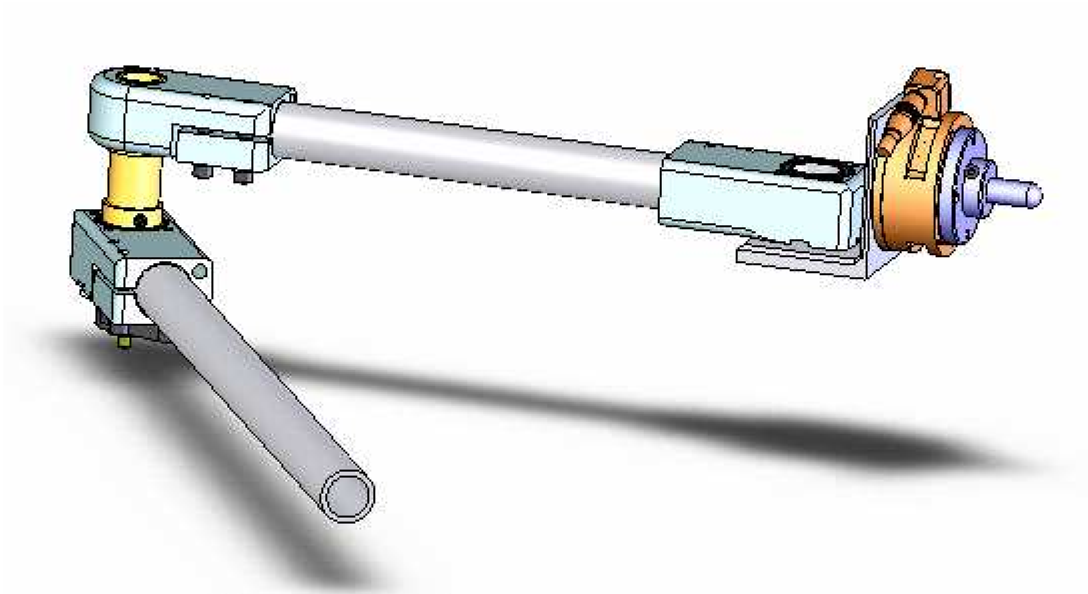

Figure 52: View of manipulator arm with force sensor

For a detailed mechanical design, Figure 53 shows an exploded view of the force sensor system with notations. It is important to ensure sufficient clearances between the mounted transducer and other fixtures and that total stack height is acceptable. Also make sure that the user could have access to the mounting screws for attaching the transducer.

The mounting adapter plate is machined for attaching to the robot. All user-supplied screws must be flush with the inside of the mounting adapter to ensure proper clearance for the electronics inside the transducer.

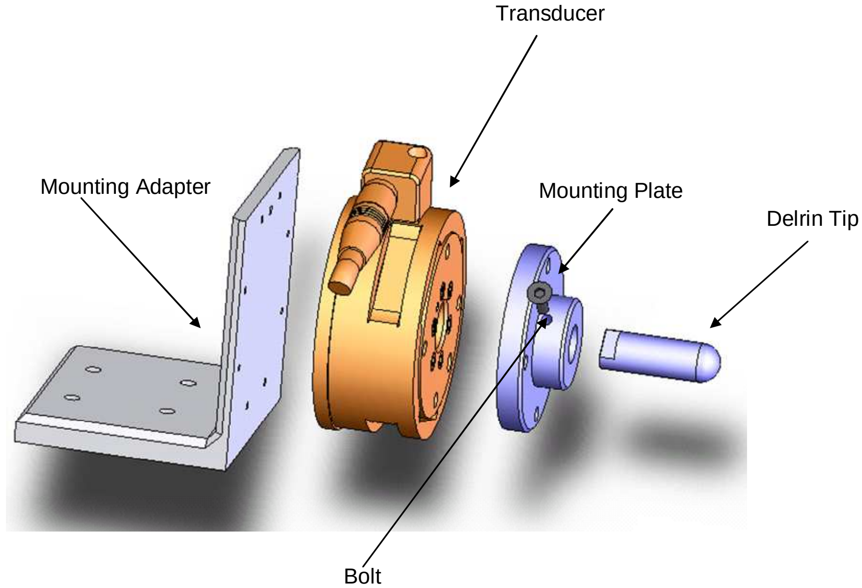

Figure 53: Exploded view of force sensor with notation

The other side of the transducer also provides screw slots to mount an end-effector for manipulation task. In our design, we machined a mounting plate with delrin tip which would provide compliant contact with the environment to enhance contact stability. The overall WMM with mounted force sensor is shown in Figure 54

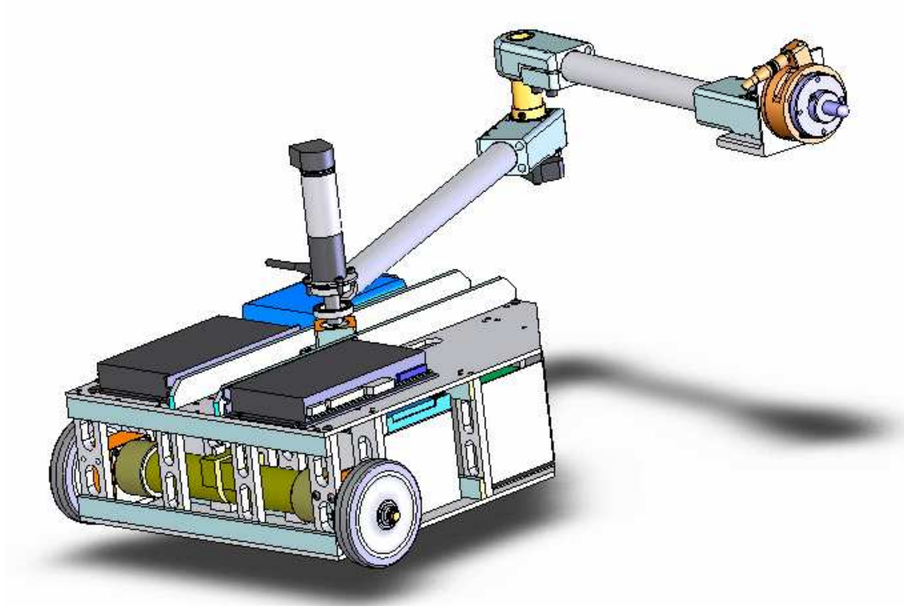

Figure 54: WMM with mounted force sensor

7.5 Force Control Simulation

The force control scenario is shown in Figure 56 where a two link manipulator is regulated to get in contact with a vertical wall. In the simulation test, we would adopt a hybrid impedance control technique and verify it in the two link manipulator arm. The task space impedance controller has the following form

$$\underline{u} = \underline{\ddot{x}}_d + k_v \underline{\dot{e}} + k_p \underline{e} + k_f (\underline{F}_d - \underline{F}_E) \qquad [7.4]$$

To increase the stability, we add some damping term in the task space and get the new controller with the form

$$\underline{u} = \underline{\ddot{x}}_d + k_v \underline{\dot{e}} + k_p \underline{e} + k_f (\underline{F}_d - \underline{F}_E) - k_v \dot{x} \qquad [7.5]$$

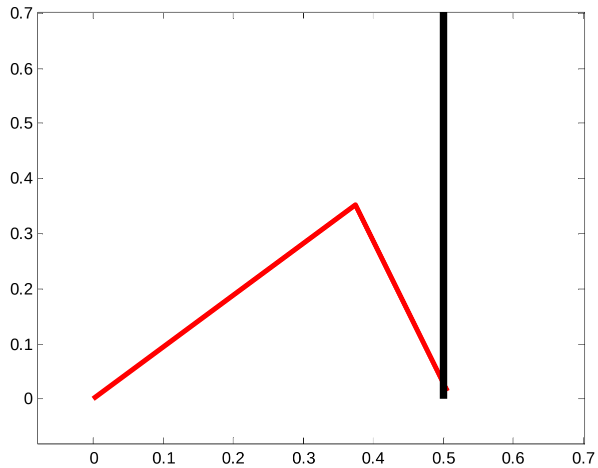

Figure 55: Two link manipulator in contact with vertical wall

The overall control scheme is implemented in MATLAB SIMULINK using RealTime xPC Target[TM] as shown in Figure 56.

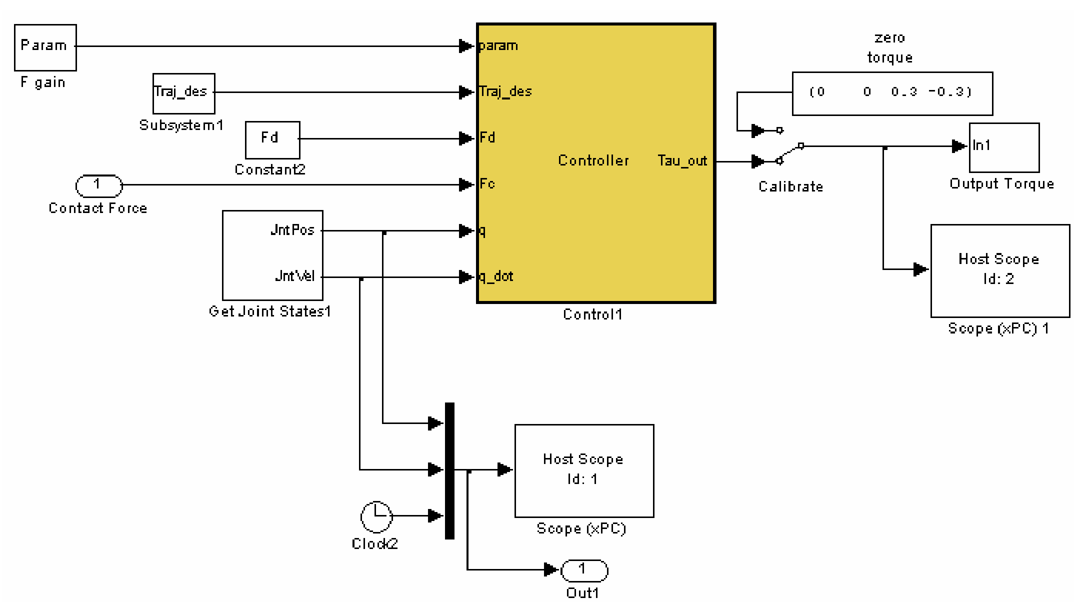

Figure 56: Diagram of xPC Target

The simulation result for the contact force profile is shown in Figure 57.

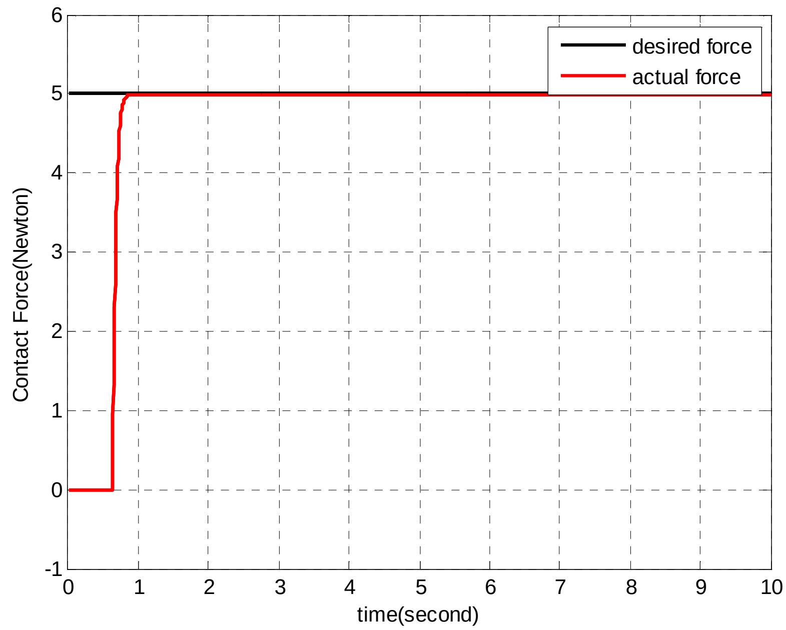

Figure 57: Force profile under HIC regulation

7.6 Force Sensor and Motor Calibration

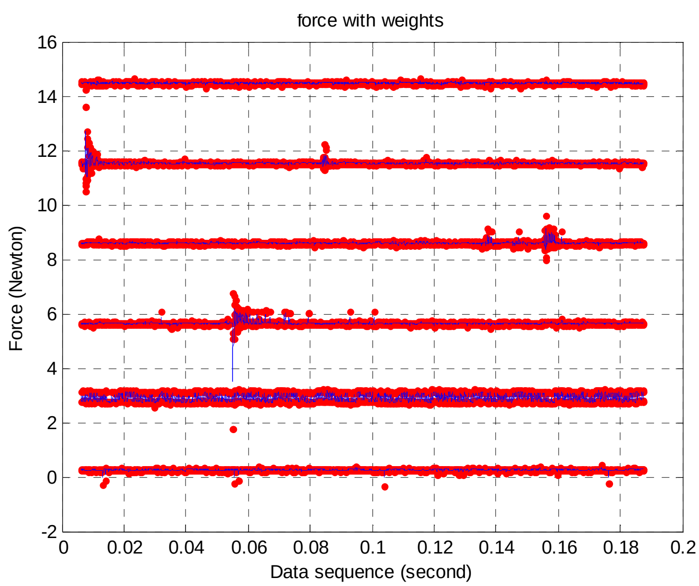

Figure 58: Force reading with 0-5 weights

By varying the number of weights from 0 to 5, we test the static reading of the force sensor in the –Z direction, as shown in Figure 58. With this static calibration, we can calibrate the force sensor and find out the software calibration setting.

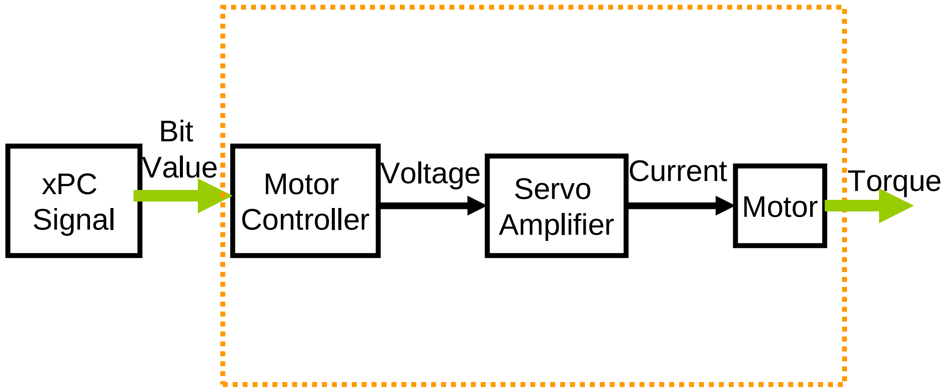

Figure 59: Schematic of motor control implementation

With this preparation, we can have a look at the robot hardware implementation. Since the computed torque would be transformed into bit values which are used are the direct control signal for the motor controller. It is imperative to find out the mapping from the computed torque to the real bit-torque value. We consider all the system in the dash line box as a black box and we can test the output force with different bit value.

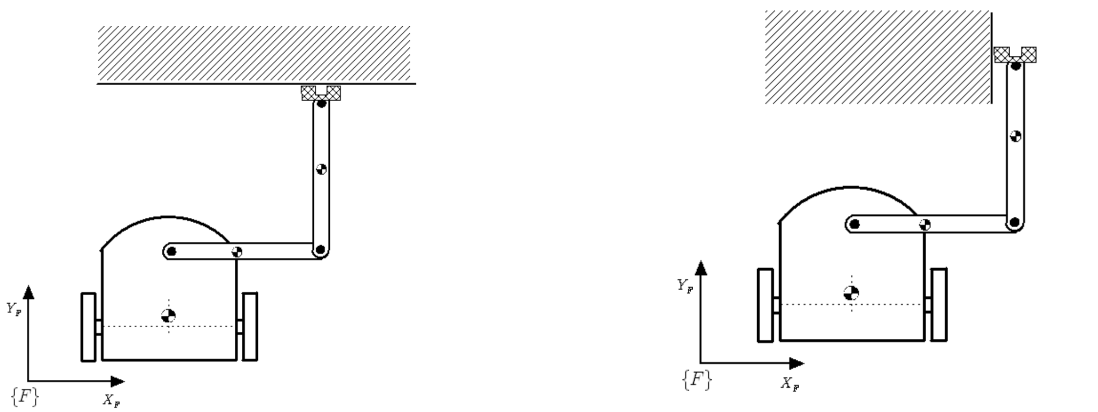

(a) **(b)**

Figure 60 : Robot configuration of motor calibration

Our test is performed in the WMM system with the two link part as the test platform. With the different configuration of the robot arm as shown in Figure 60, we can find out the bit-torque mapping for motor 1 and motor 2. The calibrated results are illustrated in Figure 61 (a) and (b).

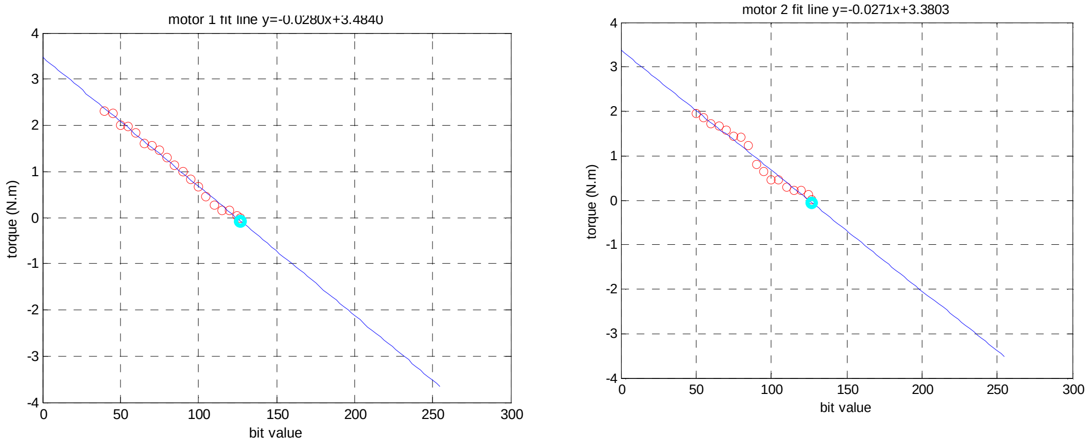

(a) **(b)**

Figure 61: (a) Calibration of motor 1; (b)Calibration of motor 2

With the calibrated sensor and motor torque, we perform the control routine in the hardware system and the force control profile is shown in Figure 62. We can see that there is some force burst in the beginning and there is some noisy signal in the control process. One important problem is the steady state error.

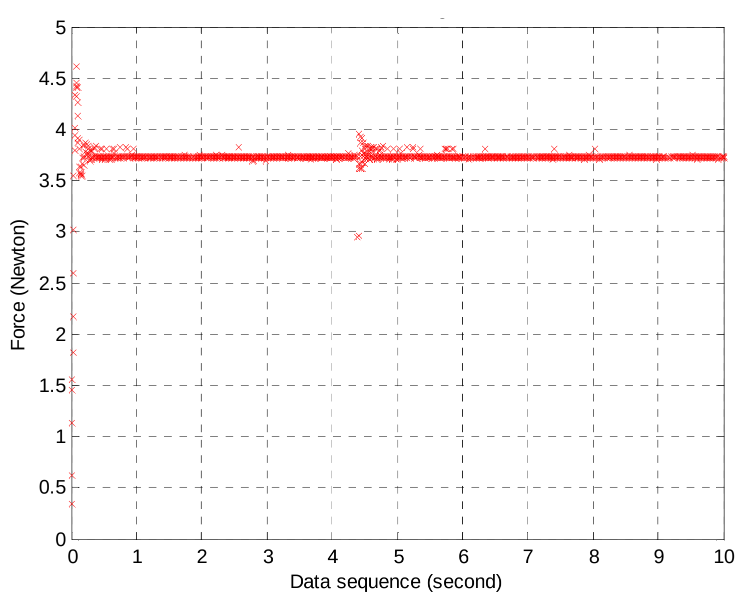

Figure 62: Experiment force data

8 Conclusion and Future Work

8.1 Summary

In Chapter 1, we reviewed some related works on mobile manipulator collectives, from the multiple agent robots, multiple finger hand and multiple legged robots. We analyzed the related issues in the cooperative control systems.

Chapter 2 discussed a variety of preliminary knowledge on modeling and control of constrained mechanical systems. Some detailed background theory includes operational space dynamics and control, constrained Lagrange dynamics.

Chapter 3 is about the force control review, and because the focus of this thesis is on force control of manipulators, we will introduce and categorize some popular force control schemes developed since three decades ago in. We will also highlight the benefits and limitations of some approaches and show some empirical and visionary perspective basing on the existing experiment results and some related literature.

Chapter 4 focuses on the modeling and control of WMMs. We begin by investigating the kinematic and dynamic model of WMR, and then the similar analysis would be performed in the WMM system with a focus on task space consistent dynamic control method. As a main body of this thesis, the multiple grasp modeling would be investigated therein and the decentralized control of WMM collectives would be presented in this chapter.

Chapter 5 investigates the formation control of a group of WMMs. The mobile robot formation problem is investigated first for a basic study, and this problem is split into trajectory tracking and static obstacle avoidance, formation control and cooperative obstacle avoidance. All of these results are generalized to mobile manipulator cases.

Chapter 6 presents simulation results for various interesting cases studies using the dynamic equation formulated in Chapter 3. In particular, the first two case studies were performed for the dynamic payload transport scenario. The subsequent two cases were targeted at mobile manipulator collective formation control.

Chapter 7 introduces the experimental setup and verification procedure. A force sensor calibration and manipulator torque calibration method is proposed therein.

8.2 Future Work

Force Control Algorithm

One of the difficult issues met in the experiment is that the system is quite sensitive to control parameters. One remedy is to perform delicate system identification, but it is necessary to note that some dynamic effects like the Coulomb friction is difficult or impossible to be identified, and even these models are perfected obtained, a stable controller is still an important problem to be solved.

Force Signal Processing

In our implementation, the sensed signal is filtered through a first order low pass filter, but in fact, the sensed data also contains the sensors acceleration, environment disturbance and some noise. Some researchers have begun to study these problems and have proposed some algorithms. The application of these algorithms into WMM is still rare.

Force Control Implementation on WMM

Since the system modeling problem, our system is still too sensitive to control parameter, so the force control implementation on WMM still needs further investigation.

Reference

[1] Y. U. Cao, A. S. Fukunaga, A. B. Kahng, and F. Meng, "Cooperative mobile robotics: Antecedents and directions," Pittsburgh, PA, USA, 1995, pp. 226-234.

[2] T. Arai, E. Pagello, and L. E. Parker, "Editorial: Advances in Multi-Robot Systems," *IEEE Transactions on Robotics and Automation*, vol. 18, pp. 655-661, 2002.

[3] C. Reynolds, "Flocks, Herds, and Schools: A Distributed Behavioral Model " in *ACM SIGGRAPH '87 Conference Proceedings*, Anaheim, California, 1987.

[4] T. L. Huntsberger, A. Trebi-Ollennu, H. Aghazarian, P. S. Schenker, P. Pirjanian, and H. D. Nayar, "Distributed control of multi-robot systems engaged in tightly coupled tasks," *Autonomous Robots*, vol. 17, pp. 79-92, 2004.

[5] A. Nakamura, J. Ota, and T. Arai, "Human-supervised multiple mobile robot system," *IEEE Transactions on Robotics and Automation*, vol. 18, pp. 728-43, 2002.

[6] J. K. Salisbury and J. J. Craig, "Articulated hands: force control and kinematic issues," Charlottesville, VA, USA, 1981, pp. 2-1.

[7] V. Kumar and K. J. Waldron, "Force distribution in closed kinematic chains," Philadelphia, PA, USA, 1988, pp. 114-19.

[8] S. Arimoto, F. Miyazaki, and S. Kawamura, "Cooperative motion control of multiple robot arms or fingers " in *IEEE International Conference on Robotics and Automation.*, 1987.

[9] O. Khatib, "Inertial properties in robotic manipulation. An object-level framework," *International Journal of Robotics Research*, vol. 14, pp. 19-36, 1995.

[10] M. Zribi and S. Ahmad, "Predictive adaptive control of multiple robots in cooperative motion," in *Proceedings of the 30th IEEE Conference on Decision and Control*, 1990.

[11] K. T. Kosuge, D.; Fukuda, T.; Sakai, M.; Kanitani, K., "Decentralized coordinated motion control of manipulators with vision and force sensors
" in *Proceedings of IEEE International Conference on Robotics and Automation*, 1995.

[12] K. O. Kosuge, T.; Seki, H., "Decentralized control of multiple manipulators handling an objectin coordination based on impedance control of each arm," in *Proceedings of IEEE/RSJ International Conference on Intelligent Robots and Systems*, 1997.

[13] Y.-H. Liu and S. Arimoto, "Decentralized adaptive and nonadaptive position/force controllers for redundant manipulators in cooperations," *International Journal of Robotics Research*, vol. 17, pp. 232-47, 1998.

[14] J. Szewczyk, F. Plumet, and P. Bidaud, "Planning and controlling cooperating robots through distributed impedance," *Journal of Robotic Systems*, vol. 19, pp. 283-97, 2002.

[15] G. Montemayor and J. T. Wen, "Decentralized collaborative load transport by multiple robots," Barcelona, Spain, 2005, pp. 372-377.

[16] J. P. Desai and V. Kumar, "Motion planning for cooperating mobile manipulators," *Journal of Robotic Systems*, vol. 16, pp. 557-79, 1999.

[17] H. G. Tanner, S. G. Loizou, and K. J. Kyriakopoulos, "Nonholonomic navigation and control of cooperating mobile manipulators," *IEEE Transactions on Robotics and Automation*, vol. 19, pp. 53-64, 2003.

[18] Y. Kume, Y. Hirata, Z.-D. Wang, and K. Kosuge, "Decentralized control of multiple mobile manipulators handling a single object in coordination
" in *IEEE/RSJ International Conference on Intelligent Robots and System*, 2002.

[19] Y. K. Hirata, Y.; Sawada, T.; Zhi-Dong Wang; Kosuge, K., "Handling of an object by multiple mobile manipulators in coordination based on caster-like dynamics
" in *IEEE International Conference on Robotics and Automation*
2004.

[20] Y. K. Hirata, K., "Coordinated motion control of multiple robots without positioninformation of each robot
" in *Proceedings of the 39th IEEE Conference on Decision and Control* 2000.

[21] O. Khatib, K. Yokoi, K. Chang, D. Ruspini, R. Holmberg, and A. Casal, "Coordination and decentralized cooperation of multiple mobile manipulators," *Journal of Robotic Systems*, vol. 13,

pp. 755-64, 1996.
[22] J. Tan and N. Xi, "Integrated Task Planning and Control for Mobile Manipulators," *International Journal of Robotics Research*, vol. 22, pp. 337-354 2003.
[23] R. Bhatt, C. P. Tang, M. Abou-Samah, and V. Krovi, "A screw-theoretic analysis framework for payload manipulation by mobile manipulator collectives," Orlando, FL, United States, 2005, pp. 1597-1606.
[24] M. Abou-Samah, C. P. Tang, and R. M. B. V. Krovi, "A kinematically compatible framework for cooperative payload transport by nonholonomic mobile manipulators," *Autonomous Robots*, vol. 21, pp. 227-242, 2006.
[25] R. W. Brockett, "Asymptotic Stability and Feedback Stabilization," in *Differential Geometric Control Theory*, R. S. M. R. W. Brockett and a. H. J. Sussmann, Eds.: Boston, MA: Birkhauser, 1983, pp. 181-191.
[26] O. Khatib, "A unified approach for motion and force control of robot manipulators: the operational space formulation," *IEEE Journal of Robotics and Automation*, vol. RA-3, pp. 43-53, 1987.
[27] J. Park and O. Khatib, "A haptic teleoperation approach based on contact force control," *International Journal of Robotics Research*, vol. 25, pp. 575-91, 2006.
[28] V. De Sapio, O. Khatib, and S. S. Delp, "Task-level approaches for the control of constrained multibody systems
" *Multibody System Dynamics*, vol. 16, pp. 73-102, 2006.
[29] E. L. Faulring, K. M. Lynch, J. E. Colgate, and M. A. Peshkin, "Haptic display of constrained dynamic systems via admittance displays," *IEEE Transactions on Robotics*, vol. 23, pp. 101-11, 2007.
[30] N. Hogan, "IMPEDANCE CONTROL: AN APPROACH TO MANIPULATION: PART III - APPLICATIONS," *Journal of Dynamic Systems, Measurement and Control, Transactions ASME,* vol. 107, pp. 17-24, 1985.
[31] Y. Shen and K. Huper, "A joint space formulation for compliant motion control of robot manipulators," Niagara Falls, Ont., Canada, 2005, pp. 362-9.
[32] M. H. Raibert and J. J. Craig, "Hybrid position/force control of manipulators," *Transactions of the ASME. Journal of Dynamic Systems, Measurement and Control*, vol. 103, pp. 126-33, 1981.
[33] C. H. An and J. M. Hollerbach, "Kinematic stability issues in force control of manipulators," Raleigh, NC, USA, 1987, pp. 897-903.
[34] R. Holmberg and O. Khatib, "Development and control of a holonomic mobile robot for mobile manipulation tasks," *International Journal of Robotics Research*, vol. 19, pp. 1066-74, 2000.
[35] G. Campion, G. Bastin, and B. D'Andrea-Novel, "Structural Properties and Classification of Kinematic and Dynamic Models of Wheeled Mobile Robots," *IEEE Transactions on Robotics and Automation*, vol. 12, pp. 47-62, February 1996.
[36] J. Borenstein, B. Everett, and L. Feng, *Navigating Mobile Robots: Systems and Techniques*. Wellesley, MA: A. K. Peters, Ltd., 1996.
[37] J. Angeles, *Fundamentals of Robotic Mechanical Systems: Theory, Methods, and Algorithms* Springer, 2003.
[38] V. Kumar, X. Yun, E. Paljug, and N. Sarkar, "Control of contact conditions for manipulation with multiple robotic systems," Sacramento, CA, USA, 1991, pp. 170-5.
[39] R. Murray, Z. Li, and S. Sastry, *A Mathematical Introduction to Robotic Manipulation*: CRC Press, 1994
[40] D. Williams and O. Khatib, "The virtual linkage: a model for internal forces in multi-grasp manipulation," Atlanta, GA, USA, 1993, pp. 1025-30.
[41] K. Kosuge and Y. Hirata, "Coordinated Motion Control of Multiple Manipulators," in *Robotics and Automation Handbook*, T. Kurfess, Ed.: CRC Press, 2005.
[42] T. Balch and R. C. Arkin, "Behavior-based formation control for multirobot teams," *IEEE Transactions on Robotics and Automation*, vol. 14, pp. 926-39, 1998.
[43] H. G. Tanner, "ISS properties of nonholonomic vehicles," *Systems & Control Letters*, vol. 53, pp. 229-35, 2004.
[44] S. Mastellone, D. M. Stipanovic, and M. W. Spong, "Remote formation control and collision avoidance for multi-agent nonholonomic systems," Roma, Italy, 2007, p. 6 pp.
[45] S. Mastellone, D. M. Stipanovic, C. R. Graunke, K. A. Intlekofer, and M. W. Spong, "Formation control and collision avoidance for multi-agent non-holonomic systems: Theory and experiments,"

International Journal of Robotics Research, vol. 27, pp. 107-126, 2008.
[46] G. Leitmann and J. Skowronski, "Avoidance control," *Journal of Optimization Theory and Applications*, 1977.
[47] I. ATI Industrial Automation, "ATI Net F/T Manual," Apex, NC, 2007.

Appendix

Mechanical Design

This section includes the mechanical drawings for all the parts needed to construct the physical prototype. The solid models and drawings were created using Solid Works Educational Edition 2006.

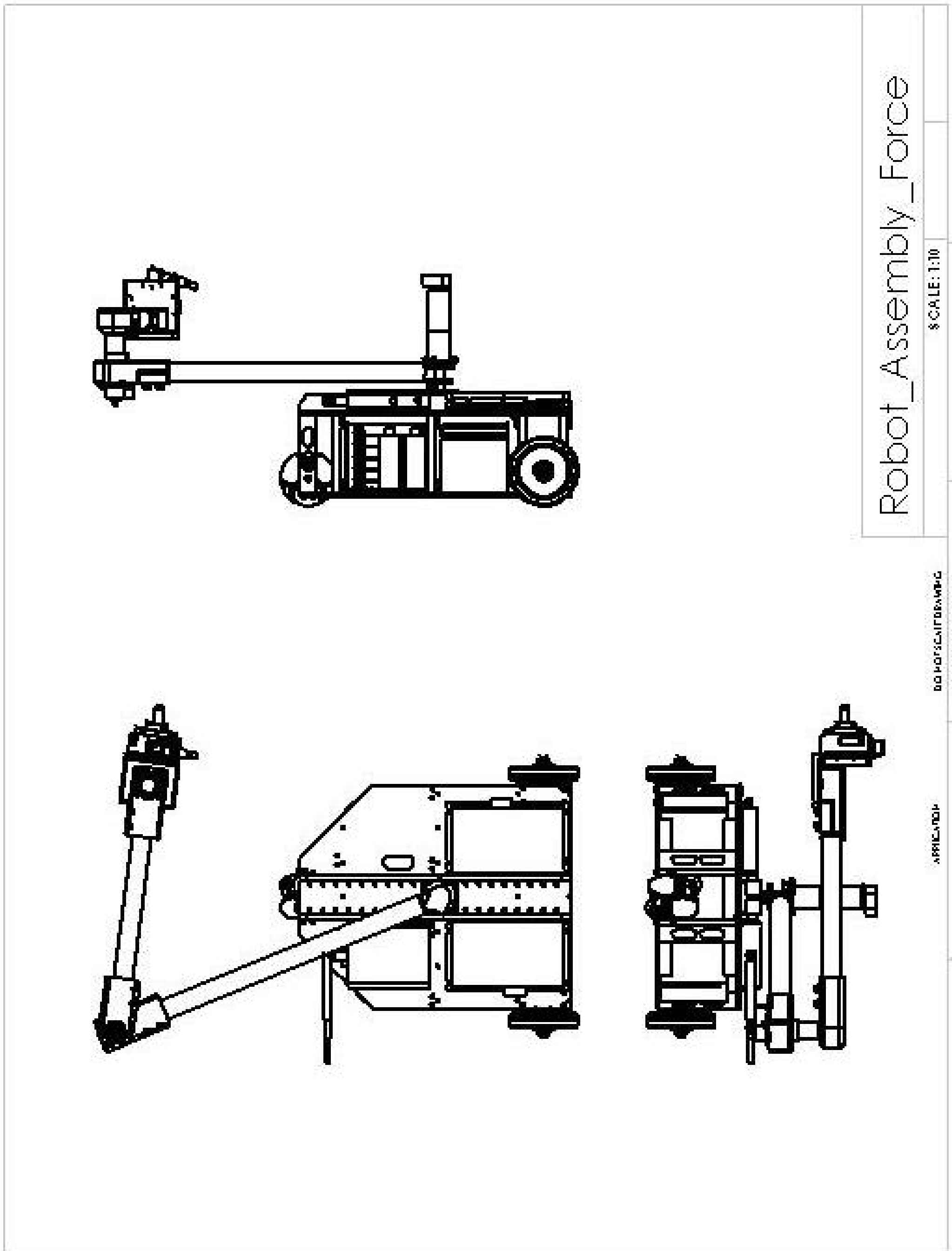
Robot_Assembly_Force
SCALE: 1:10

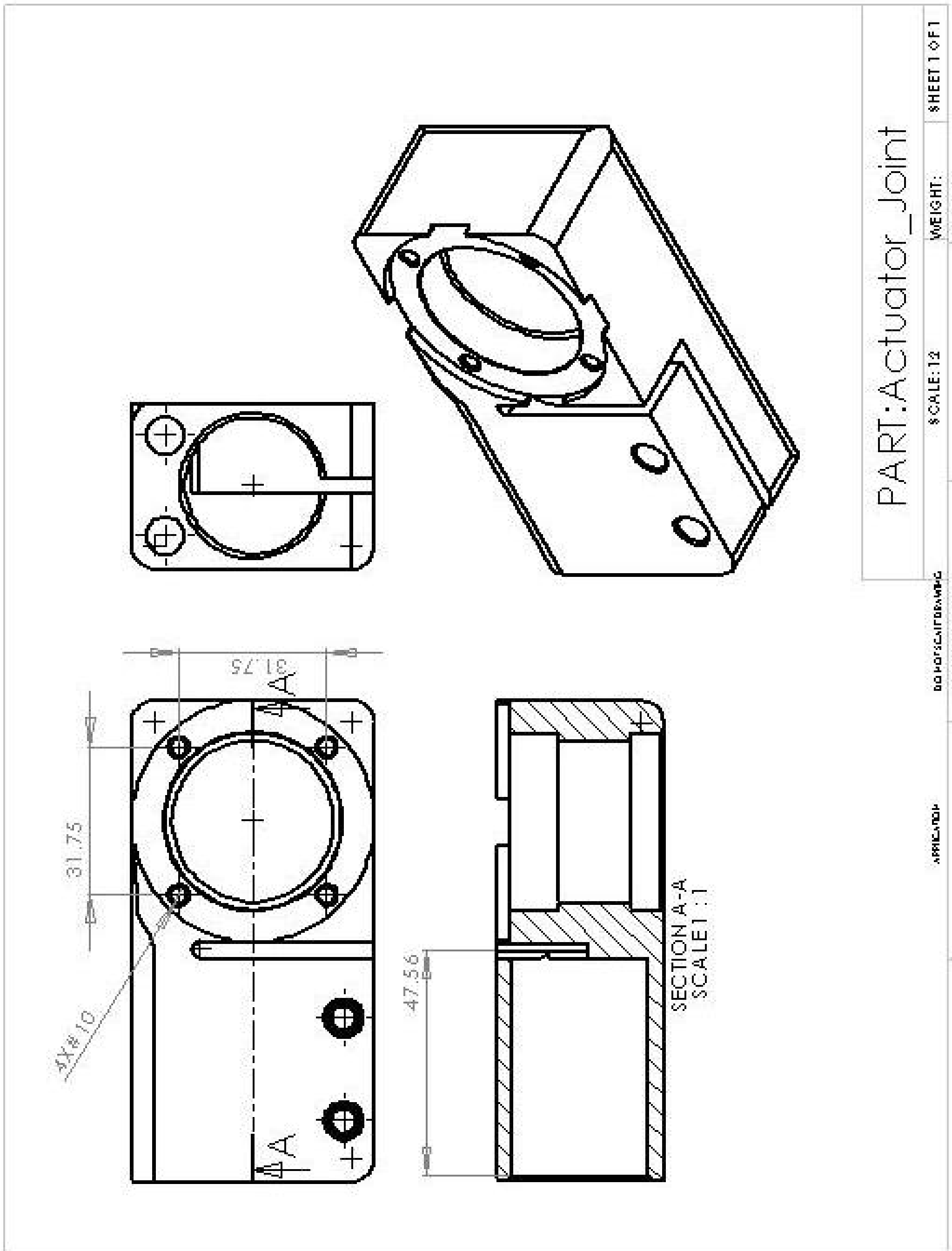
PART:Actuator_Joint
SCALE:1:2
WEIGHT:
SHEET 1 OF 1
31.75
31.75
47.56
4X#10
A
A
SECTION A-A
SCALE 1 : 1

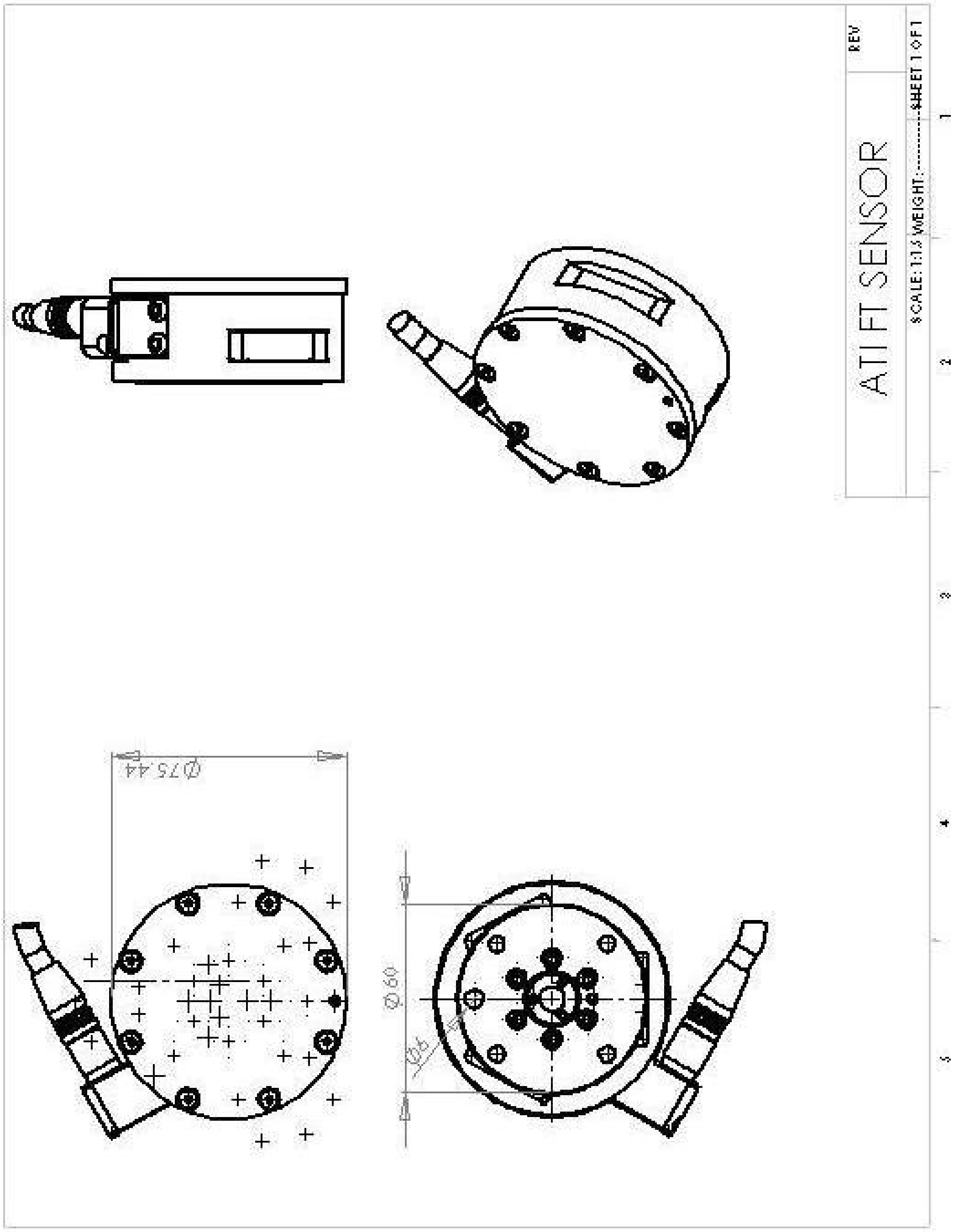
ATI FT SENSOR
REV
SHEET 1 OF 1
Ø75.44
Ø60

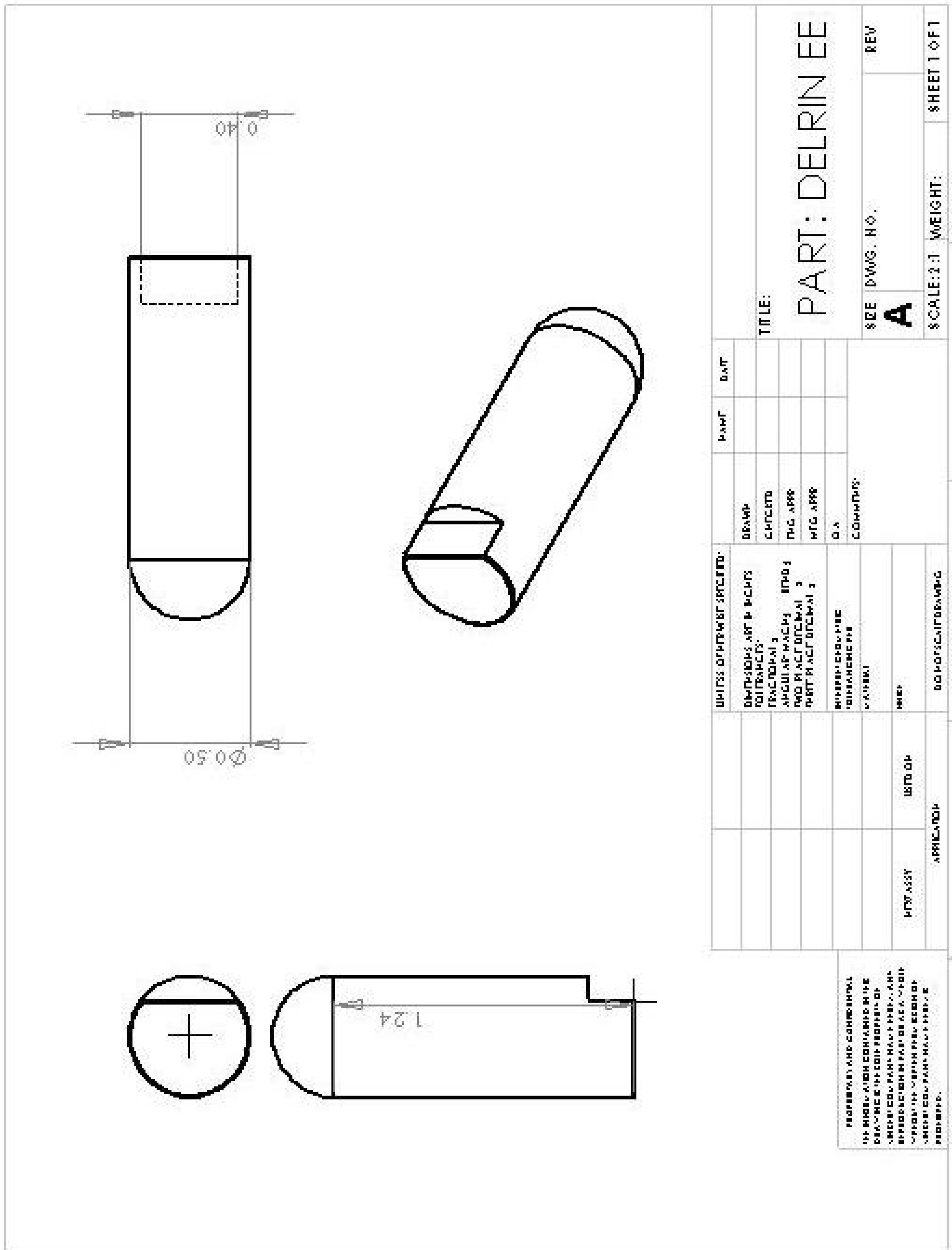
0.40
Ø0.50
1.24
TITLE:
PART: DELRIN EE
SIZE
A
DWG. NO.
REV
SCALE:2:1
WEIGHT:
SHEET 1 OF 1

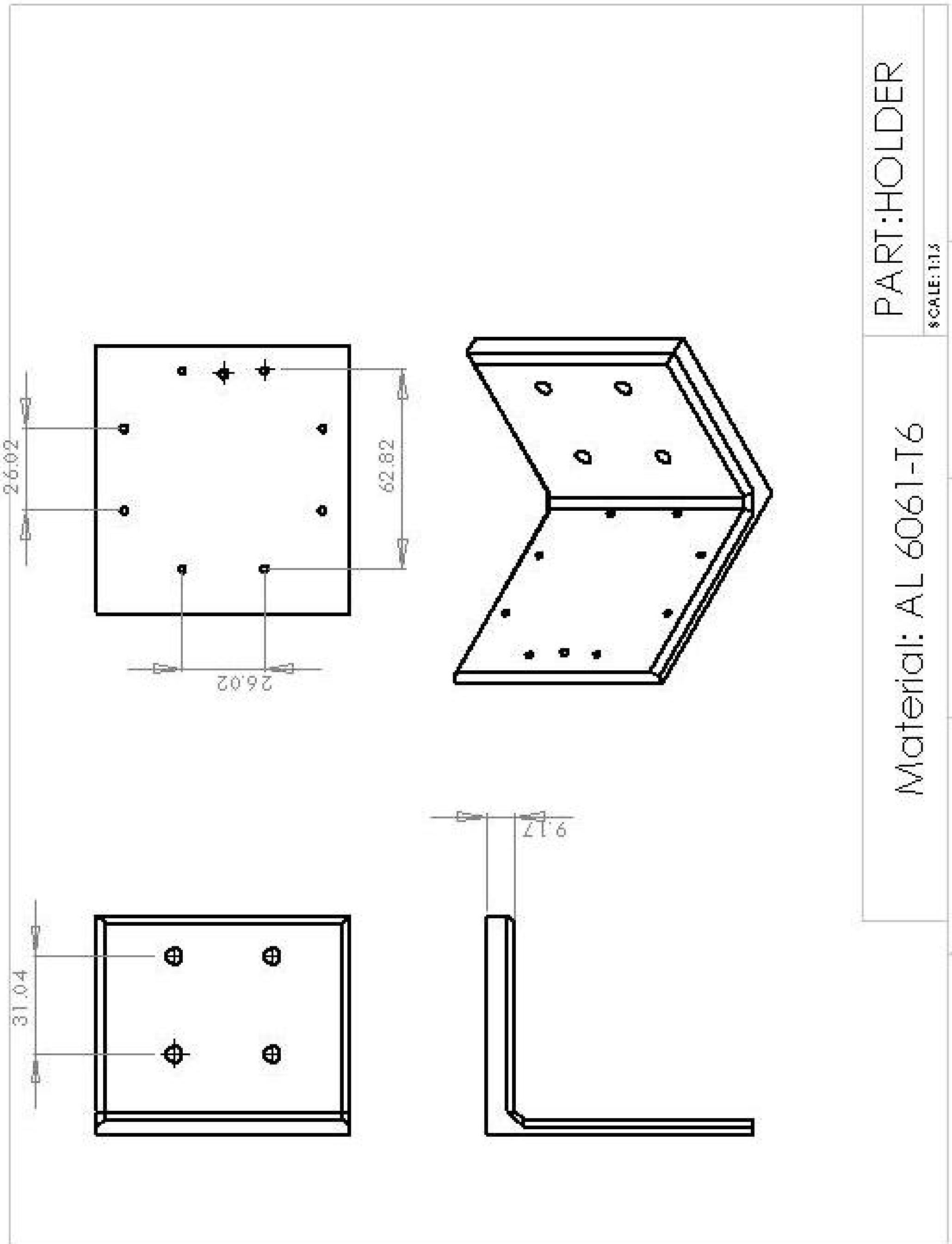
PART:HOLDER
SCALE: 1:1.3
Material: AL 6061-T6
26.02
62.82
26.02
31.04
9.17

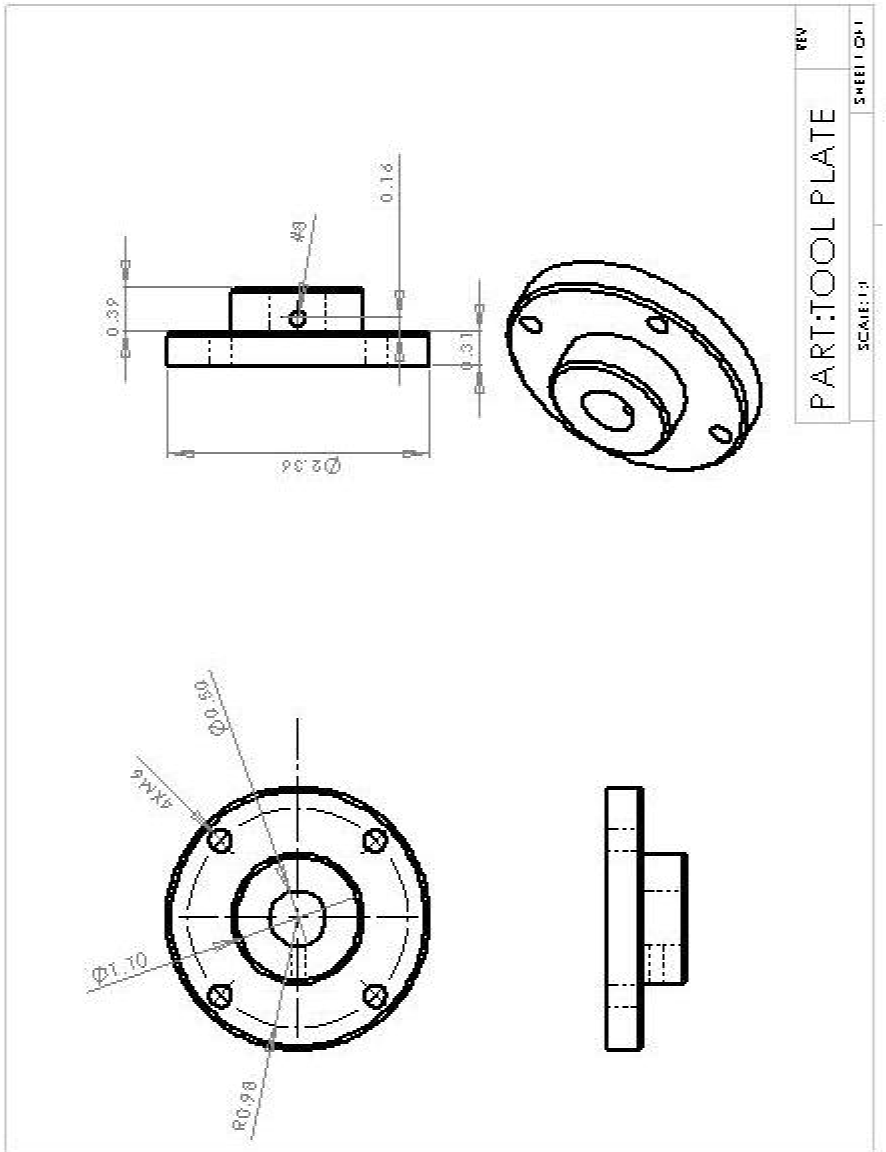
PART:TOOL PLATE
REV
0.39
#8
0.16
0.31
Ø2.36
Ø0.50
4XM6
Ø1.10
R0.98